UCRL-50016-82-1

Mechanical Engineering Department Technical Review

Scientific Editor: R. B. Carr

General Editors: L. Abrahamson

R. M. Denney

B. E. Dubois

January 1, 1982

Lawrence Livermore National Laboratory

DISCLAIMER

DISCLAIMER

Work performed under the auspices of the U.S. Department of Energy by Lawrence Livermore National Laboratory under Contract W-7405-Eng-48.

UCRL-50016-82-1
Distribution Category UC-38

Mechanical Engineering Department Technical Review

Scientific Editor: R. B. Carr

General Editors: L. Abrahamson

R. M. Denney

B. E. Dubois

Manuscript date: January 1, 1982

LAWRENCE LIVERMORE LABORATORY
University of California • Livermore, California • 94550

Available from: National Technical Information Service • U.S. Department of Commerce
5285 Port Royal Road • Springfield, VA 22161 • $3.50 per copy • (Microfiche $8.00)

PREFACE

The Mechanical Engineering Department Technical Review is published to inform readers of various technical activities in the Department, promote exchange of ideas, and give credit to personnel who are achieving the results.

The report is in two parts: technical achievments and publication abstracts. The first is divided into seven sections, one for each division in the Department.

These technical achievement articles are summaries of ME work. For additional details on a subject, please contact the individual(s) listed at the end of each article. Inasmuch as most projects are the result of cooperative efforts, the article contact may refer you to another individual who can best answer your question.

The second part of the biannual Technical Review contains the titles or abstracts of laboratory reports published by Mechanical Engineering Department personnel since the previous issue.

The ME Technical Review Committee members include:

R. B. Carr, Deputy Department Head
E. W. McCauley, Nuclear Test Engineering Division
D. W. Ravenscroft, Nuclear Explosives Engineering Division
J. H. Pitts, Energy Systems Engineering Division
A. S. Zolnay, Weapons Engineering Division
R. H. Bossi, Engineering Sciences Division
J. D. Lee, Magnetic Fusion Engineering Division
H. H. Humpal, Materials Fabrication Division
R. M. Denney, General Editor

CONTENTS

Nuclear Test Engineering Division

Nuclear Explosives Engineering Division

Weapons Engineering Division

Energy Systems Engineering Division

Engineering Sciences Division

Magnetic Fusion Engineering Division

Materials Fabrication Division

NUCLEAR TEST ENGINEERING DIVISION

The Nuclear Test Engineering Division (NTED) provides mechanical engineering and technical expertise for a wide range of activities in three LLNL programs: nuclear test, nuclear systems safety, and energy.

Nuclear Test Program

Our nuclear testing responsibilities involve design, structural evaluation, fabrication, and proof testing of diagnostic and device canisters that position radiation detectors and protect nuclear explosives in an underground environment. We synthesize, procure, and certify the arming and firing systems, and we develop downhole and containment systems to meet zero-detectable radioactivity release requirements. Our advanced development projects include studies of new engineering concepts, analytical and design methods, and diagnostic techniques. In carrying out this work, we strive to improve data quality and field operations, maximize safety, and optimize cost-effectiveness and resource utilization. Included in this programmatic support is spill effects testing under the Liquefied Gaseous Fuels Program.

Nuclear Systems Safety Program

The safety of nuclear power plants and associated facilities is the major concern of the Nuclear Regulatory Commission (NRC). We are responsible for providing technical data relating to reactor safety on which the NRC can base licensing decisions and assessment tools to protect public health and safety. Facilities in the nuclear fuel cycle—fuel processing and fabrication, reactor containment systems, interim waste storage, and spent fuel reprocessing—are considered from the viewpoint of safety and structural integrity.

Our multidisciplinary work is grouped into four categories: seismic and structural safety, reactor engineering, systems/operations, and licensing reviews. The NRC relies on the Laboratory as the primary facility for research on the seismic safety of nuclear power plants. Our multiyear Seismic Safety Margins Research Program (SSMRP), for example, defines the adequacy of seismic design for the safety of nuclear power plants in the U.S. Reactor engineering work involves accident analysis and studies of thermal-hydraulic and fluid-structure interaction phenomena. Systems/operations projects are concerned with risk assessment and control room design reviews. We also provide technical assistance to the NRC licensing staff on reactors operating or under construction.

In addition, our engineering mechanics expertise is applied to specific projects in other areas, including effort for the Magnetic Fusion Program, the Plant Engineering Department, H Division, and W Division.

Energy Program

We provide mechanical engineering support to several of the Laboratory's smaller energy projects and to a number of efforts for the Earth Sciences (K) Division. Current work is under way in oil shale retorting, underground coal gasification, radionuclide migration, spent reactor fuel storage, and geophysics research. We are responsible for designing, building, and operating both Laboratory experiments and off-site field engineering tests.

(For further information, contact R.J. Wasley, Ext. 2-9966.)

Technology Transfer and Development of Computer-Aided Engineering with the University Community

Computer-aided engineering (CAE), the process of using the computer interactively for modeling, analysis, and design with graphical representation for both input and output, is becoming an increasingly important contributor to engineering productivity. The demand for persons skilled in CAE is growing rapidly. However, it appears that the need for such skills will exceed the ability of the university community to supply competent personnel unless something is done now.

We have initiated a new technology transfer project in cooperation with the university community. The objectives of this program are to increase the student's use of and familiarity with the

computer in engineering schools, and ultimately to assist in increasing engineering productivity.

For most universities, available CAE exposure is offered in graduate school. The major responsibility for CAE training is left to industries and research facilities that specifically require the skills. It appears that the university community has been slow in developing CAE curricula for two reasons: first, interactive graphic and computational equipment costs have been too large for most universities to afford; second, the normal learning experience through which instructors are trained and curricula are developed (research, grants, publications, and ultimate introduction into the classroom) is impeded in CAE.

The costly equipment and the rapidity with which the CAE field has developed has meant that many universities have been unable to respond and affect research. Because the institutional academic structure emphasizes research and publications for advancement, there is limited incentive and time for instructors to develop courses that do not benefit their research. With the new developments in powerful and low-cost microcomputer hardware, the first factor can be overcome. The major impediments to development, then, are the institutional requirements and the resulting limitations on the instructor's time. Rather than to try to alter the institutional requirements or to wait for them to change, it is expedient to work with members of the university community to develop a CAE curriculum externally. This process will include: (1) the standardization, collection, development, and documentation of software that is suitable for CAE curriculum use and is adaptable to microcomputer implementation; (2) curriculum development; and (3) dissemination to the university community. This process is designed to minimize the instructor's learning and preparation time.

This article is intended both as an announcement and as an invitation, particularly to microcomputer practitioners who have developed engineering software that might be useful to this project.

(For further information, contact W.J. Comfort, III, Ext. 2-4908, B.E. Brown, Ext. 2-1261, B.R. Bowman, Ext. 2-0325, or A. Harral, III, Ext. 2-8695.)

New X-Ray Fluorescence Analysis System Developed to Account for Nuclear Fuel During Reprocessing

Process control information and material accountability are key factors in nuclear fuel reprocessing operations. Using the LLNL X-Ray Fluorescence Analysis (XRFA) system, both speed and accuracy can be vastly improved over methods presently used.

Nuclear Test Engineering Division personnel, in collaboration with the Nuclear Chemistry Division, have developed a system utilizing x-ray emission stimulated by a ^{57}Co source (see Fig. 1). The XRFA system provides improved concentration measurement accuracies for pure and mixed actinide solutions, and plutonium isotopes. The XRFA system also is much more adaptable than the chemical analysis process presently in operation at the Savannah River Plant near Aiken, South Carolina. For example, the x-ray's ability to penetrate several millimetres of stainless steel makes it advantageous to build the analysis system right into a reprocessing line.

Energy-dispersive XRFA utilizes photons from radioactive sources or x-ray tubes to stimulate x-ray emission. Radioactive ^{57}Co emits a 122.05-keV gamma ray that is very effective in fluorescing uranium (K_{ab} = 115.59 keV) and plutonium (K_{ab} = 121.72 keV) K x rays. Both the 122.05 keV exciting radiation and the actinide K x rays have sufficient energy to penetrate several millimetres of stainless steel. Therefore, this technique can easily be adapted for on-line, at-line, or off-line measurements.[1,2]

In the Savannah River Plant application, the solution is contained in a plastic test tube 11-cm high, 20-mm o.d., and 1-mm wall thickness. Two 10-mCi sources are collimated to irradiate the solution as shown in Fig. 2. The radioactive isotope is electroplated onto a 1.6-mm-diam spot on nickel foil and is encased in a welded stainless steel capsule 4.8-mm-diam by 3.2-mm thick. Since ^{57}Co also emits x rays at lower energies, a substantial amount of correctly placed shielding is required both for operator safety and detector shielding from stray photons. The 37-mm tungsten collimator shielding thickness gives an optimum

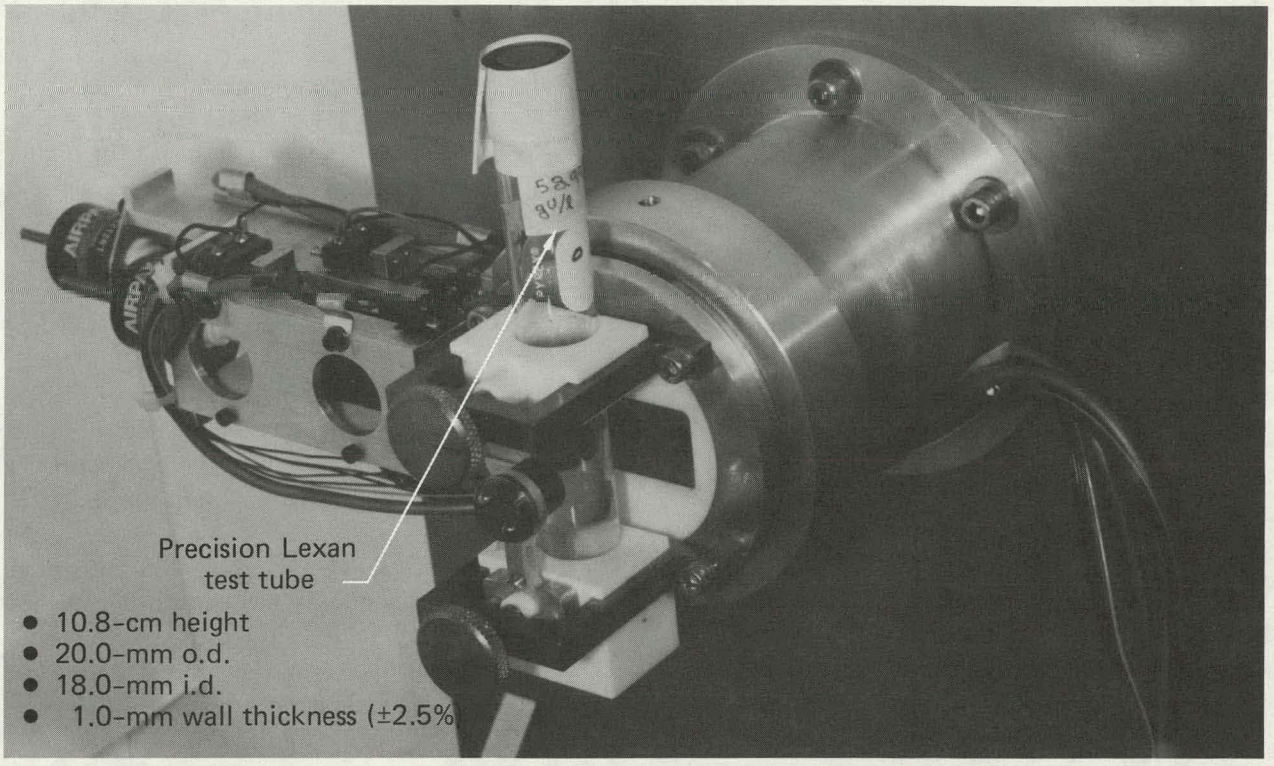

FIG. 1. Mechanical system for the x-ray fluorescence analysis system.

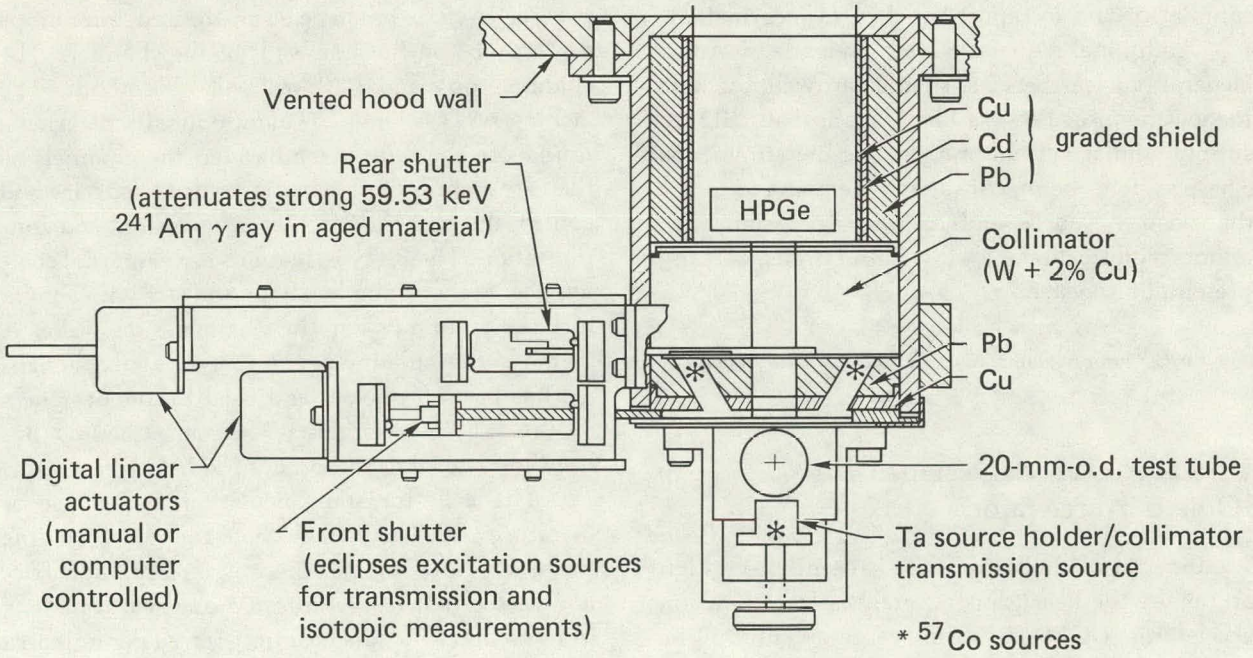

FIG. 2. Schematic of sample, source, and detector assembly.

signal-to-background ratio. Cadmium and/or copper liners and surfaces attenuate lead or tungsten x rays that are created. A third similarly constructed, less intense, ^{57}Co source is housed in a hollow tantalum collimator. A 0.5-mm exit hole in a faceplate located 12.5 mm from this source allows a 122-keV beam to pass through the solution into the detector straight on. Actinide x-ray intensity is proportional to solution concentration while the transmitted intensity indicates changes in solution density at a fixed concentration. Two shutters are controlled manually or by computer. When closed, the front shutter (2.5-mm tungsten) eclipses the two exciting sources, allowing solution radioactivity to be measured. The rear shutter (1-mm Cd) is used to attenuate the 59.53-keV x ray of ^{241}Am when it is incompletely separated in aged material. Linear digital stepping motors are used to drive the shutters by computer command.

All supporting electronic equipment except for a used terminal is enclosed in a locked, air-conditioned, two-rack enclosure to prevent unauthorized access and to minimize contamination in the event of a spill. The system requires the operator to insert a filled test tube of liquid and address the computer terminal to begin the counting cycle. The computer makes the two types of measurement required (process control information and material accountability), inserting shutters and initiating count cycles, and then reduces the accumulated data to report the desired information.

Additional requests have been made by Allied General Nuclear Services Plant, Barnwell, SC, and Idaho Chemical Process Plant, Idaho Falls, ID, to supply similar systems for on-line measurements. These systems being considered are going to utilize the existing source and collimating design with minor modifications to the liquid transport and presentation system.

(For further information, contact J.D. Eckels, Ext. 2-6686.)

Upgraded Target Designed for IONAC Accelerator

Special methods were used recently to design and make the heat transfer analysis for a new ion accelerator (IONAC) beam target that will be cooled internally with water. The IONAC accelerator is used as a subkilovolt x-ray source for diagnostics calibration to support the nuclear test program.

The IONAC accelerator will be upgraded to provide a higher ion beam power than at present; however, the present target cannot accept higher power without damage, so an upgraded target also is necessary.

The upgraded target will consist of a copper plate with internal water cooling channels located 0.015 in. below the target surface to provide cooling for a 0.75-in.^{2} area. The channels are parallel, 0.08-in. wide, 0.03-in. deep, and are separated by 0.025-in.-thick lands. The target will be made with a technique previously used at LLNL to fabricate targets for the Rotating Target Neutron Source II (RTNS-II).[3]

The cooling passages, inlet plenum, and outlet plenum will be chemically etched into the surface of an oxygen-free, high-conductivity copper plate. Figure 3 shows the prototype target following etching. Then a layer of copper will be electroplated over the etched plate while the channels and plenum are protected by a wax filler. After the wax is removed, the channels and plenum are left as internal water passages. The water will be admitted and discharged through holes in the back of the target.

Turbulence generator bumps will be provided on the channel walls to enhance heat transfer to the flowing water. The chemical etching process can provide any size or shape bump desired, but bumps can only be on the side walls of the channels. The channel tops and bottoms will be smooth. The etching process tends to smooth out sharp corners, round off the bumps, and widen the channels as they are etched. Experience is needed to specify and control the process to achieve the desired end configuration. The RTNS-II targets have internal cooling passages of a similar shape and size with similar turbulence bumps on the channel side walls. A method of calculating heat transfer in such a channel has been developed and used by the designers of the RTNS-II targets.[4] The same method has been used to design the new IONAC target.

The heat transfer calculation makes use of literature data showing that for flow in the transition-flow regime, there is an optimum friction factor that results in optimum heat transfer.[5] In transition flow, the heat transferred per unit area can be increased by about a factor of 2 over what would be possible in a smooth tube by optimally

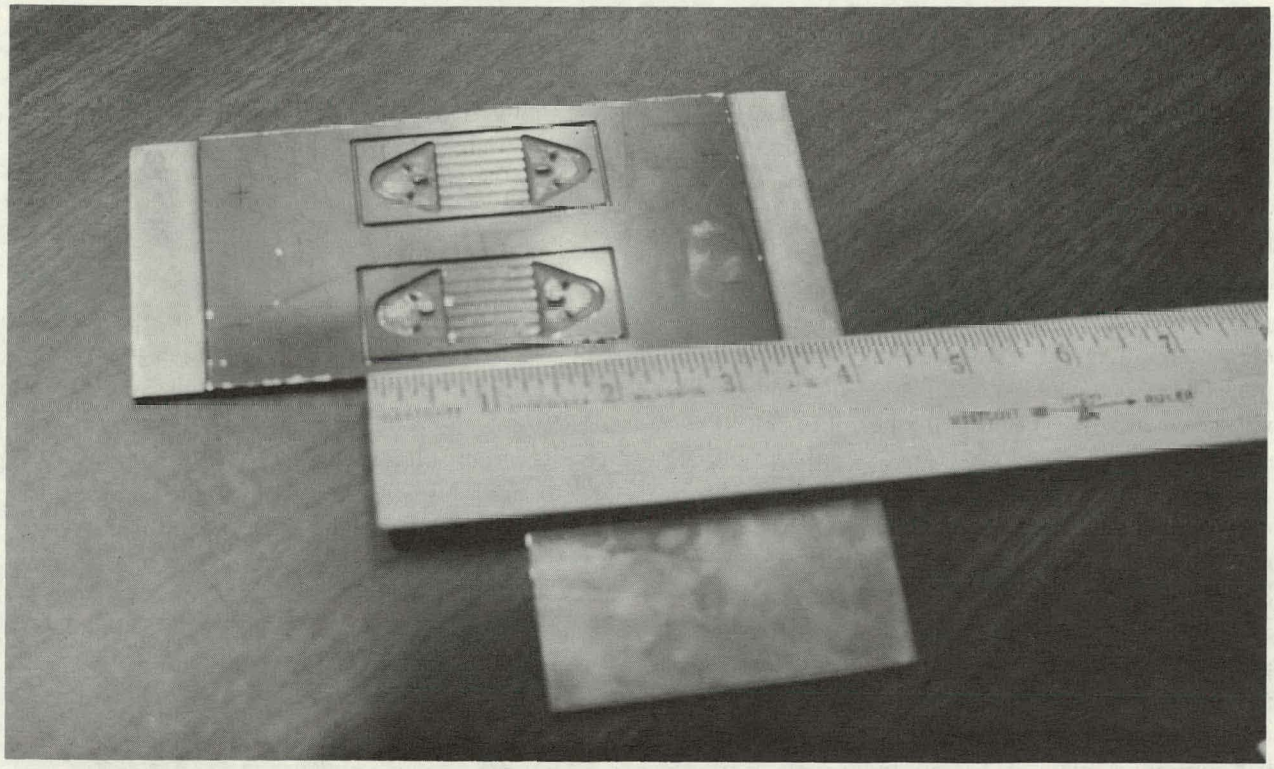

FIG. 3. Prototype targets after etching. Measurements are being made of these targets to better characterize the etching process so that the desired configuration can be reliably achieved.

roughening the surface. Increasing the surface roughness in a system already in fully rough flow, however, will decrease the heat transferred per unit area because the flow velocity drops as friction rises, while the augmentation in heat transfer coefficient does not keep up.

Calculations for the upgraded IONAC target show that the target surface temperature will be about 310°F. To prevent boiling, water will be kept under pressure in the channels. By including the effects of turbulence generator bumps, the maximum heat flux is 1990 W/cm^2, which corresponds to a 1-cm-diam beam of 1560 W. For comparison, smooth wall channels of the same hydraulic radius result in a maximum heat flux of 1150 W/cm^2 (a 910-W, 1-cm-diam beam) for the same conditions. The heat-transfer coefficient for the smooth wall case is calculated using the standard Dittus-Boelter equation, which gives the heat-transfer coefficient as a function of Reynolds number and fluid properties.

(For further information, contact D.I.. Hipple, Ext. 2-4958, I.M. Wiseley, Ext. 2-1762, or R.D. Ernst, Ext. 2-7860.)

Transient Measurement of Relative Permeability Under Study

Relative permeability is an empirical parameter used to predict simultaneous flow of immiscible fluids in a porous medium. The flow prediction is an integral part of the Nuclear Test Engineering Division's containment analyses. In an effort to improve flow prediction capabilities, an analytical/experimental study was initiated with the objective of developing a method suitable for *in situ* determination of relative permeability of geologic formations.

The relative permeability is to be calculated from measured pressure history by computer simulation using parameter estimation techniques. The pressure histories are to be measured in one-dimensional and two-dimensional experiments conducted in a controlled laboratory environment. The results from the new parameter estimation technique will be checked with one-dimensional experiments, which will also provide data to determine relative permeability of the same sample using classical methods. The test medium will be consolidated sand.

A code for simulation of one-dimensional immiscible fluid flow through a porous medium has been written and debugged. The code is being modified to accept experimental input data. The code will be further modified for calculation of two-dimensional immiscible fluid flow and for parameter estimation.

A method for consolidating epoxy-coated sand has been developed for preparing an adequate porous medium for the scheduled experiments. The consolidation method was developed from visual inspection of the internal structure and from measurement of specific permeability of consolidated one-dimensional flow samples. Special apparatus was designed and fabricated for measurement of specific permeability. Visual inspection of sectioned samples indicate that controlling the tamping intensity, the tamping duration, and the initial layer thickness were sufficient to produce an adequately uniform sample. Measurements of specific permeability indicate that controlling the epoxy-sand ratio, and sand-particle distribution were adequate for production of a porous medium with acceptable properties in the 1-to-10-D range.

Acquisition, design, and fabrication of equipment for both the one- and two-dimensional experiments have been completed. Figure 4 shows the core and the shell of the injector-detector probe for the two-dimensional experiments. The core, which contains the injector passage and provisions for mounting two pressure transducers, is sealed to the shell with O-rings; each of the seven sets of ports may serve as injector or detector ports. The injector-detector is nominally 3-in. diam by 6-ft long and weighs about 200 lb.

The one-dimensional samples will be nominally 2-in. diam by 24-in. long. The two-dimensional test medium is approximately 6-ft diam by 8-ft high. The tamping procedure for producing samples for one-dimensional experiments has been developed. The porous medium for the two-dimensional experiment will be consolidated in place as soon as tamping procedures are selected from smaller scale tamping tests.

Tamping parameters for producing the two-dimensional porous medium will be selected from results of consolidating epoxy-coated sand in a 55-gal drum. The consolidated sample in the 55-gal drum will contain an embedded injector and pressure transducer ports to permit two-dimensional experiments to be conducted on a smaller scale. The consolidated sample will be cored for proof of adequate uniformity before the tamping technique is used in the 6-ft by 8-ft tank.

(For further information, contact W. Lai, Ext. 2-0324.)

Microcomputer-Aided Engineering

An opportunity to test the utility of a microcomputer in a significant engineering task arose when a study was initiated to develop an *in-situ* method to determine relative permeability. The microcomputer aided in two distinct areas:

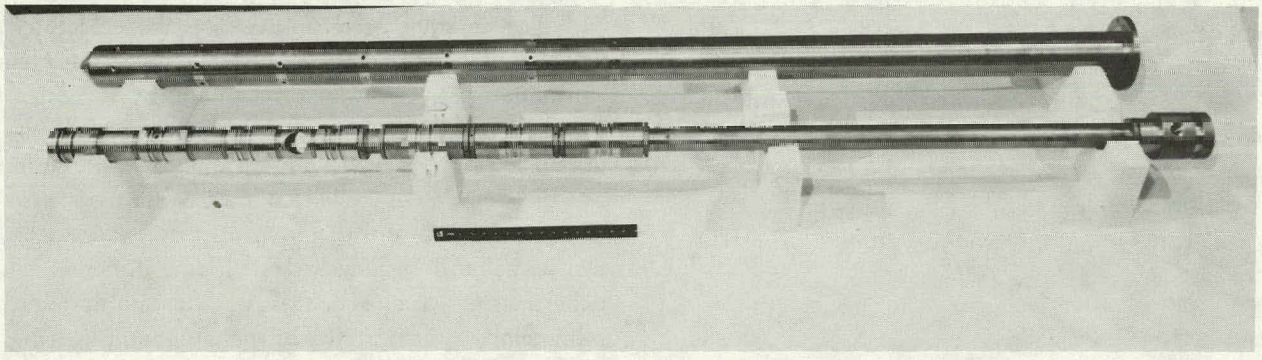

FIG. 4. Injector-detector probe for two-dimensional experiments.

development of a computer simulation code to estimate relative permeability, and text composition (i.e., word processing) to report the findings. Experience in these two areas of microcomputer-aided engineering is summarized here.

This report is most applicable to stand-alone microcomputer systems. Depending on the manufacturer, size, and configuration, these systems can be less than $500 to more than $10 000. The experience is limited to a modified upper-lower case Model 1, TRS-80 with 48k bytes memory, cassette tape storage, three disk drives, and the line printer II. The system costs about $3000, or about half the price of a new subcompact automobile; the cost is about equally divided among the basic computer (i.e., the keyboard, computer, and video display), the disk drives, and the printer.

The computer was purchased with Level II Basic. Basic seems to be the resident language for microcomputers. The TRS-80 disk operating system, TRSDOS, is supplied with disk drives. Although other languages and disk operating systems are available at extra cost, I preferred to use the standard packages. SCRIPSIT was used for word processing.

The simulation code for estimation of relative permeability involves simultaneous numerical solution of two nonlinear partial differential equations which describe the flow of each immiscible fluid component; the relative permeability is a nonlinear proportionality constant relating derivatives of saturation and fluid pressure. An implicit-pressure, explicit-saturation, finite-difference method was selected for the numerical solution. The implicit procedure gives rise to a tridiagonal matrix which was solved using the Thomas algorithm. The implicit solution was iterated until the old and new pressures differed by less than 0.0001.

Instructionally identical one-dimensional flow codes were developed in parallel for the microcomputer and the CDC 7600 in the LLNL LTSS; the code for the microcomputer is written in Basic and that for the LLNL LTSS is written in LRLTRAN. The instruction set for Basic is more limited, but similar to Fortran. Writing the code in the two languages provided a continuous check on syntax and logic which I estimate ultimately reduced the total development time by one quarter or one half.

Programming limitations of the Basic language are not excessively restrictive. One restriction which can cause problems is that subroutines are called by line numbers in Basic so that arguments are essentially passed by common; arguments are common by default and not by declaration so that this restriction has a positive side. Another is the limited format instructions in Basic; the easiest method to format tabular output is with the TAB instruction which performs the same function as on a typewriter. Because variable names start with a letter and can only be two characters long in LEVEL II Basic, care must be exercised to avoid duplication in writing large programs. Basic permits use of the same name for different variable types, but undeclared type variables are single-precision-real by default; single precision is six significant figures. Finally, undeclared array dimensions default to 11 (i.e., from 0 to 10).

The code developed for the microcomputer is 141 lines long, has 11 subroutines, and occupies about 6300 bytes of memory. It contains 23 one-dimensional arrays; 19 arrays have 61 elements and 4 have 50 elements. About 10% of the lines contain multiple instructions. Computed results are identical to those from the LRLTRAN LTSS code. Identical runs take about 1000 times longer on the microcomputer than on the CDC 7600; a compiled Basic code will be signficantly faster.

The slowness of the uncompiled code compared to the CDC 7600 is offset by the fact that the microcomputer is a dedicated machine. The results from computations that require a long time may be stored on a cassette tape, stored on a diskette, or printed. Because the interpreter mode permits quick turnaround tests, microcomputers are ideal for testing algorithms and for parametric studies. Also, the reported code development task indicates that personal microcomputers can be used to advantage in engineering analyses.

Text describing completed portions of this study were composed and stored on diskettes for later retrieval and assembly of the final report. Accustomed to the time-honored method of writing, insert, delete, erase, and cut-and-paste, I was not certain that I could make the transition to writing on a video display. The transition was effortless, however, and I compose as easily if not easier on the microcomputer; all of the accustomed editing procedures are built into the word processor. There

is the added advantage of a clean text that is always available for revision. Though the completed text may not be ready for publication, its condition is much easier for preparation by other professionals. This experience has shown that text composition with a general purpose personal microcomputer can be very effective.

(For further information, contact W. Lai, Ext. 2-0324.)

Analysis of Transient, Erosive Flows

Theoretical analysis has been made of surface heating history when a surface is exposed to transient thermal fluxes from a turbulent compressible boundary layer. The conservation equations were solved by means of a factored alternating-direction-implicit (ADI) numerical method. Results showed high heat fluxes at the surface, causing sufficient rise in surface temperatures to quickly reach melting in some substances. The melting liquid-layer case is also briefly discussed.

The present work was undertaken to describe the transient surface phenomena involved in high temperature propellant flows in order to investigate the dominant mechanisms of surface erosion. To study the interaction between the interior surface and the hot flowing gas, a time-dependent description of the flow field in the boundary layer adjacent to the wall is formulated which includes reacting species, turbulence, and propellant additives, taking into account the conditions of unsteady core flow and heat transfer at the surface. The analysis thus involves simultaneous solution of the various conservation equations in the transient boundary layer. The generalized formulation also includes finite-rate chemical reactions and a two-equation closure model for the turbulent-flow situations.

In view of the complex nature of the hot-gas erosion, as well as of the various coupled conservation equations that describe the phenomena, a step-by-step approach is taken in the present analysis. Thus initial effort has been primarily directed toward solving the mass, momentum, and thermal energy equations in the unsteady boundary layer as a first phase in this systematic approach. The timewise change in the surface temperature due to the heat flux at the wall is also determined along with the solution of the conservation equations for the adjacent viscous layer. In the transient boundary-layer flow situations, thermodynamic equilibrium is assumed for the present and the turbulent case is accounted for by the use of the zero-equation model along with the eddy-diffusivity expression of Cebeci and Smith.[6]

Numerical solution of unsteady-flow equations, especially boundary-layer and Navier-Stokes equations, has been the subject of many investigators. In the present work the transformed, time-dependent, nonlinear partial differential equations were solved by a method patterned after the ADI scheme of Douglas and Gunn.[7] This method is second-order time accurate, spatially factored, and noniterative. The conservation equations in the alternated-sweep form are then solved under prescribed (transient and streamwise varying) core-flow conditions applied at the edge of the boundary layer. For the turbulent case, a variable grid size scheme is implemented in order to facilitate accurate computations near the wall where very steep flow gradients exist.

The numerical scheme was tested for its validity on some well-studied physical cases. The first of these was the case of an incompressible unsteady laminar flow over a flat plate. A Blasius velocity profile on the upstream boundary and the "Rayleigh-Stokes" flow field were prescribed on all downstream stations as initial conditions. As time elapsed, all the velocity profiles developed into the Blasius profile. Hall[8] originally obtained a solution to this problem and our results agreed well with his. The scheme was next applied to compressible laminar flows of perfect gases with a Prandtl number of unity. The resulting thermal profiles matched the velocity profiles, another proof of correctness of the present scheme. Figure 5 shows the timewise development of the turbulent velocity profile downstream from the leading edge. The change in the profiles near the wall and the increase in boundary layer thickness compared to the laminar cases are evident. These turbulent profiles compared well with those obtained by Blottner.[9] The turbulent thermal profiles demonstrate behavior similar to that of the turbulent velocity profiles over time.

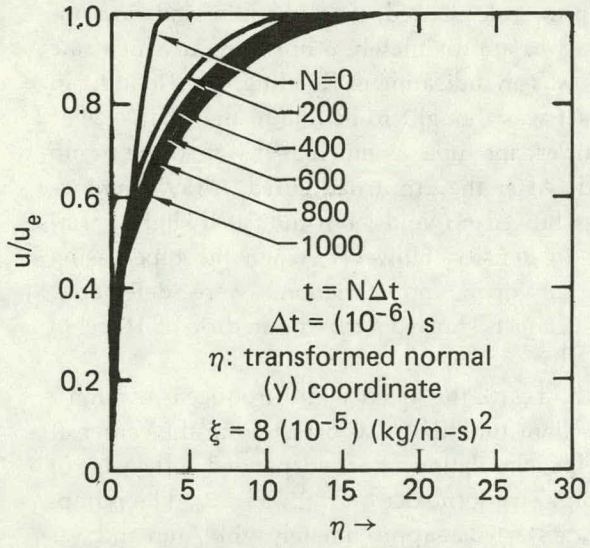

FIG. 5. Timewise development of turbulent velocity profiles.

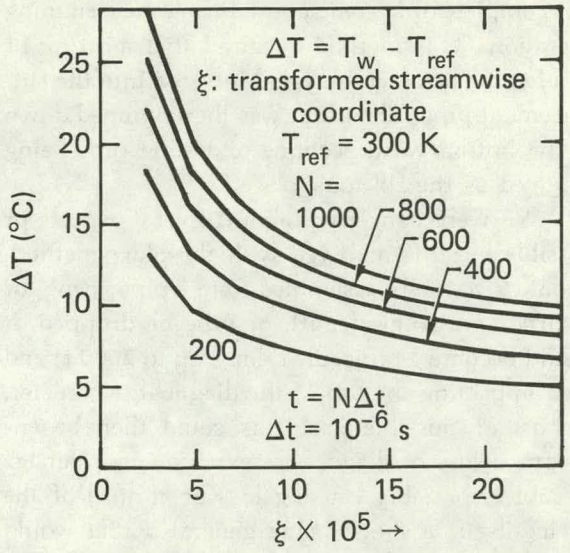

FIG. 6. Wall-temperature history along a steel surface: turbulent flow.

The case of spatially and temporally varying total energy potential between the wall and the flow was next studied. In the "responding wall" model, heat from the core flow is transferred through the boundary layer to the wall, causing wall temperature T_w to rise. From the unsteady thermal profile distributions in the direction normal to the flow, it is possible to obtain the heat-transfer rate at the surface. Figure 6 shows the corresponding wall temperatures for these times for a steel surface whose thermal conductivity and thermal diffusivity were held constant. Sizable increases in surface temperature with time are demonstrated, especially in the upstream region.

Continuous exposure to high heat fluxes at the wall (surface) could result in the surface temperature reaching the melting point. Under the sample conditions under discussion, this point is arrived at in approximately 1 s. Thereafter, melting of the solid will commence at the surface and the resultant liquid layer will be swept downstream due to the high shear at the interface between the liquid layer and the (gas) turbulent boundary layer. Assuming a Couette-type flow for the liquid layer, the conservation equations for the liquid flow have been derived, which yield the melting rate, the streamwise interface velocity and the heat flux at the interface. Preliminary results show very low values of the interface velocity and the interface temperature much higher than the melting point, suggesting that the no-slip condition at the interface is a physically reasonable boundary condition and that much of the heat flux from the hot turbulent boundary layer is expended in melting the solid material at the surface.

(For further information, contact S.-W. Kang, Ext. 2-7233.)

New Method Improves Emplacement Pipe Grouting

The Containment Group of the Test Systems Section of NTED has tested and successfully fielded a less hazardous and more efficient emplacement pipe grouting method. The tests were conducted in mid-February 1981, just prior to the Seco Event. The new method of emplacing the grout at the top of the pipes has been used for the Seco, Vide, Harzer, and Niza Events; time savings have been approximately 6-8 h per event compared to the old method.

We believed that the emplacement pipe grouting method developed during the 1970's for containment purposes was expensive and potentially hazardous to equipment. This led us to pursue an alternative method. The established method was to grout emplacement pipes after emplacement

was complete or at some point during the stemming operation. This method required that a string of tremie pipe be assembled and lowered into the emplacement pipe. The grout was then pumped down to the bottom with sections of tremie pipe being removed as the fill took place.

We were concerned about several aspects of possible hazards involved with the older method. Should a partially assembled tremie pipe string, or as little as a single length of pipe be dropped, it would become a projectile falling up to 2000 ft and then impacting the top of the diagnostics canister. A host of possible problems could then be envisioned: loss of diagnostics experiments; damage to cables, possibly causing loss of control of the device itself; a shock being generated that would cause separation of the emplacement string at a coupling, a compromise of the containment assurance if the tremie pipe fell into a partially grouted emplacement pipe.

In an attempt to eliminate these potential problems, we tested a proposed new emplacement pipe grouting method—performing the grouting operation from the surface. To answer these questions, two tests were conducted at the vertical pull test facility at the Nevada Test Site:

1. Can grout be practically emplaced from the surface?
2. Is there a pumping rate that should not be exceeded?
3. What will be the effects on grout densities?

The tests consisted of pumping the grout into a 600-ft-long string of 5-1/2-in.-diam pipe casing. Two nozzle designs (see Fig. 7) were used to pump the grout, a 50/50 Pozmix with 2% bentonite. The pumping rate was gradually increased until flooding occurred. Each pipe string was filled with approximately 250 ft of grout. The grout was then allowed to set and cure for several days. After the grout had cured, the pipe strings were disassembled and each grouted section was inspected. Air entrapment and voids were checked by the material balance and an x-ray examination. In both tests the balance was within one lineal foot, or approximately 0.3 ft^3 of the calculated elevation. Each pipe section was also subjected to a pressure test.

For Test 1 we used a peripheral design to introduce the grout at the pipe wall; the air return was through a centrally located 2-in.-diam tube (nozzle on left, Fig. 7, and closeup in Fig. 8). The pumping rate started at 2 bbl/min and was increased to approximately 6 bbl/min, at which rate there was an indication of flooding. The flooding in this set was thought to be due to the small size of the air escape tube, as much as it was to the pump speed. After the grout had cured, x-ray examinations showed no voids, but indicated slight variations in density. However, when the pipe casing was cut open, no variations were detectable. Pressure tests showed a maximum drop of 10 psi in 1-1/2 h.

In Test 2 the grout was introduced through a 2-in.-diam tube that was offset from the center of the pipe, simulating a hose suspended at the edge of the pipe string (nozzle on right, Fig. 7). The pumping rate started at approximately 4 bbl/min and was increased to 7 bbl/min, which was the maximum pumping speed of the equipment. There were no signs of flooding. However, in this test there was some CaCl introduced due to residue left in one of the pump tanks. X-ray examinations revealed numerous short "pipes" or holes lengthwise through the grout sections. Pressure tests confirmed that the "pipes" were connected and continued through the entire grout sections. The "pipes" were thought to be caused by the CaCl in the grout, because this phenomena has been observed in other samples of grout containing CaCl. X-ray examination also showed numerous areas of varying density, although slight, probably caused by the presence of the CaCl.

Our tests confirmed that emplacement pipe grouting from the surface is practical. Operational safety has been enhanced and costs have been decreased by elimination of tremie pipe emplacement/removal and its required equipment and manpower effort. Furthermore, besides being a much safer operation, the new method can be employed while other stemming is underway. In this method's subsequent use for the Seco, Vide, Harzer and Niza Events, time savings have been approximately 6 to 8 h per event compared to the old grouting method.

Grateful acknowledgment is made to B.G. McMahan of Fenix and Scisson, Inc., for his experimental work in testing the new method, and to D.L. Paquette of LLNL for her help in preparing a description of the grouting method.

(For further information, contact B.L. Maranville, Ext. 2-9278.)

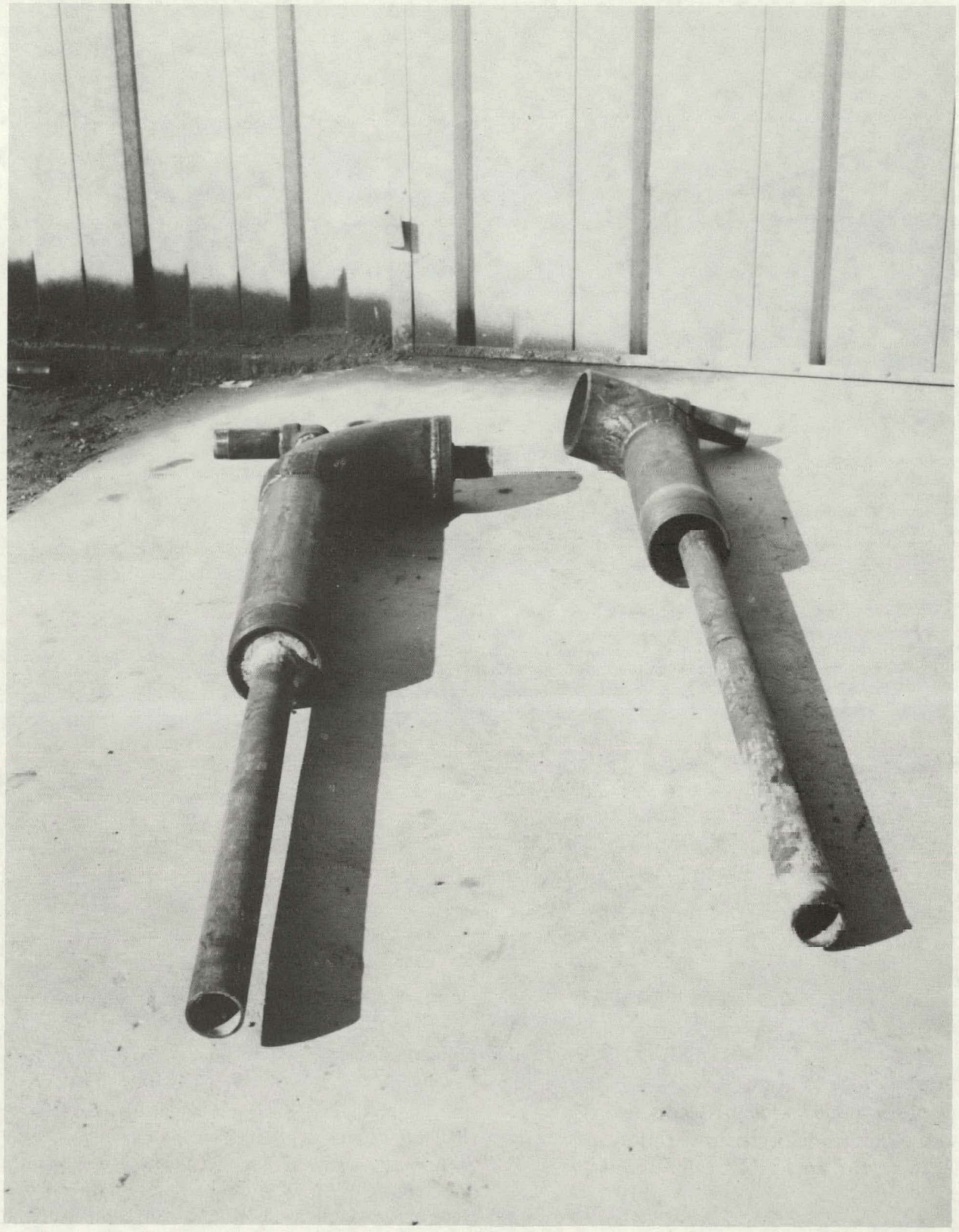

FIG. 7. Experimental nozzles.

FIG. 8. Closeup of peripheral nozzle.

Computer-Aided Design Used to Make Piping and Instrumentation Diagrams for an LNG Spill Facility

A computer-aided design terminal was used advantageously to draw piping and instrumentation diagrams (Fig. 9) for the liquefied natural gas spill facility at Frenchman Flat, NV.

The drawing, which is a schematic layout of all valves, gauges, piping, and storage tanks, is prepared by means of simple commands to create lines, arcs, circles, radius, and text. Since there are many valves and symbols that can be repeated many times, a library of parts is drawn. Some of these parts are shown in Fig. 10. With this library of parts at hand, it is simple to use them anytime they are needed.

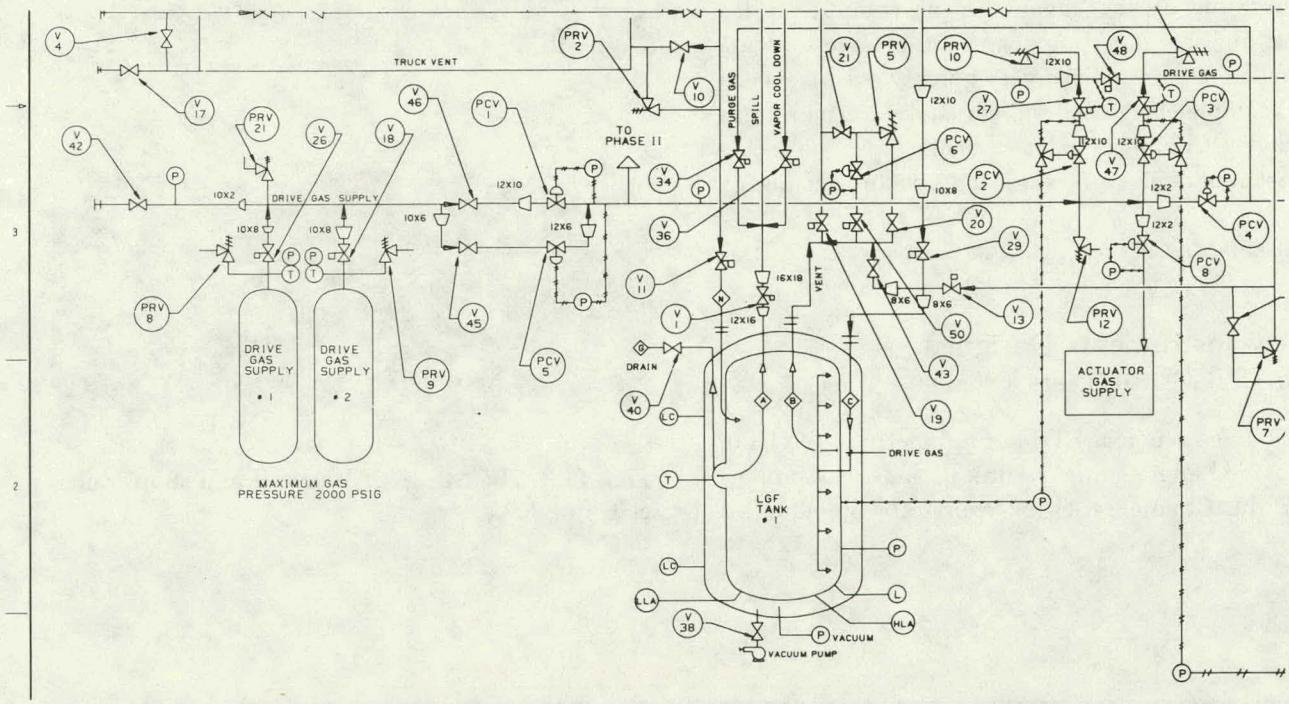

FIG. 9. A portion of the piping and instrumentation drawing done by the computer-aided design terminal.

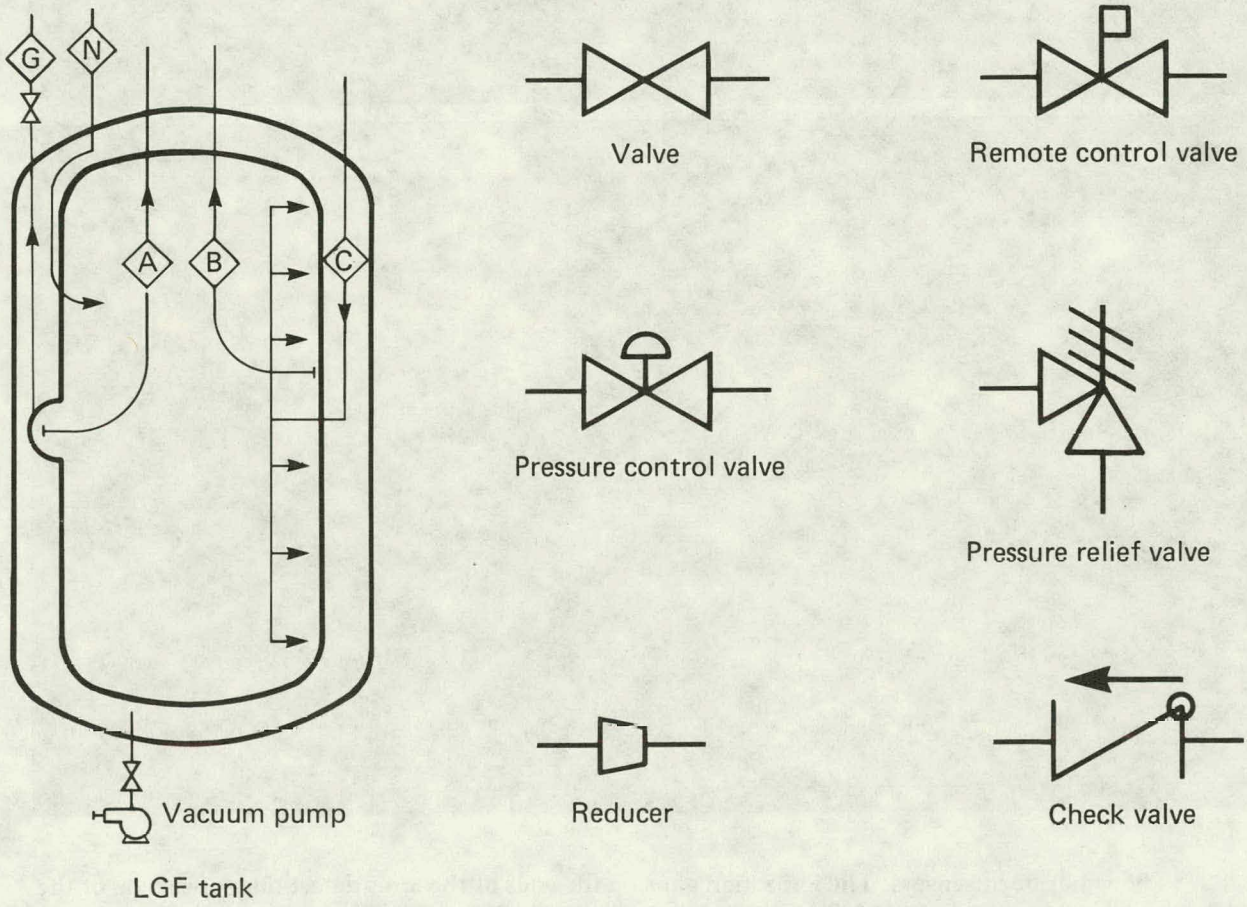

FIG. 10. The library parts that are available.

Some of the advantages of computer-aided drafting are that components on a large drawing can be erased or moved very quickly. Also, text can be completely erased or edited by certain commands. Computer-aided drafting can make the most mundane work simpler to do in drafting.

(For further information, contact M. Ochoa, Jr., Ext. 2-9273.)

New Instruments Designed for LNG Spill Tests

The Nuclear Test Engineering Division provided engineering, technical, and field support for the Coyote series of spill tests on liquefied

FIG. 11. The ME gas laboratory and shop trailer at China Lake.

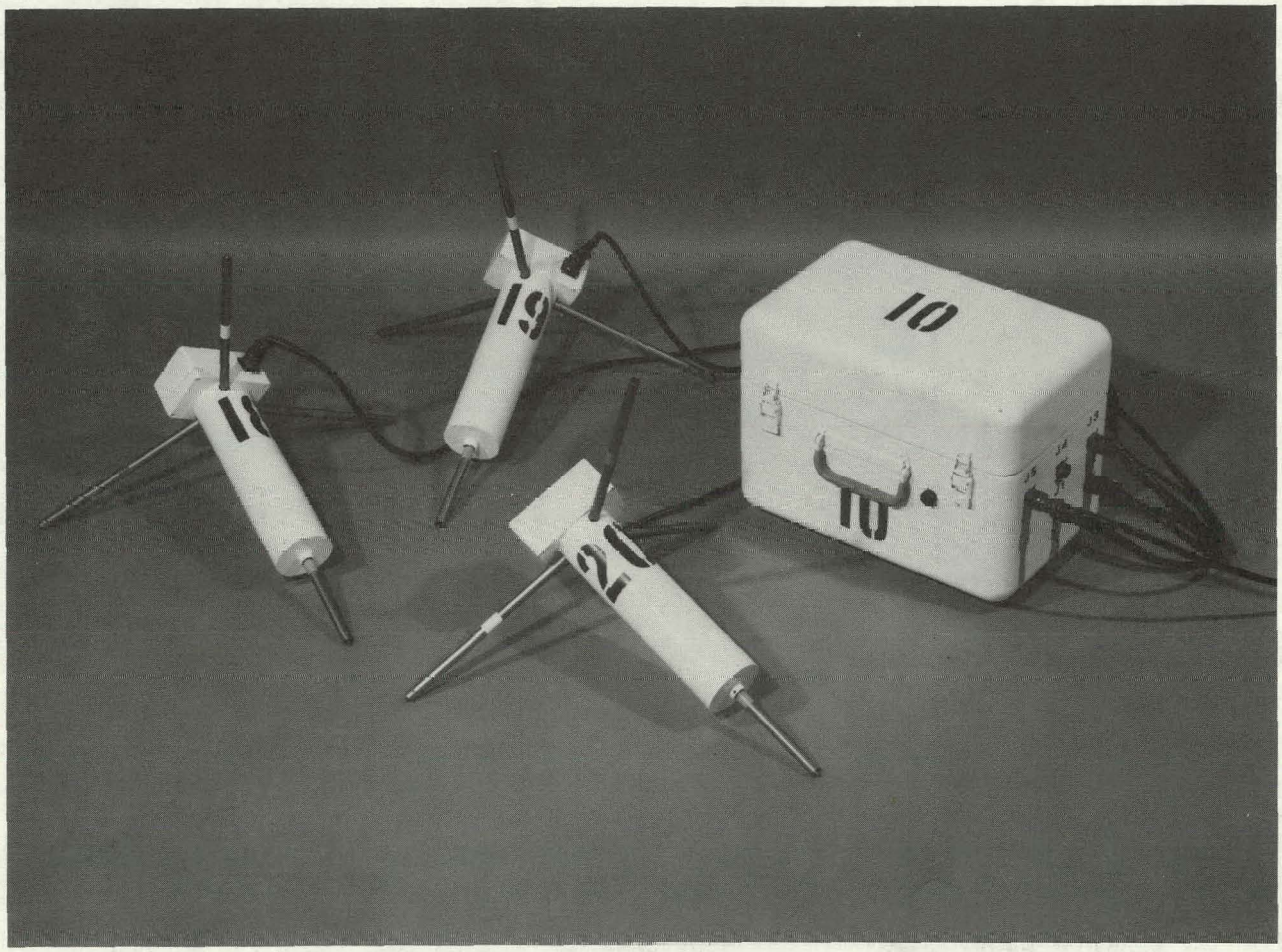

FIG. 12. The vapor burn sensors. The ionization gaps on the ends of the arms detect time-of-arrival of the flame front.

natural gas (LNG) at China Lake, CA, in the summer and fall of 1981. The entire trailer park and instrumentation array was demobilized after the 1980 tests at China Lake. The division remobilized the trailers and tower array in the spring of 1981 and started tests in June. Figure 11 shows the trailer housing the ME Gas Laboratory and Shop.

The Coyote series of LNG spill tests included dispersion and burning of vapor clouds and RPT (rapid phase transition) explosions. A new instrument designed and fabricated for cloud burns was the vapor burn sensor (VBS) (see Fig. 12). The VBS consists of four ionization gaps on variable-length arms that detect the time of arrival of the flame front. The arms were mounted on 38-foot towers.

Another new instrument built by the division was a continuous gas sampling system to measure LNG vapor boiloff from the spill pond. Probes were mounted just above the water surface, and underwater hoses were run from the probes to the existing infrared absorption sensors on shore. Gas pumps were used to force the gas through the sensor heads, and a water-warmed probe was placed in the exit nozzle of the spill pipe to continuously sample LNG as it left the pipe. The gas hose was brought to the Anarad gas analyzer on shore. A pump forced water through an enclosed channel in the probe tip to vaporize the LNG, and a gas pump forced the LNG vapor through the gas analyzer. This group of instruments was used to dynamically measure the major constituents of LNG to try to relate the changing composition to the time of occurrence of rapid phase transitions.

(For further information, contact W.C. O'Neal, Ext. 2-8369, R.E. Blocker, Ext. 2-9207, or G.M. Bianchini, Ext. 2-6686.)

Aluminum Tower Survivability Tested in LNG Vapor Cloud Fires

Concern has been raised as to the damage that flames of approximately 2000°F could do to 38-ft-high aluminum towers during liquefied natural gas spill tests at China Lake, CA. The towers support the instrumentation for the tests.

During a vapor burn test, two metallurgical events could occur that would affect the strength of the towers. First, pure aluminum melts at 1220°F. Second, the alloying elements in heat-treatable aluminum will go into solution when metal temperatures are between 650 and 1100°F, with a resultant reduction in strength. The amount of loss depends on the metal temperature reached and exposure time at that temperature.

Because of many constraints, it was necessary to devise a plan to make a passive temperature measurement of the tower metal and institute actions if the indicated metal temperature fell in certain ranges. Temperature-sensitive paints ranging from 100 to 1200°F in 100°F increments, were applied to the towers. Each temperature is identified by a color, and the surface finish changes from flat to glossy when the metal reaches the indicated temperature of a particular color paint. One drawback to this system is that the paint is water soluble and must be reapplied after it is subjected to rain.

After a vapor burn test is completed, the temperature-sensitive paint is visually inspected. If the maximum metal temperature is less than 600°F, the tower is certified ready for the next test. If, however, the metal temperature indication is greater than 1100°F, the tower is replaced by another tower and the original one is inspected and tested before it can be returned to service. If the metal temperature indication is between 600 and 1100°F, a pull test equivalent to one and one half times the maximum design load is applied. If the tower fails this test, it is replaced; if it passes, it is certified as serviceable.

Maximum metal temperatures observed on several vapor burn tests performed were less than 500°F. But on the initial vapor burn test, several plastic items were damaged (see Fig. 13) and the observed metal temperature was less than 300°F. These included the polyvinyl chloride jacket around the electronic cables, polypropylene propellers on the bivane anemometers, nylon screws holding the fins on the bivane anemometer, and the nylon hub on the cup anemometer.

(For further information, contact W. Wakeman, Jr., Ext. 2-1227, or G.M. Bianchini, Ext. 2-6686.)

Development of a Downhole Dry Ice Cooling System

In testing nuclear weapons, it is sometimes necessary to provide extreme thermal environments that are dictated by the particular weapon's stockpile-to-target sequence (STS). Currently and in the past, low temperature environments have

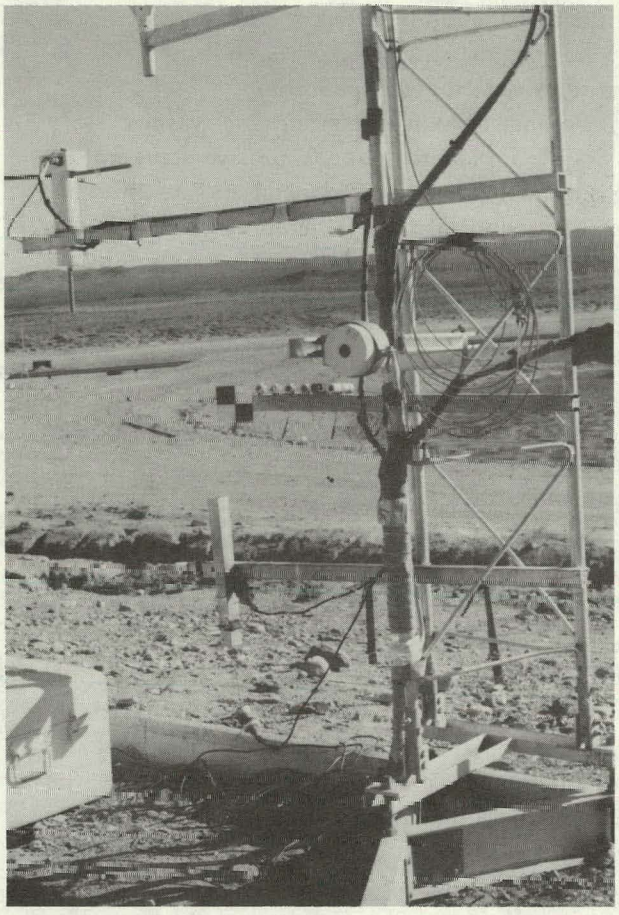

FIG. 13. A view of a portion of the tower after the first test.

been produced using conventional vapor compression mechanical refrigeration systems. As the required temperature approaches –50°C, mechanical systems must be staged. This staging, or cascading, results in mechanical complexity and the necessity of dissipating the energy rejected from multiple compressors.

The Nuclear Test Engineering Division is currently involved in the development of cooling systems using dry ice. The low temperature and high heat of sublimation of dry ice and the mechanical simplicity of such a system provide an attractive alternate means of producing low temperature environments for nuclear device testing.

We have performed limited testing of two types of dry ice cooling systems: one in which CO_2 gas is circulated around a container of dry ice, and another in which the gas flow is directed through the ice container.

The first system to be built and tested is shown schematically in Fig. 14; a cross section of the ice container is shown in Fig. 15. The design requirements were to maintain the device at –54°C in an environment at 27°C for 1000 h. Excess CO_2 gas was to be vented to the surface through 1-in.-diam tubing and a series of solenoid or vacuum-operated valves. The ice container and device box were welded of one-eighth-in. aluminum and insulated with multiple layers of styrofoam. The connecting ductwork was fabricated from 4-in. aluminum tubing insulated with molded polyurethane foam insulation. Two muffin-type fans were used to circulate the CO_2 gas. The ice container was suspended from a static test fixture using a single double-bridge load cell, and a floor jack was used to stabilize the container during loading and inspection operations. Slip joints in the ductwork prevented any load from being carried by the device box. Figure 16 shows the system in the test configuration. The unavailability of molded urethane duct insulation required the ducts to be insulated with fiberglass. This modification led to a predicted test lifetime of 700 h.

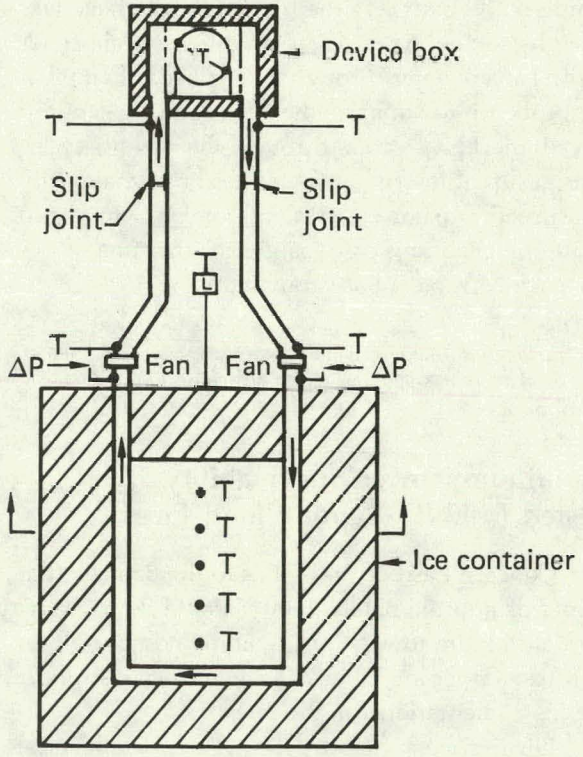

FIG. 14. Schematic drawing of the cooling system and test instrumentation: T = temperature-recording points; P = pressure differential; and L = load cell.

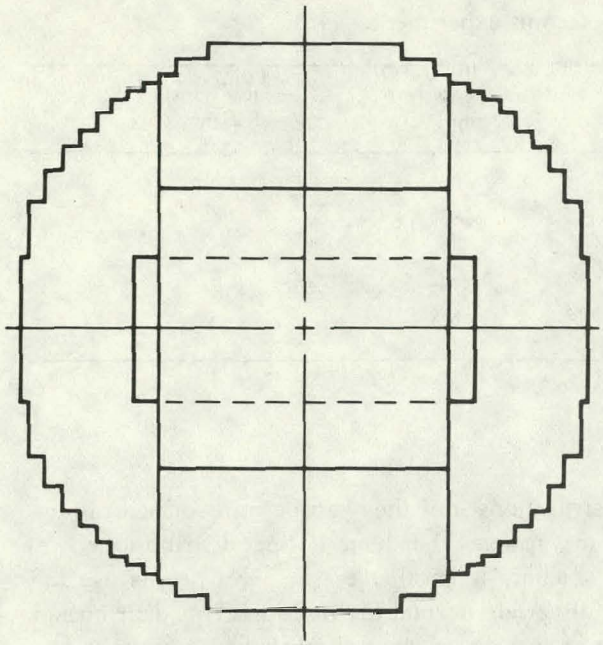

FIG. 15. A cross section of the ice container.

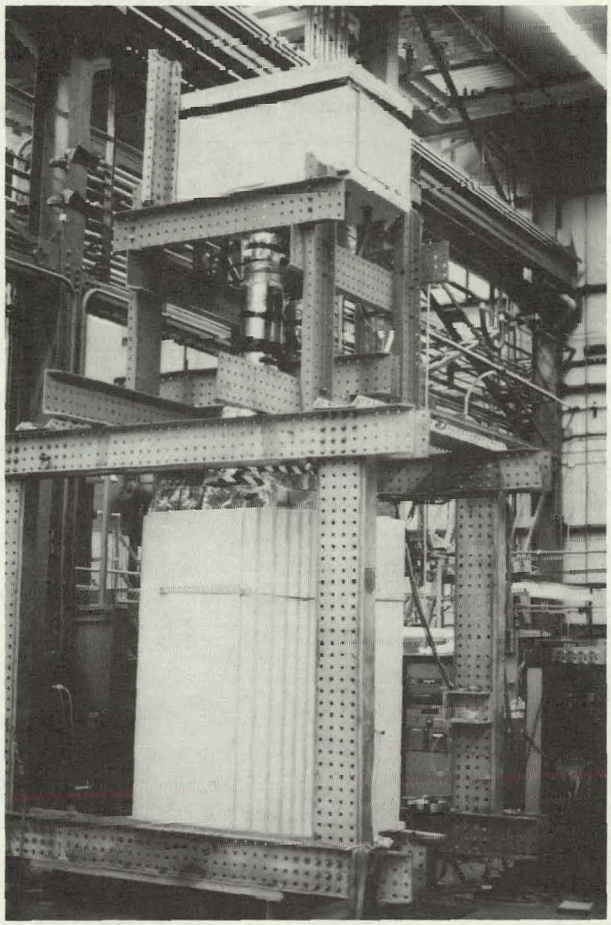

FIG. 16. The cooling system in the test stand.

The ice container was loaded with approximately 2800 lb of dry ice and the test was begun. The device temperature reached its desired level at about 68 h. After running the test for 114 h, operations were halted and the front door of the ice container was removed to examine the condition of the dry ice.

After the first 24-h transient, a linear least-squares fit to the data revealed a steady-state ice usage rate of 7.2 lb per hour.

After the inspection, the door was replaced and an attempt was made to continue the experiment. Unfortunately, use of the floor jack during the inspection was responsible for opening one of the slip joints, creating an open circuit for the cold gas and terminating the experiment.

The steady-state dry ice usage rate would have led to an operating time of only about 350 h, rather than the predicted 700 h. The unevenness of the welded ice container walls prevented tight insulation, particularly at major joints. This excessive usage can be entirely attributed to small gaps at these joints. Analysis of the data revealed that this system had an average heat-transfer effectiveness of only about 34%.

A second system was designed to attempt to overcome some of the difficulties encountered in the first. The ductwork and device box were replaced with a short, heated test loop and the ice container was modified to allow flow through crushed dry ice rather than around the ice container. Three load cells under the container were used to measure the ice weight. The heater could supply up to 400 W, a heat load about 60% larger than that anticipated by the largest device under consideration for cooling.

A series of tests were performed on the second system to evaluate its performance. Table 1 summarizes the results of these tests.

It is apparent that the system in which the gas flow is directed through the ice is considerably more effective and has the capability of maintaining even a very large device at the required temperature.

We are currently planning additional experiments aimed primarily at reducing the heat load on the ice container through the use of better insulation. Extended time testing, system control, and gas

TABLE 1. Results of the second experiment.

Test No.	Fans	Heater	Ice usage rate (lb/h)	Average loop temp (°C)	Heat transfer efficiency (%)
1	Off	Off	4.42	NA	NA
2	On	Off	5.72	-76	48
3	On	200 W	7.41	-74	70
4	On	400 W	10.02	-69	68
5	Off	Off	2.01	NA	NA

vent simulation will be part of the new test procedure.

Creating low temperature environments for nuclear testing appears to be readily feasible using dry ice cooling systems.

(For further information, contact R.W. Martin, Ext. 2-1263.)

What Does Portfolio Analysis Have in Common with Reliability Engineering for Nuclear Systems?

Both use the multivariate normal distribution to model random processes, and both use opinions to estimate parameters of the distribution. The parameter estimators for the distribution help reliability engineering and portfolio analysis. We derived the parameter estimators at LLNL.

Why do people use the multivariate normal distribution to model random processes in portfolio analysis and in reliability engineering for nuclear systems? The normal distribution is the multivariate analog of the familiar bell-shaped probability distribution function. Portfolio analysts assume returns on investments have the multivariate normal distribution because of the random walk theory of stock price fluctuation. The random walk theory says the probability distribution of a stock price tomorrow, given today's price, is the same as the probability distribution given the whole history of stock prices, including today's. Reliability engineers assume strengths of components have the multivariate normal distribution because the strength histograms from test data fit the familiar bell-shaped curves. (Sometimes component strengths are assumed to have lognormal distributions, but they can be transformed to random variables that have normal distributions.)

There is another reason why people use the multivariate normal distribution. This distribution represents dependence of returns on investments or of component strengths with one parameter, correlation. We have found that, if strengths are normally distributed, reliability is twice as sensitive to correlation as to variance. If strengths are lognormally distributed, reliability is infinitely sensitive to correlation in the neighborhood of zero correlation. So correlation is important to reliability analyses and to investment decisions too.

We use subjective percentiles as data and least squares as the method to estimate means and standard deviations of distributions from opinions.[10] A subjective percentile is an opinion of the value of strength at which a specified percent of components fail. We ask experts their opinions of several percentiles. We then find the mean and standard deviation that minimize the sum of squared errors between the subjective percentiles and the cumulative normal distribution function (Fig. 17).

Subjective percentiles are convenient for several reasons. We can test whether the assumption of a normal distribution is valid. We can ask opinions about low percentiles to determine information about weak components. Most experience is in the neighborhood of low percentiles because few strong components fail, so experts have opinions about low percentiles even if they don't have opinions about means and standard deviations.

Until now, there was no way to obtain correlation estimates from subjective percentiles. We have recently developed two ways. They differ in the types of questions asked the experts. Both use least

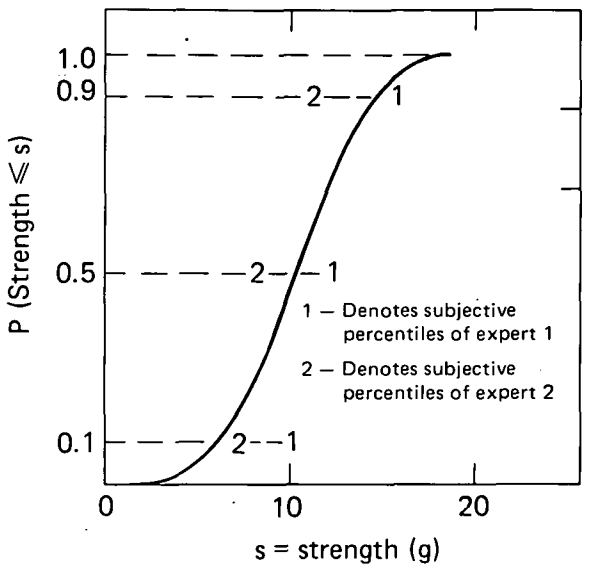

FIG. 17. Strength at failure distribution of miscellaneous small valves in terms of acceleration due to gravity.

squares to estimate means, standard deviations, and correlations.

The first way is to ask an expert for subjective percentiles of the strength conditional on the knowledge another component has failed at a specified strength. This can be repeated for several specified strengths. If the conditional and unconditional percentiles differ, the expert is telling us the component strengths are dependent (see Fig. 18).

The other way is to ask the expert: What is the joint probability of simultaneously having the strengths of two components less than two of his previously specified percentiles,

P(Strength 1 ⩽ percentile 1 and Strength 2 ⩽ percentile 2)?

If the expert says this probability is not the product of the two percents ÷ 10 000, he is saying the strengths are dependent (Fig. 19 shows the extremes of no correlation and perfect correlation).

Sometimes experts ask what is a conditional percentile or what is a joint probability. All probabilities are probabilities of events, and conditional percentiles are probability statements. Usually, careful definition of events helps experts give subjective percentiles or probabilities regardless of the events as long as they can quantify their experience with the events in terms of probabilities. Experience with common mode failures and dependent events is growing, so we hope to find a few experts who can answer our questions about conditional and joint events.

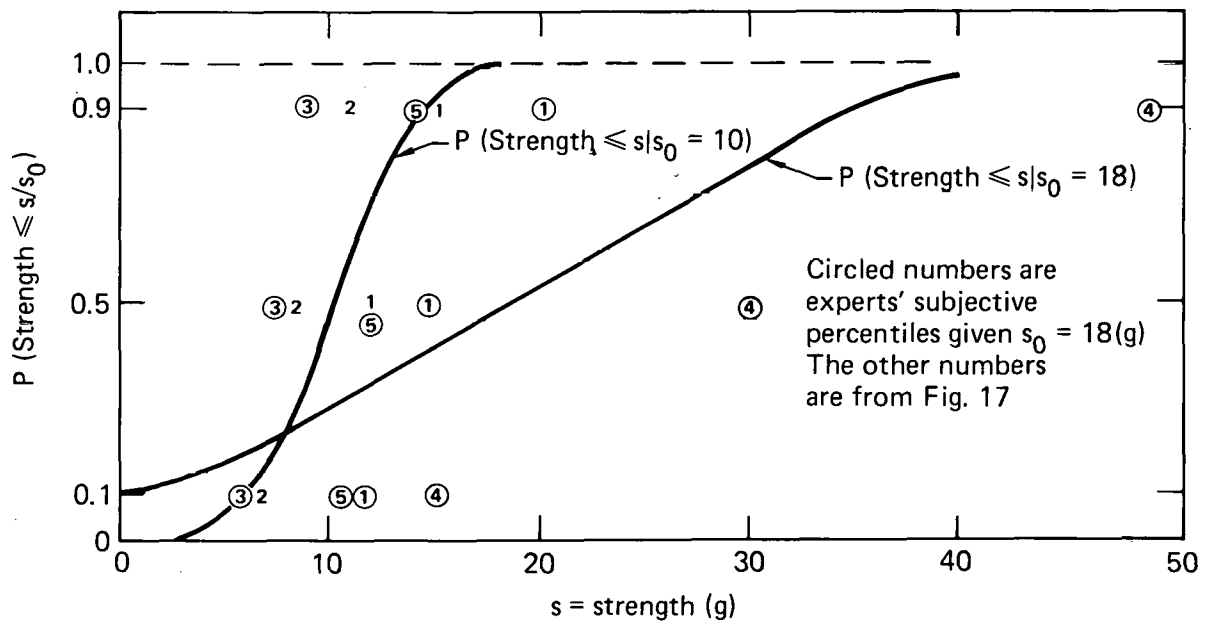

FIG. 18. Conditional strength at failure distributions of miscellaneous small valves given another small valve failed at strength s_0.

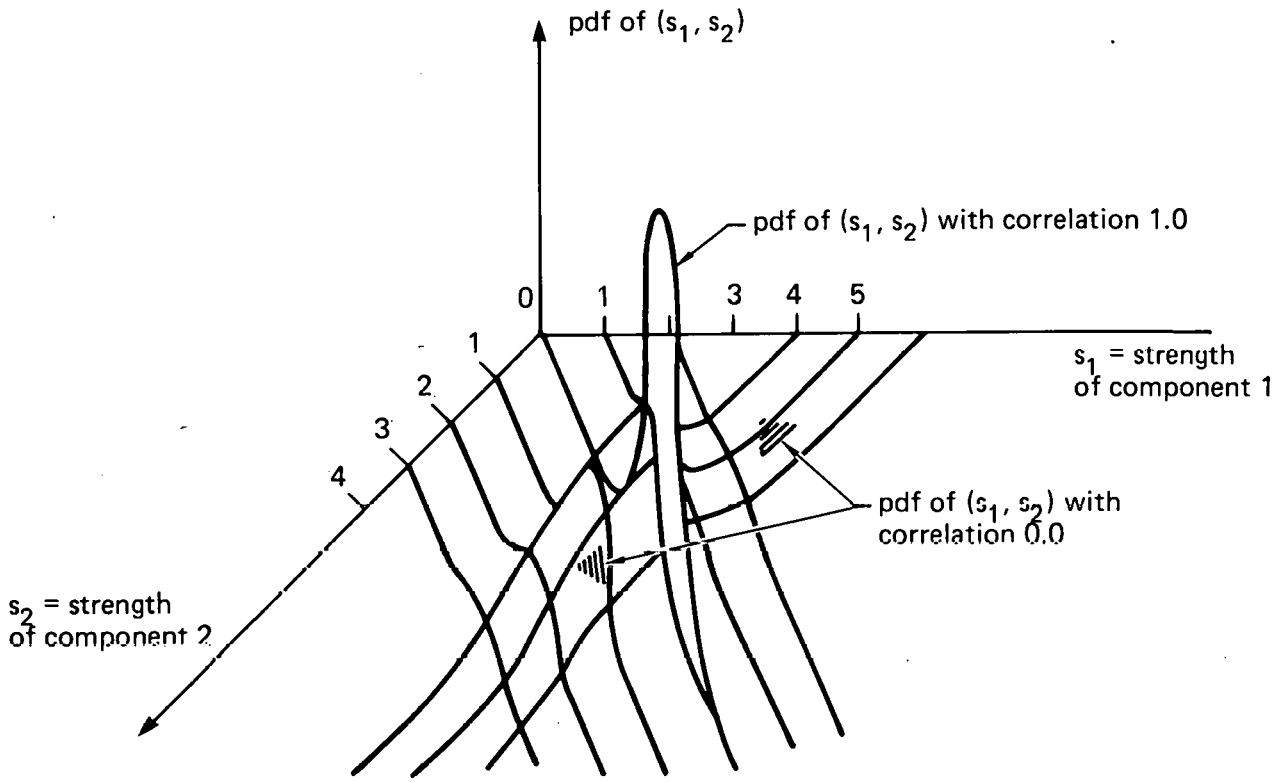

FIG. 19. Correlated and uncorrelated bivariate normal probability density functions of two strengths.

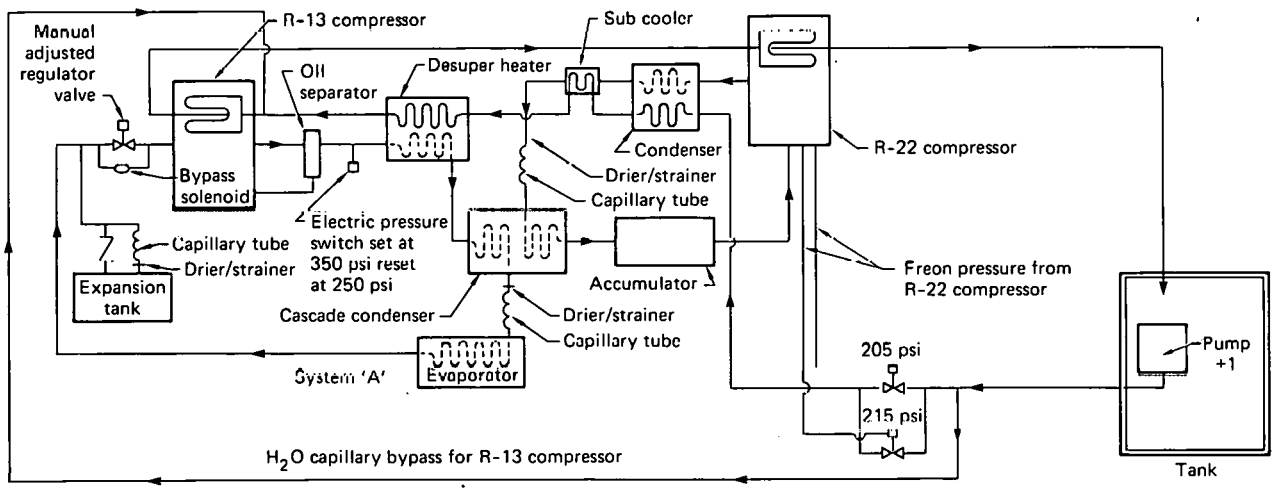

FIG. 20. Schematic of the cascade cooling system for the Islay Event.

The answers are important because the U.S. Nuclear Regulatory Commission and the utility industry must assure the reliability of nuclear systems. If reliability can be assured, cheap power will be available and utility returns on investment will rise. That is another thing portfolio analysis has in common with reliability engineering for nuclear systems.

(For further information, contact L.L. George, Ext. 2-9590.)

Downhole Mechanical Cooling System Tested on Islay Event

A new requirement specifying a device temperature of −65° ±5° was applied for the Islay Event, which was undertaken in late August 1981. With the device at −70°F, the performance was as predicted. The diagnostic measurements and containment were satsifactory.

A mechanical "cascade" refrigeration system was used for the Islay Event (see Fig. 20). A cascade system is two refrigeration units, usually with different freon refrigerant charges. One unit is used to cool the refrigerant in the other unit which cools the cold box. The Islay refrigerator was a commercial type of freezer modified to fit the shot conditions. The principal modification was to add water cooling to the motor/compressors and to provide water for a heat sink in the device canister.

An extensive test program was carried out on the refrigeration system to prove its feasibility for use downhole. The testing involved the Nuclear Test Engineering and Weapons Engineering divisions and Plant Engineering.

(For further information, contact R.P. Stock, Ext. 2-8932.)

Nuclear Reactor Containment Response Due to Postulated Loss-of-Coolant Accidents

As part of the Systematic Evaluation Program (SEP), 10 of the oldest nuclear power plants in the U.S. are being reanalyzed by using the latest computer codes (RELAP4/mod 7) to document deviations from current safety criteria.

The analysis involves determining the transient pressure and temperature response of the containment atmosphere from various postulated reactor loss-of-coolant accidents. The loss-of-coolant accidents include rupture of a main coolant pump suction line and also a main steam line. Using the computer code RELAP4/mod 7, calculations are undertaken to determine mass and energy release to the containment. The containment pressure and temperature response are in turn calculated using the CONTEMPT-LT/028 computer code with mass and energy release data as input.

Results of analyses completed for five plants showed containment pressure design conditions were exceeded for two plants. The methodology for performing the calculations is presented here.

The containment structure encloses the reactor, the steam generators, and associated pumps and coolant piping, and is the final barrier against the release of radioactive fission products in the event of an accident (see Fig. 21). The containment structure must be capable of withstanding the pressure and temperature conditions resulting from postulated primary coolant line and steam-line break accidents.

Pressurized water reactors (PWR) use a dry cylindrical reinforced concrete-type containment. The safety systems provided to reduce containment pressure and temperature during an accidental pipe break discharge of water and steam usually include the containment air recirculation system, containment water spray system, and safety water injection systems. The safety injection system consists of pressurized water tanks, high pressure pumps, and low pressure pumps. Often it is postulated that a loss of off-site power and failure of one diesel generator occurs and therefore safety injection is degraded by loss of a high pressure pump and a low pressure pump, and containment heat removal is degraded by loss of one containment spray pump and one fan cooler.

For PWR plants, the types of high-energy line breaks that must be analyzed include primary and secondary system breaks. A break on the primary side generally results in the most severe pressure response in the containment, whereas a break on the secondary side results in the most severe temperature conditions in the containment.

Two separate calculations are required for the containment analysis for a postulated pipe break. The first includes the mass and energy release which, for primary system pipe breaks (LOCAs), includes blowdown, reflood, and post-reflood phases. The results are mass and energy release rates into the containment. The second calculation is the containment response analysis, which results in the containment temperature and pressure response to the mass and energy release from the postulated break.

Primary System Breaks

The initial mass of water in the reactor coolant system is based on the system volume calculated for the temperature and pressure conditions existing at 102% of full power.

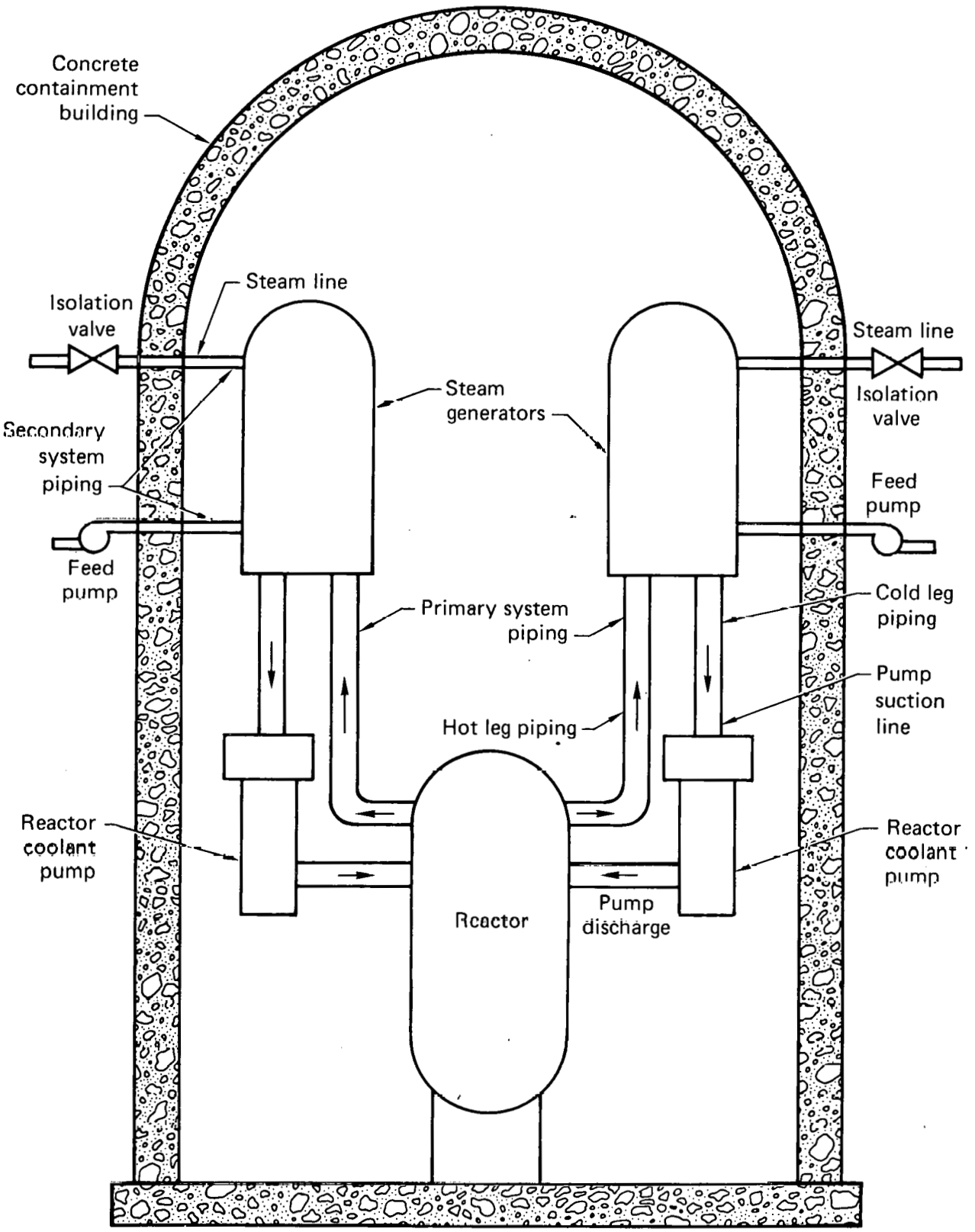

FIG. 21. Pressurized water reactor containment with two-loop PWR primary coolant system.

For the containment peak pressure analysis, a double-ended guillotine break at the reactor coolant pump suction line is postulated.

Following a postulated break in the pump suction line, steam and water are released into the containment. Initially, the water in the reactor coolant system is subcooled at a high pressure. When the break occurs, a portion of the water flashes to steam at the low pressure in the containment. Break flow rates are calculated with the Moody critical flow model for saturated flow and the Henry-Fauske model for subcooled flow.

When loss of off-site power occurs, the reactor is shut down. The recirculation pumps trip off, and the steam generators are isolated at the time of the break. The end of blowdown is defined as the time when the reactor pressure drops below the containment pressure. Natural convection heat transfer was used for the secondary coolant in the steam generator for tube surfaces immersed in water.

The mass and energy release rates are calculated with the code RELAP4-mod7. Figure 22 shows a typical computer model for a blowdown calculation.

Following blowdown, the reactor core refills with water from the safety injection system. This phase is conservatively omitted and reflood is assumed to begin immediately after blowdown. Initial conditions for the start of the reflood phase are based on the end-of-blowdown results. At the start of reflood, the water remaining in the reactor vessel is assumed to be saturated at the containment pressure and at the level of the bottom of the active core.

At the end of blowdown, the core power level drops to approximately 6% of the initial power. The reactor coolant pumps coast down and the rotors lock.

Safety injection (SI) water enters the reactor downcomer. As the downcomer fills, a driving head across the vessel forces water into the core. The SI water entering the core is converted to steam, which entrains water into the hot legs at a high velocity. Water continues to enter the core and releases the stored energy of the fuel and cladding as the water level in the core rises. The core is assumed to be quenched when the liquid level is 2 ft from the top of the core.

The heat transfer from the secondary coolant to the steam generator tubes is based on natural convection heat transfer for tube surfaces immersed in water. For tubes not immersed in water, condensing heat transfer is assumed. Steam leaving

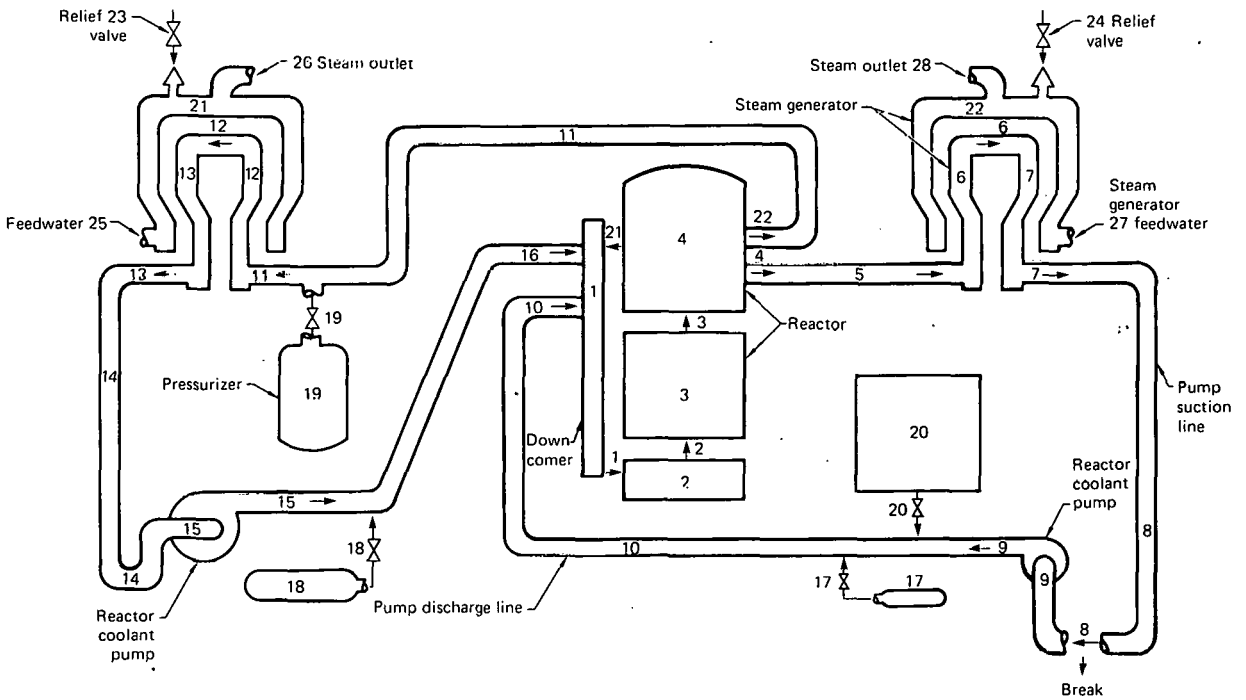

FIG. 22. Schematic of RELAP4 code model for a pressurized water reactor.

the steam generators is conservatively assumed to be superheated to the temperature of the secondary coolant.

In the post-reflood phase, all remaining stored energy in the primary and secondary systems (and accounting for decay heat) is removed. This is done by conservatively assuming that all the energy in the secondary system and primary heat structures is released in 1 h after the end of reflood. The decay heat released over the 1-h duration was based on the ANS standard decay heat curve plus 20%.

The containment pressure and temperature response were calculated by assuming that the blowdown, reflood, and post-reflood energy is released directly to the containment.

The containment response was calculated by using the CONTEMPT-LT/028 computer code. The program uses a three-region containment model consisting of the containment atmosphere (vapor region), the sump (liquid region), and the water in the reactor vessel. Mass and energy are transferred between the liquid and vapor regions by boiling, condensation, or liquid dropout. Each region is homogeneous, but a temperature difference can exist between regions.

The containment spray systems and containment structures are available for heat transfer energy removal. The Tagami and Uchida heat transfer correlations were used for all structural heat sinks, the Tagami until the end of blowdown and thereafter the Uchida. A typical containment pressure response transient for a LOCA is given in Fig. 23.

Secondary System Pipe Breaks

The containment response to a secondary system pipe break is also analyzed. For PWRs, the most limiting break is in a main steam line with pure steam blowdown. The steam-line-break accidents are analyzed for various plant conditions from hot standby to 102% of full power.

The postulated accidents analyzed were a double-ended guillotine break in a main steam line at 102% of full power and the same break at hot standby. In both of these cases, the mass and energy release rates were calculated assuming that off-site power was available. Single active failures considered for the 102% of full power case, and the hot standby case include the main steam isolation valve and the main feed isolation valve failure and loss of one train of containment heat removal systems.

The blowdown mass and energy release rates were calculated using a four-volume RELAP4 model. One volume models the primary side of the affected steam generator and the other three model the feedwater line, the secondary side of the steam generator, and the steam line. A schematic of the four-volume model is shown in Fig. 24. A description of the model follows.

Steam Generator—On the primary side of the steam generator, steady-state flow conditions at 102% of full power are conservatively assumed throughout the blowdown. On the secondary side of the steam generator, the actual plant conditions are used. An infinite bubble rise velocity was assumed on the secondary side, which precludes moisture carry-over and ensures a pure steam blowdown. Heat transfer between the primary and secondary sides in the steam generator is modeled. A forced convection heat transfer coefficient on the primary side was assumed. On the secondary side, nucleate boiling heat transfer was assumed.

Steam Line and Feedwater Line—The blowdown of the steam line and feedwater line was accounted for by a one-volume RELAP4 model for each line. The size of each volume was adjusted to account for the mass of steam or water in the line up to its respective isolation valve.

Sources of stored energy for release to the containment include the following:

- The affected steam-generator vessel tubing and water.

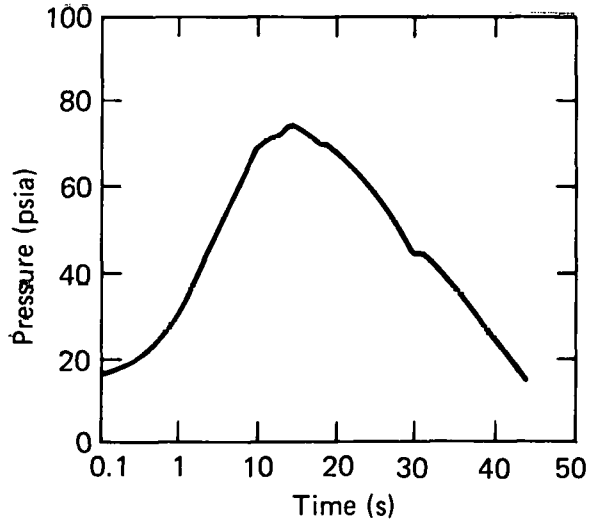

FIG. 23. Containment atmosphere pressure for a primary system break.

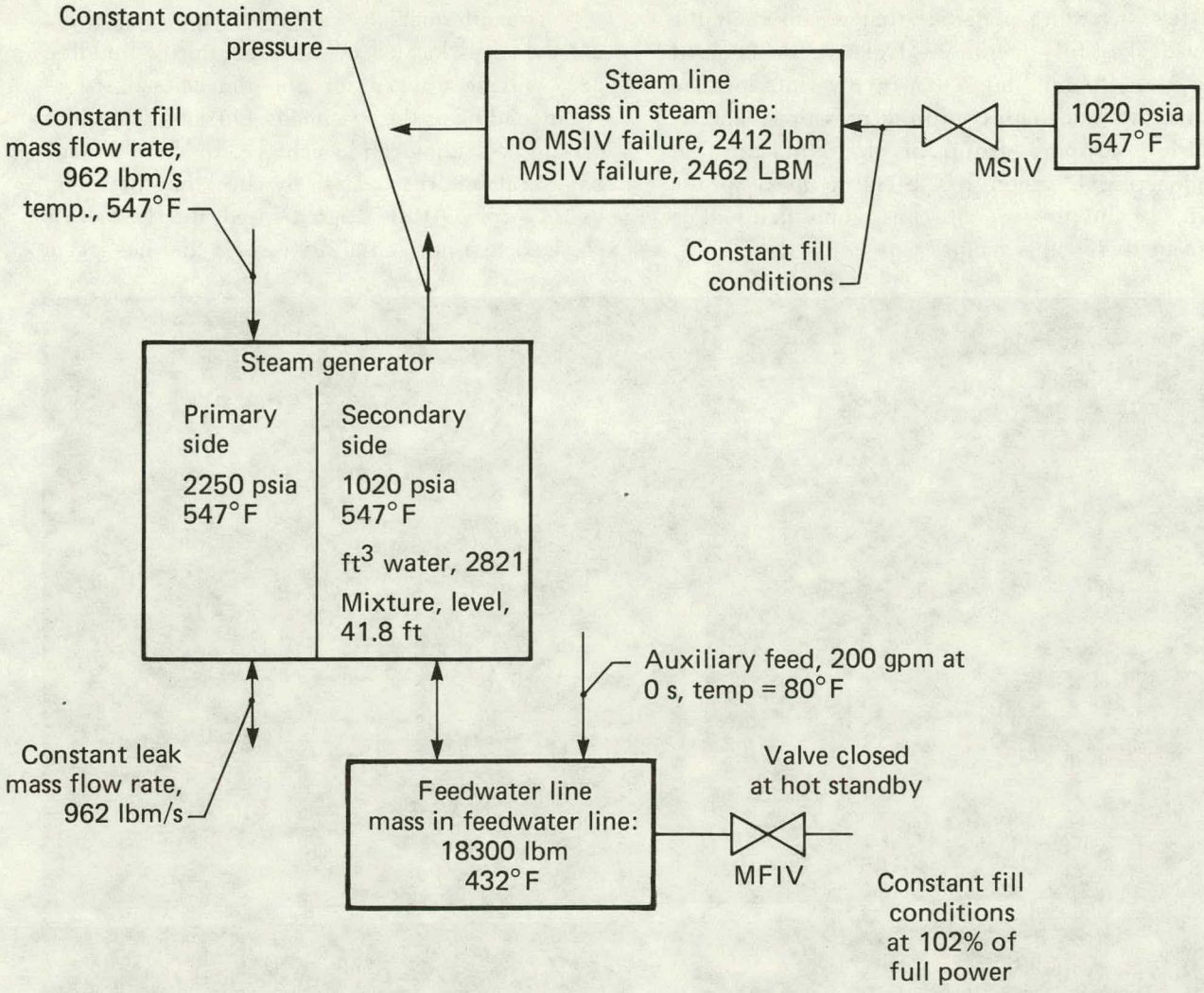

FIG. 24. Schematic of analytical model for a steam line break.

- Feedwater transferred before the isolation valves close.
- Steam transferred from the unaffected steam generators before the isolation valves close.
- Heat transfer from the primary coolant to the water in the affected steam generator.

A typical containment pressure and temperature response is given in Fig. 25.

(For further information, contact W. Stein, Ext. 2-0323, or D.G. Vreeland, Ext. 2-5775.)

Strain-Rate Apparatus Used for Dynamic Testing of NTS Containment Materials

The Earth Sciences (K) Division is involved in measuring the physical properties of coal tar epoxy

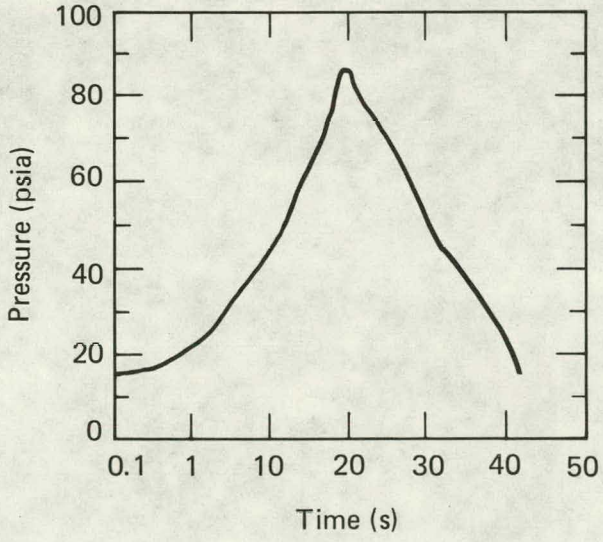

FIG. 25. Containment atmosphere pressure for a steam line break.

plastics stemming materials that are used in the Nevada Test Site operations. Data will be obtained under *in-situ* conditions that involve intermediate strain rates and high confining pressures. The K-division support group of the Nuclear Test Engineering Division has been involved in the design of the pressure vessel assembly that will be used in these experiments.

The intermediate strain-rate apparatus (Fig. 26), which is located in the Laboratory's Building 231, will be utilized for one-dimensional stress-strain loading of the specimens. Different velocities of sample loading can be achieved by coupling one of several motors to a large flywheel that rotates up to 1000 rpm. At the desired speed, the flywheel is engaged to a horizontal drive shaft that has a cam

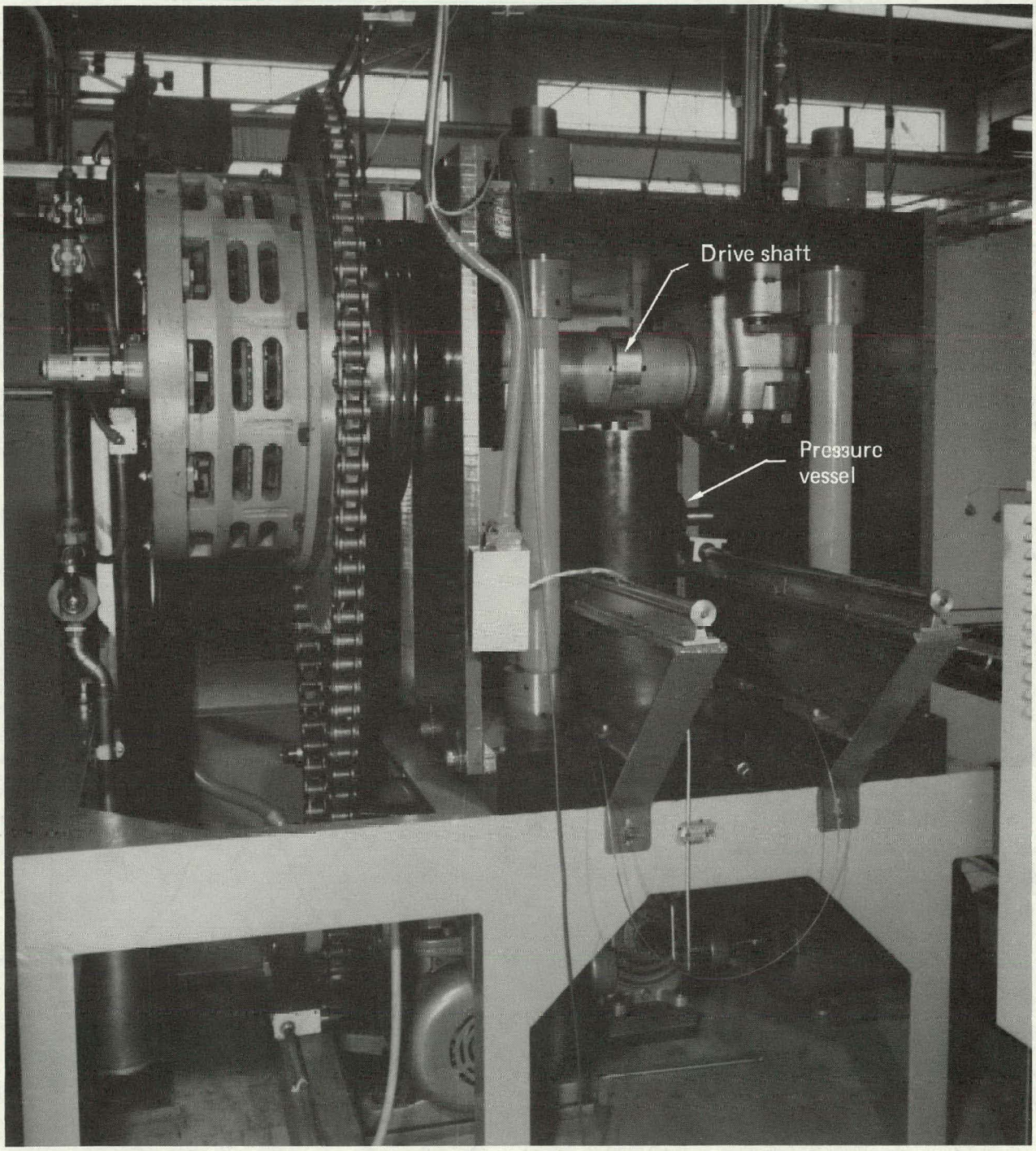

FIG. 26. Strain-rate apparatus used for dynamic testing of containment materials.

to drive a follower located on the sample loading piston. Various strain-time signatures at the specimen may be obtained by varying experimental parameters, including shaft velocity, cam design, and piston loading relative to the flywheel.

The pressure vessel assembly shown in Fig. 27 consists of an AISI-4142 steel vessel with associated hardware for dynamically loading the specimen and for obtaining specimen property measurements during an experiment. Specimens of 3/4- and 1-in. diam by 1-in. long will be loaded at rates from 10^{-2} to 10^{2} in./in./s. Specimens will be confined under 7000 psi of nitrogen at 150°F. Eddy current transducers will be used to obtain longitudinal and radial strain data. We expect to begin operations in the near future.

(For further information, contact E.W. Russell, Ext. 2-6398.)

Piping Reliability Model Developed in Load Combination Program Can Adequately Estimate Piping Failure Probability

During Phase I of the Load Combination Program, a probabilistic fracture mechanics model was developed to evaluate the reliability of nuclear power plant piping. In this model, initial crack size, crack length and depth aspect ratio, material properties, operating transient and seismic stress histories, preservice and in-service inspections, as well as leak detections, are considered as random variables. Mechanisms affecting the crack growth considered in the fracture mechanics model are fatigue and stress corrosion. Stress introduced by operating transient, seismic motion, vibration, as well as residual effect are included. Monte Carlo technique is used to simulate the crack growth through time for the various loading conditions.

This model was used to estimate the failure probability for the primary coolant loop of a pressurized water reactor (PWR) plant. [Details are given in a nine-volume report issued by LLNL for the U.S. Nuclear Regulatory Commission (NRC).[11]] As a result of this evaluation, two important licensing requirements are in the process of being modified by the NRC. They involve asymmetric blowdown loss-of-coolant accident (LOCA) in PWR plants, and the combination requirement for LOCA and a safety shutdown earthquake in the design of a nuclear power plant.

This model was also used to analyze cracking incidents in PWR feedwater lines. By the end of June 1980 there were 16 operating PWR plants reported to have detected feedwater line cracking incidents among the 35 PWR plants inspected. Within the 16 plants, LLNL obtained detailed information on 5 plants. The piping reliability model was used to analyze these five plants. The analytical results correlated with the observed cracking experiences. For example, in one plant, the actual leak occurred 11 mo after the reactor was placed in commercial operation. Our result showed a 0.90 probability of a leak at the end of the 11 months of operation. The results of the five-plant evaluation are given in Table 2.

Sensitivity studies were conducted to evaluate the potential remedial actions. The studies show

TABLE 2. Summary of observed cracks and estimated leak probability.[a]

Plant	Operating time to defect discovery (yr mo)	Max crack depth (in.)	Pipe thickness (in.)	Crack depth/thickness (in.)	Leak probability simulated to defect discovery date	
					With[b] ISI, PSI	Without ISI, PSI
A	11 mo	0.57	0.57	1.0	0.68	0.9
B	2 9 mo	0.235	0.875	0.27	0.32	0.63
C	4 3 mo	0.028	0.75	0.04	0.0022	0.074
D	9	0.75	1.21	0.62	0.08	0.29
E	10	0.107	0.843	0.13	0.55	0.92

[a]Leaking was discovered at plant A in May 1979; in March 1980, the other four plants reported having defects.

[b]ISI = in-service inspection, PSI = preservice inspection; ISI was based on ASME XI inspection program A, 1980.

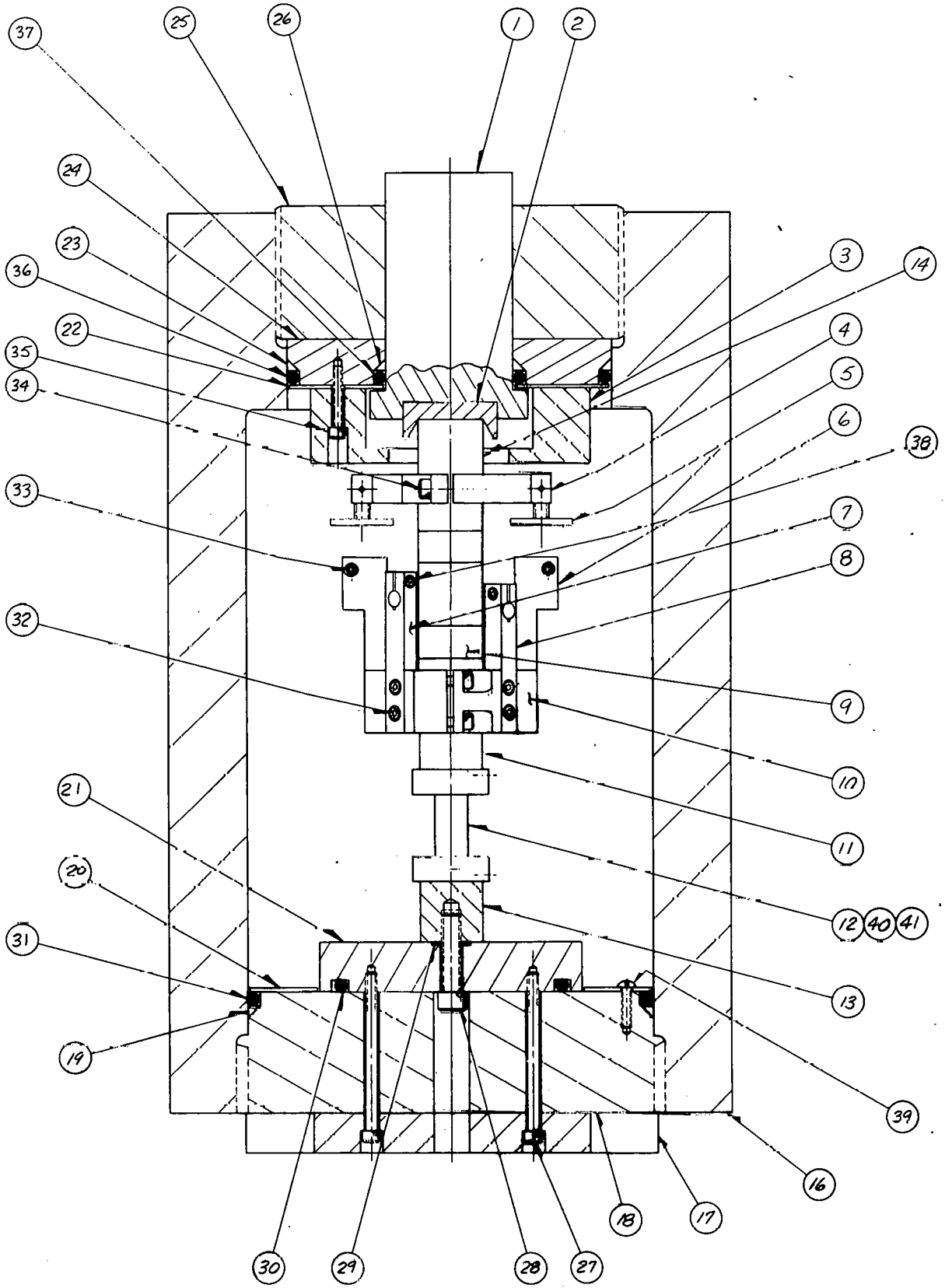

FIG. 27. Schematic of pressure vessel assembly used for dynamic property measurement of NTS containment materials.

Legend for Fig. 27.

Item	Part No.	Material/description	Req'd	Spec. No.
41	81-110647	Load cell TAB-03	1	
40	81-110647	Load cell TAB-02	1	
39		R.H.M.S. No. 8-32 unc × 375 lg. stl.	9	
38		S.H.C.S. No. 4-40 unc × 375 lg. stl.	4	
37		"O"-ring 1,948 in. i.d. × 139 wall Parker No. 2-226	1	Buna-N
36		"O"-ring 4,725 in. i.d. × 210 wall Parker No. 2-351	1	Buna-N
35		S.H.C.S. No. 8-32 unc × 1.00 stl.	3	
34		S.H.C.S. No. 8-32 unc × .750 stl.	1	
33		S.H.C.S. No. 4.40 unc × .625 stl.	2	
32		S.H.C.S. No. 8-32 unc × .625 lg. stl.	12	
31		"O"-ring 5.975 in. i.d. × .210 wall Parker No. 2-361	1	Buna-N
30		"O"-ring 3.225 in. i.d. × .210 wall Parker No. 2-339	1	Buna-N
29		"O"-ring		Buna-N
28		S.H.C.S. No. 3/8-24 unf × 1.25 in. lg. stl.	1	
27		S.H.C.S. No. 10-32 unf × 2.50 in. lg. stl.	4	
26	74-113870	Ring-piston seal TAB-02	1	
25	76-103258	Plug-top	1	
24	76-103257	Ring-chamber sealing	1	
23	74-113875	Ring-inner plug seal TAB-03	1	
22	76-103256	Retaining ring-top	1	
21	77-101830	Adapter bottom	1	
20	76-103250	Retaining ring-bottom	1	
19	74-113875	Ring-inner plug seal TAB-04	1	
18	76-100699	Plug, bottom TAB-01	1	
17	76-100698	Plate, base	1	
16	76-100695	Pressure ring sub-assy	1	
15	81-110644	Calibration sample TAB 01-06	Ref.	
14	81-110646	Spacer block TAB-02	1	
13	81-110648	Lower mount	1	
12	81-110647	Load cell TAB-01	1	
11	81-110646	Spacer block TAB-01	1	
10	81-110645	Coil fixture	1	
9	81-110643	End plug sample	2	
8	81-110642	Radial coil mount TAB-02	2	
7	81-110642	Radial coil mount TAB-01	2	
6	81-110641	Linear coil mount	2	
5	81-110640	Target	2	
4	81-110639	Target fixture	1	
3	81-110638	Catcher	1	
2	81-110637	Insert, piston	1	
1	81-110636	Piston with insert	1	

that augmented in-service inspections and improved flaw-detection methods can reduce the failure probability. The use of improved operational procedures to mitigate the thermal stratification is a positive and direct way to increase the reliability of PWR feedwater lines.

(For further information, contact C.K. Chou, Ext. 2-0315.)

References

1. D.C. Camp and W.D. Ruhter, "Determination of Actinide Process and Product Stream Concentrations Off-Line or At-Line by Energy Dispersive X-ray Fluorescence Analysis," from *Proc. 3rd ESARDA Symp. on Safeguards and Nuclear Material Management*, Karlsruhe, West Germany (May 6–8, 1981).
2. D.C. Camp and W. D. Ruhter, *On-Line Determination of Uranium and Plutonium Process and Product-Stream Concentrations by Energy Dispersive X-Ray Fluorescence Analysis*, Lawrence Livermore National Laboratory, Livermore, CA, UCRL-52883 (1979).
3. "RTNS-II: A Tool for Studying Neutron Damage," in *Energy and Technology Review*, Lawrence Livermore National Laboratory, Livermore, CA, (March 1978), p. 16.
4. B. Schumacher, Lawrence Livermore National Laboratory, private communication (June 1981).
5. Dippery and Sabersky, "Heat and Momentum Transfer in Smooth and Rough Tubes at Various Prandtl Numbers," *Intern. J. Heat and Mass Transfer* 6, 329–353 (1963).
6. T. Cebeci and A.M.O. Smith, *Analysis of Turbulent Boundary Layers* (Academic Press, New York, 1974).
7. J. Douglas and J.E. Gunn, "A General Formulation of Alternative Direction Methods," *Numerische Mathematik* 6, 428-453 (1964).
8. M.G. Hall, "A Numerical Method for Calculating Unsteady Two-Dimensional Laminar Boundary Layers," *Ingen-Arch* 38, 97-106 (1968).
9. T.G. Blottner, "Nonuniform Grid Method for Turbulent Boundary Layers," *4th Intern. Conf. Num. Methods in Fluid Dynamics*, Boulder, CO (June 1974).
10. L.L. George and R.W. Mensing, "Using Subjective Percentiles and Test Data for Estimating Fragility Functions," in *Proc. Dept. of Energy Statistical Symp* (October 1980), Berkeley, CA.
11. *Probability of Pipe Fracture in the Primary Coolant Loop of a PWR Plant*, Lawrence Livermore National Laboratory, Livermore, CA, UCID-18967 (1981); in nine volumes. Issued for the NRC as NUREG/CR-2189; in nine volumes.

NUCLEAR EXPLOSIVES ENGINEERING DIVISION

Our major mission is to support the Laboratory's Nuclear Explosives Program (NEP) in developing operational nuclear weapons systems for the U.S. Stockpile. We also support the Non-nuclear Ordnance Program, Organic Materials Division, and H (Physics) Division. We perform studies and develop hardware for Y-Program, Nuclear Regulatory Commission (NRC), Z-Division, and the Defense Nuclear Agency (DNA).

NEED's project teams are dedicated to specific engineering areas: conceptual nuclear design, strategic systems, development and production/liaison for nuclear weapons systems, advanced fission and fusion systems, hydrodiagnostics development, and maintenance and upgrade of the Site 300 test facilities. Our Applied Mechanics Group supports Laboratory programs with calculational expertise in solid mechanics and transport phenomena, and the Auxiliary Systems Group supports Laboratory programs with expertise in high-pressure gas technology.

(For further information, contact R.A. Corallo, Ext. 2-8301.)

An Experimental Procedure to Determine Fusion-Zone Penetration During Arc Welding

An experimental study is under way to measure the effects of weldpool fluid motion on displacement (penetration) of the liquid/solid interface. The weld procedure investigated is that of the gas-tungsten-arc process in which the molten flow under the arc is driven by the associated electromagnetic field. The apparatus consists of a high-melting point hemispherical nickel shell (anode) filled with a low-melting-point test material. The convex shell underside is impingement-cooled by an array of gas jets sharing a common plenum. The cathode is centered above the surface of the test material. Variations around the shell in heat flux and temperature are sensed by appropriate instrumentation.

Before conducting experiments with the arc, a series of steady-state experiments was performed to verify that the apparatus was functioning properly.

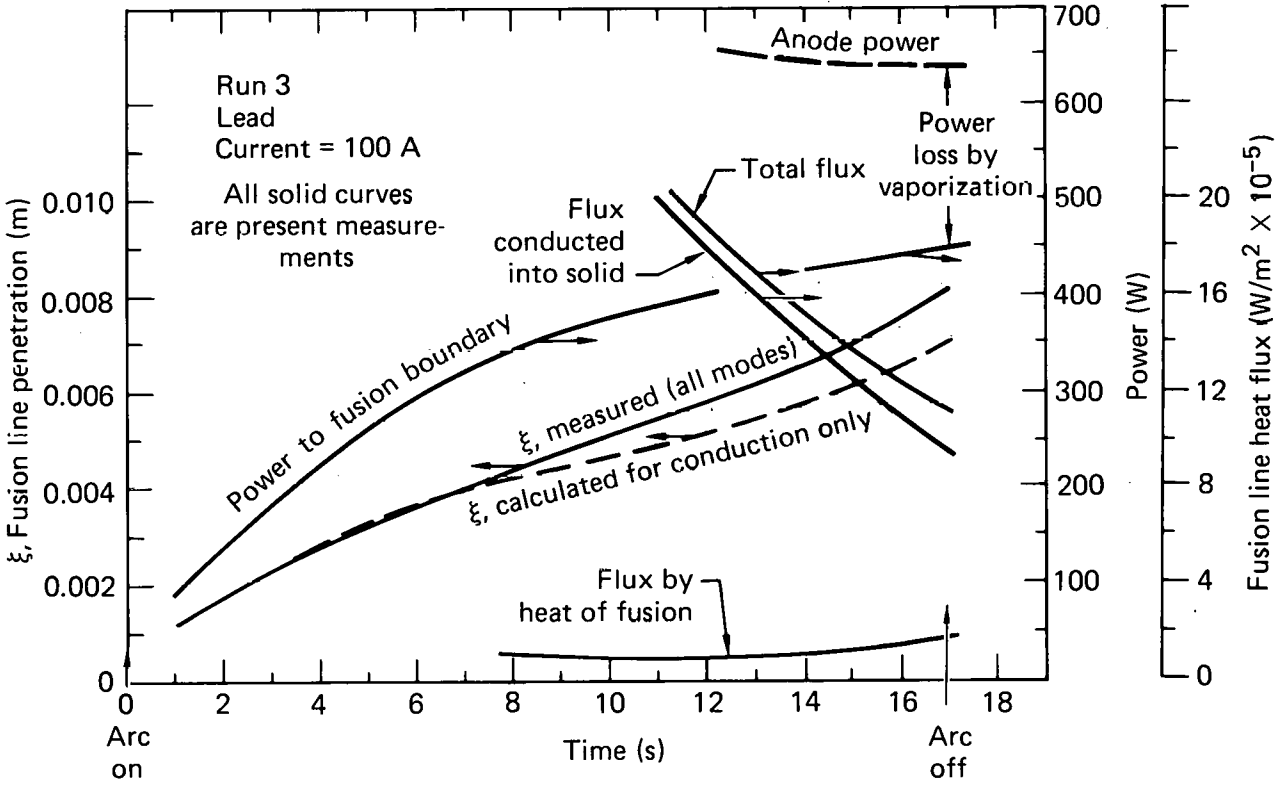

FIG. 1. Measured fusion boundary characteristics.

A soldering iron with its power monitored was substituted for the arc and contacted a very low melting point (75°C) bismuth alloy used for the test material. Gas cooling was adjusted to establish a given steady-state fusion zone radius ξ. Because no molten metal fluid motion exists for this case, the value for ξ can also be calculated by heat conduction laws. Measured and calculated values of ξ compared favorably over a range of heating (and cooling) rates.

Transient experiments with the arc, using lead as the test material, have been performed. In these tests, there is no cooling of the shell, and the arc is maintained at a constant power level as the weldpool grows. Measured shell temperature histories were used to determine the penetration of the fusion boundary ξ and the heat flux at the fusion boundary (see Fig. 1). For the case shown in Fig. 1, weldpool motion increases the penetration by about 16% over that of pure conduction. Note also the power losses by vaporization in comparing anode power[1] to fusion boundary power.

(For further information, contact C.S. Landram, Ext. 2-8569.)

References

1. R.L. Apps and D.R. Milner, "Heat Flow in Argon-Arc Welding," *Brit. Weld. J.* 2, October 1955, p. 475.

WEAPONS ENGINEERING DIVISION

The Weapons Engineering Division (WED) is responsible for engineering activities supporting nuclear weapons development, production, and maintenance of an important portion of the national stockpile. In providing these services, the Division keeps abreast of new developments in safety, and weapon control.

The activities include new weapon development, environmental testing, weapon control, initiation of systems development, engineering technology, and special materials procurement. Production work involves communicating product definition and design intent to the DOE contractors responsible for component fabrication and assembly. In addition, active monitoring of the stockpile requires a careful effort in disassembly surveillance of stockpile weapons to ensure that design requirements have indeed been met and to monitor physical changes that may eventually limit the useful life of a weapon.

The Special Materials (SM) office in WED purchases goods and services from the DOE contractors, military commands, and other governmental agencies for all LLNL programs. This office is also responsible for coordinating Laboratory guidance on weapon development activities by the DOE contractors, purchasing special isotopes used in a variety of programs, and providing the DOE with a forecast and management plan on nuclear material usage.

Because of classification restrictions, none of the numerous significant and important activities of the Weapons Engineering Division for the period covered by this issue of the Technical Review are being reported.

(For further information, contact R.E. Clough, Ext. 2-8296.)

ENERGY SYSTEMS ENGINEERING DIVISION

This division is engaged in a variety of work to provide mechanical engineering support to the Laser (Y) Program in two major categories: Laser Isotope Separation (LIS) and Inertial Confinement Fusion (ICF). In the LIS program, coherent laser light is used to selectively photoionize atoms of a given isotope in a material containing several isotopes. The ionized atoms can then be separated and enriched using extractor/collectors. The ICF effort is directed at understanding the basic physics problems associated with imploding small fusion targets with high power lasers, and at developing a fusion process to provide an unlimited source of power for use during the next century. Each major category has both military and civilian applications.

In this issue we document six studies from the numerous projects under way:

- We extended the lifetime of XeCl laser amplifiers by eliminating deposition of a reflective coating on the internal surface of the amplifier windows during operation.
- Development is proceeding on a very high temperature gas heater using positive-displacement compression at high pressure ratio. This heater will produce clean inert gas at a uniformly hot temperature for our LIS program.
- A plasma shutter to prevent light from entering the Nova laser chain from the wrong direction has been successfully tested. The shutter replaces previously considered large-aperture Faraday isolators, resulting in a cost savings of about 80%.
- One intriguing concept under construction is the two-beam Novette laser system. Each beam line is the same as will be used on Nova and includes frequency conversion from 1.05-to-0.53-μm wavelength light through the use of potassium dihydrogen phosphate (KDP) crystals.
- The KDP crystals must be manufactured with tight mechanical tolerances (± 1 μm) and precise orientation of the crystalline axis (± 30 μrad). Technology has been developed to successfully manufacture these crystals for Novette and Nova.
- All high energy optical components in a laser chain must be assembled with meticulous care for cleanliness. Particles of dust degrade performance and act as localized hot spots that damage optical components. Our class-100 clean room used for assembly is described.

(For further information, contact J.E. Keller, Jr., or J.R. Hauber, both at Ext. 2-7582.)

Procedure Developed to Preserve Window Transmission for Closed-Cycle Flow, Rare-Gas Halide Lasers

In the continuing work being done on high average power, closed-cycle flow, rare-gas halide (RGH) lasers in the Laser Isotope Separation Program at LLNL,[1] one of the main goals is to develop an XeCl (xenon chloride) laser amplifier capable of operating for hundreds of hours at high (100+ W), average power output.

In working toward the goal of a long lifetime, some factors to be considered are: corrosion resistance to the halogen gas, HCl, (in the 95% He, 4.9% Xe, 0.1% HCl gas mixture) by the materials in the electrode discharge region, system cleanliness in terms of hydrocarbon and water contamination, electronics components lifetimes, and transmission through the optical windows for laser output.

It became obvious very early in our efforts on the Closed-Cycle Test Bed (CCTB) laser[2] that one major problem was the formation of a metallic-appearing, very reflective coating on the internal surface of the windows (Fig. 1) in the laser beam pattern. This coating became a dominant factor hindering our effort to achieve long lifetime.

The problem is compounded by the fact that not only do the windows have to be made of high purity fused silica to transmit the ultraviolet (308 nm) laser light, but they are also used as the output couplers for the laser cavity. The windows are the laser gas barrier interface to the atmosphere, and therefore do not lend themselves to being changed during a laser run. The intense ultraviolet radiation, 100 to 500 mJ/shot at 1 to 3 kHz (hundreds of W/cm^2), on the inner surfaces of the windows appears to produce a photochemical reaction with the gas, resulting in the previously mentioned coating and a rapid degradation of laser output.

Experimental analysis has shown that this coating occurs only when HCl is present near the window. Further analysis of the coating by x-ray

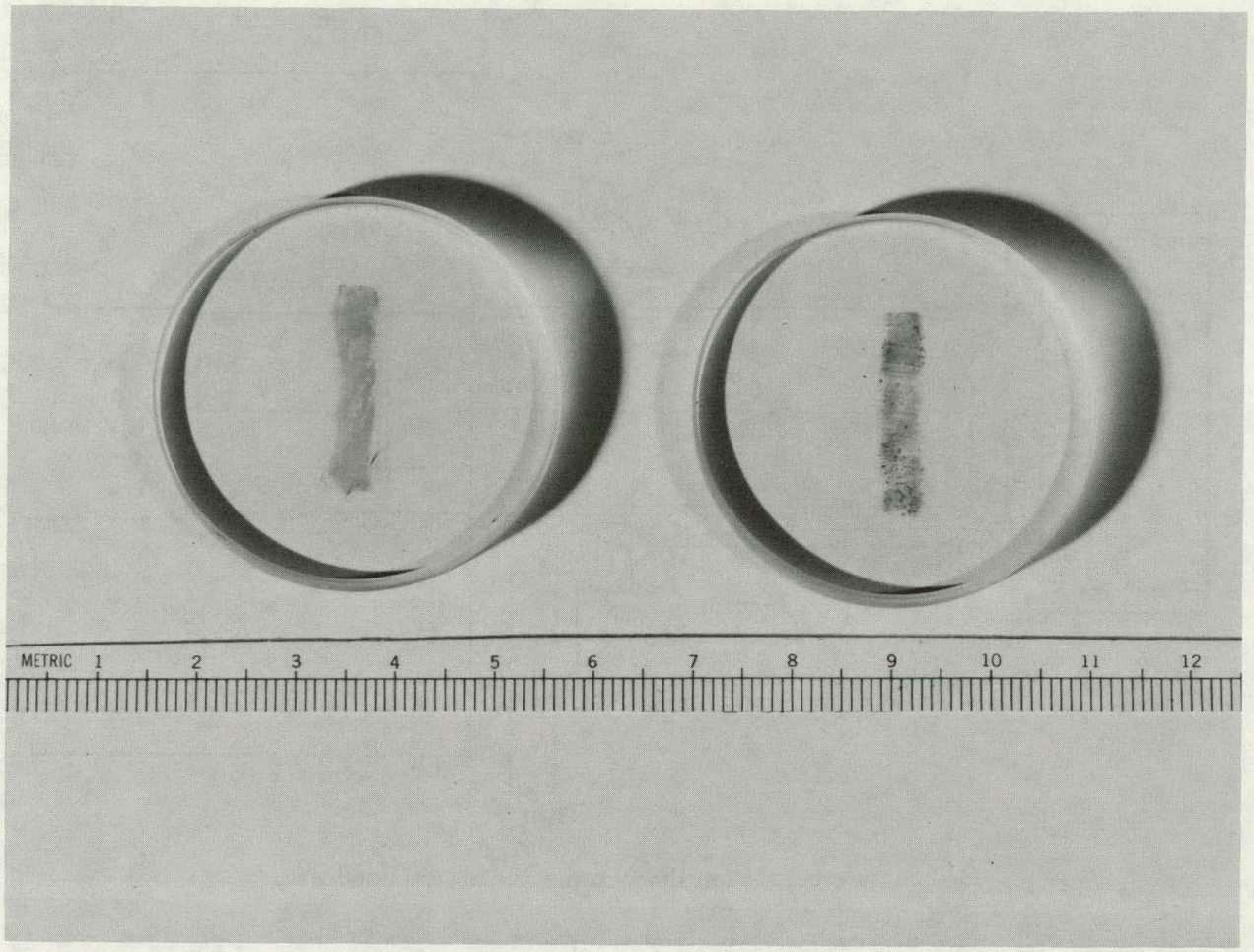

FIG. 1. Laser windows showing deposits in beam pattern.

fluorescence has shown this coating material to be made up of chlorinated hydrocarbons.

The solution to this problem was the development of a system of baffles (Fig. 2) between the main laser volume and the windows, with a moderate, 5-to-7 std l/min of clean, halogen-free gas flowing over their inner surfaces. The baffles are necessary to eliminate turbulent mixing in the window ports by the laser gas flow of 20 m/s past the ports. It is critical that during laser operation the window surfaces never come into contact with any halogens or other contaminants. By maintaining a flow of clean gas over the windows, we have demonstrated that the laser output power is no longer affected by the window surfaces during long-time laser operation.

The clean, halogen-free, Xe-He gas flow has been maintained by either bleeding off and exhausting part of the laser gas mix and adding fresh Xe-He makeup gas past the windows (with the HCl being added elsewhere in the laser), or by passing part of the laser gas mix through a chemical scrubber to remove all of the HCl and any other contaminants and returning the clean Xe-He gas past the windows, again with makeup HCl added elsewhere in the laser. In both cases, all gas flows are monitored by calibrated mass-flow meters.

It should also be pointed out that for RGH laser operation lasting hundreds of hours, some form of gas cleanup will in all probability be required anyway, so the need to flow clean gas past the windows does not constitute a major complication to the system.

(For further information, contact J.W. Dickie, Ext. 2-6262.)

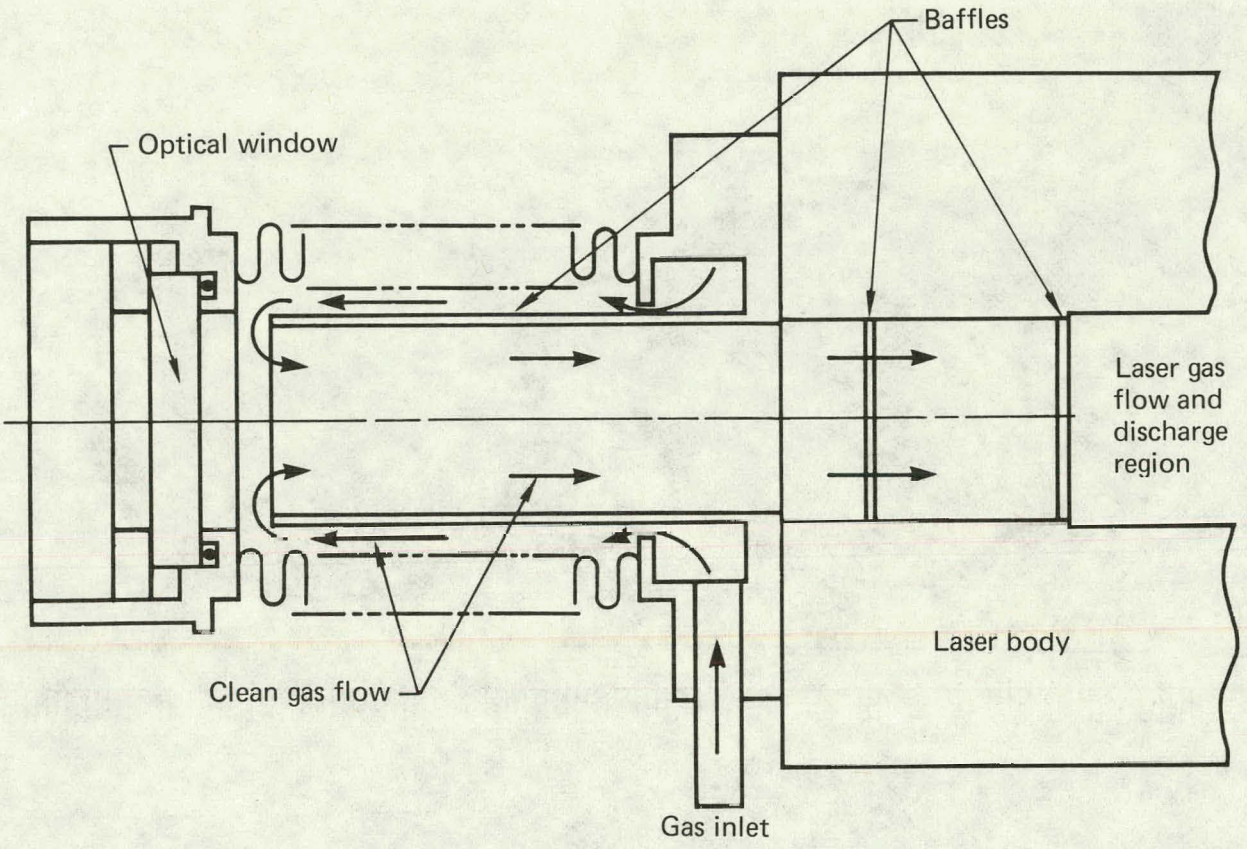

FIG. 2. A cross section through the window mount/baffle.

Very High Temperature Gas Heater Under Development for Laser Program

The Energy Systems Engineering Division is developing a very high temperature gas (VHTG) heater as a part of the laser isotope separation technology program. This heater will operate in a positive-displacement compression mode at high pressure ratio. The form is similar to the familiar Roots blower with two meshing, opposite-hand, helical-lobed rotors. They fit into a surrounding case with approximately 0.1-mm clearance to give low gas leakage without the use of sealing rings or fluids. Water cooling of the rotors and case limits component temperatures. The very high temperature of the discharge gas is the result of the high pressure ratio across the heater. We use helium-neon mixtures because they are nonreactive.

Predictions of the heater performance are shown in Table 1. Helium transfers the discharge energy and leaks more readily than neon, both processes leading to the higher temperatures shown for the all-neon conditions.

TABLE 1. Very high temperature gas heater performance prediction. (The rotor input power is 550 kW, the discharge pressure is 2 atm, and the pressure ratio is 350.)

Condition	Discharge temperature (K)	Discharge flow (g/s)	Heating efficiency (%)
Lowest temperature (helium with larger clearances)	3300	13	38
Helium design point	4000	9	31
Neon design point	7200	24	31
Highest temperature (neon with smaller clearances)	8600	14	22

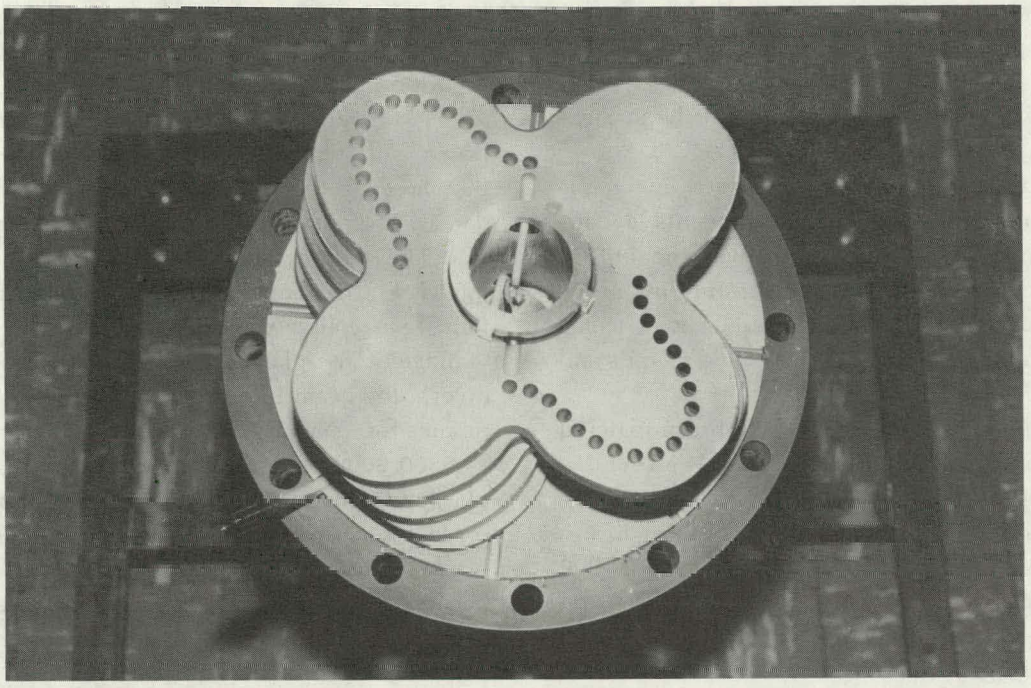

FIG. 3. Prototype impeller stack on load frame base, top wafer and filler wire removed, cooling holes left out on two lobes, blank lobes are 0.5 in. minimum over finished size.

We will deliver this hot inert gas with uniform very high temperature that is easily controlled by input power and is steady and dependable.

One of the major developmental tasks has involved the helical impellers (Fig. 3). We have found that a helical wrap of the impeller lobes, as well as an involute lobe profile, is necessary to limit the forces associated with rotor-to-rotor bumping in fault and resonant transients. Further, the high heat fluxes from very hot gas require water cooling passages to be positioned within 1.5 mm of the impeller surfaces. The only way to satisfy these requirements is to provide a water flow path that is also helical. We need continuity of the outer surface of the impeller to the body, so we provide a pattern of closely spaced helical holes near the periphery. Among a number of alternatives, we chose a copper-brazed stack of 1-in.-thick wafers with cooling holes drilled on a chord of the helix in each wafer. By centering the chord on the helical element, we get a maximum deviation of about 0.05 mm.

One of the complications of the brazed wafer mode of construction is the volume change associated with phase transformation in the 4330 V alloy steel base metal. This change, about 2% in volume or 0.7% in dimensions, is a shrinkage that occurs when the room temperature, body-centered-cubic martensite lattice transforms to face-centered-cubic austenite on heating through the 750-to-810°C transformation zone en route to the 1100°C copper brazing temperature. The endothermic work to accomplish the shrinkage results in a characteristic dip in the heating curve (Fig. 4) at the

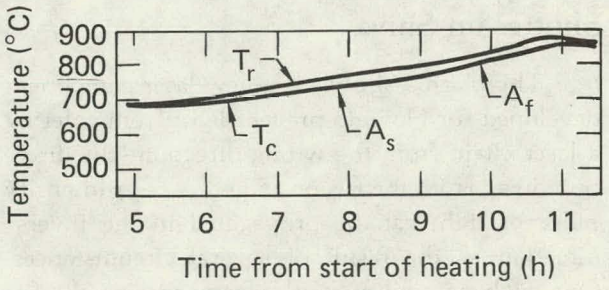

FIG. 4. A portion of the heat treat curve for 4330V workpiece showing temperature lapse associated with endothermic transformation from martensite to austenite: A_s = start of austenite formation, A_f = finish of austenite formation, T_r = temperature of gas in retort, and T_c = temperature of midpoint of workpiece. Nominal heating rate is 30°C/h to minimize transformation effects.

start of austenite formation (A_s) and a return to the normal slope at A_f. A return to martensite on cooling yields the stored energy from the closer packing, which raises the cooling curve in the martensite return zone.

The transformation cycle gives inevitable warping of the wafers, which prevents a continuous braze. We removed the warping *in situ* before reaching the brazing temperature by means of creep, driven by a 15-psi gas-bag load frame consisting of a Hastelloy-X bladder and tie rods and graphite loading disks.

We used plated copper as the braze material source over the faces of each wafer. We found it necessary to supplement this source around the peripheries of the joints with copper filler wires in grooves. All copper had to be pure to the 0.9999 level for acceptable porosity.

These techniques have given finished-form cooling passages that are helium leak-tight at the 2500 psi, centrifugal service-pressure and brazed joint tensile strengths consistently equal to the base metal yield strength.

We are preparing the prototype rotor for finish profiling, leak testing, and specimen evaluation. The service case and rotors are being fabricated, and our component and process developmental work has been essentially completed. Our schedule is to deliver hot gas this year.

(For further information, contact B. Myers, Ext. 2-7321, or F.C. Kelser, Ext. 2-6186.)

Testing the Plasma Shutter on Shiva

The plasma shutter is a new laser component developed for Nova to prevent light from entering a laser chain from the wrong direction—the direction away from the fusion target. A high-intensity pulse of light can be propagated in the inverse direction as the result of several circumstances. One such possibility results from missing the fusion target at the center of the target chamber and thereby firing an unattenuated pulse backwards into an opposing laser arm. Another possibility results from the commonly observed light that reflects back from a fusion target. This can amount to as much as 30% of the incident energy. The reason for blocking backward-propagating light is to avoid the gain remaining in the laser disk amplifiers after the laser pulse has passed through them on its way to the target. Any reflected 1.06-μm light entering a disk amplifier from either direction can potentially be amplified to the damage threshold of the optical components. This could damage expensive optics on each laser arm.

The current method for blocking reflected light is to use a Faraday rotator-polarizer combination. This relatively expensive component takes advantage of the plane polarization of the light and diverts the beam into an absorbing glass. Cost estimates for a Nova-size Faraday isolator are as high as $500 000 per arm (there are 20 arms on Nova) plus additional components necessary to account for losses caused by the isolator. For this reason the plasma shutter was developed as a relatively inexpensive replacement for the large-aperture Faraday isolators and has been estimated to cost 80 000 to $90 000 in production quantities.

The shutter takes advantage of the optically opaque nature of a dense plasma for blocking the returning light. This is the same phenomenon that causes the light to be reflected back from the fusion target. A dense plasma can be generated by passing a very high current through a metallic foil, causing it to vaporize explosively. The metal foil is initially located adjacent to the path of the laser pulse near the pinhole of a spatial filter. Figure 5 shows a diagrammatic view of the shutter mounted near the pinhole of the largest Nova spatial filter. The energy storage capacitors and high-voltage high-current switches are mounted close to the exploding foil to minimize circuit inductance and switching time.

The distance from the plasma shutter to the target is only 60 m and at the speed of light the reflected pulse will return to the shutter in only 300 ns. The plasma shutter must not be allowed to interfere with the outgoing pulse and yet must fill the beam path with dense plasma only 300 ns later. This is accomplished by passing 600 kA from a 35-kV power supply through a small aluminum foil, thus forming the plasma. The high-voltage switch that accomplishes this task was developed at LLNL; it is the most compact unit of its kind known to the author.

A prototype of the plasma shutter was tested on Shiva in 1981 to determine if it could generate a plasma of sufficient density to either block an intense laser pulse outright or refract the light out of

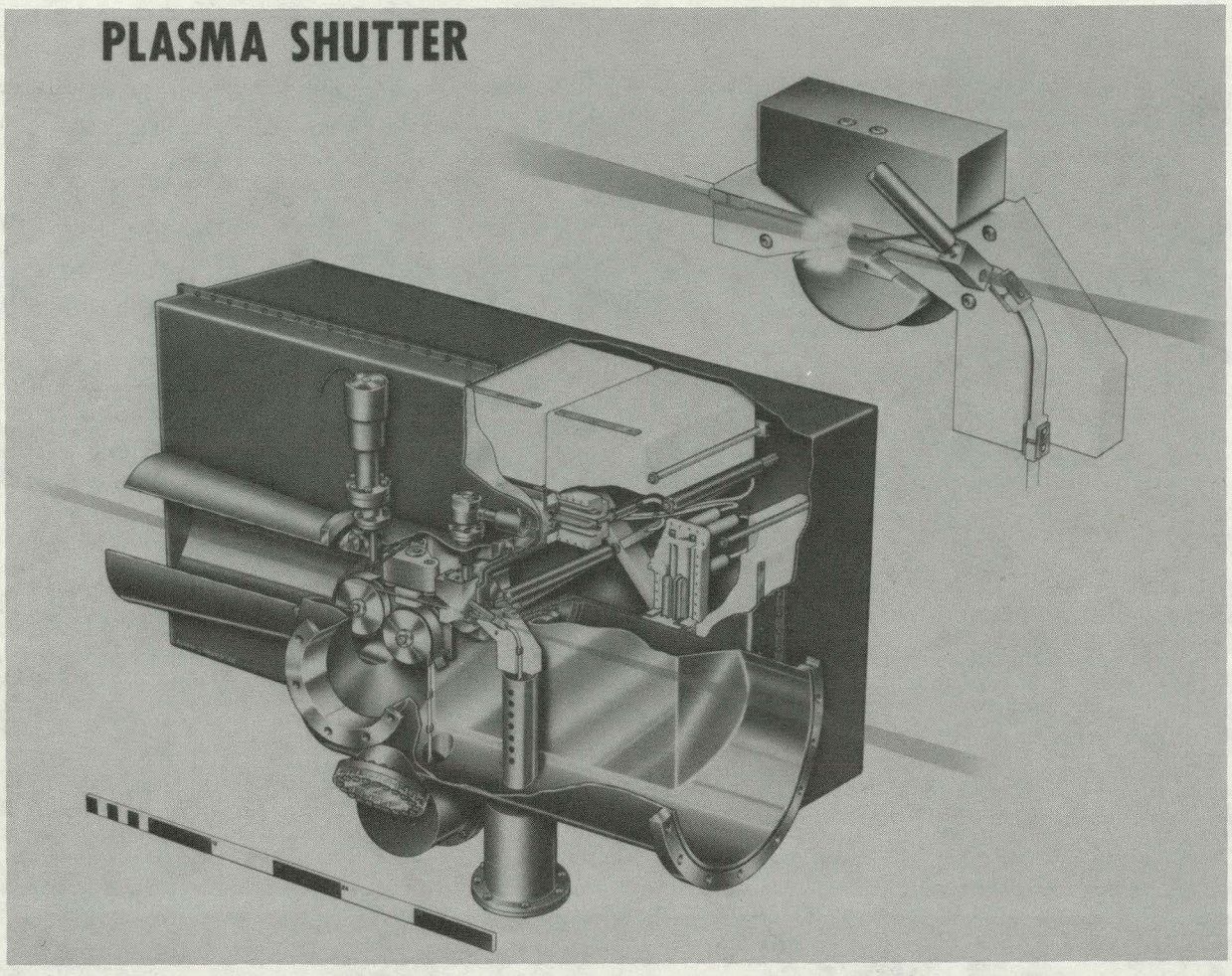

FIG. 5. Artist's rendering of the Nova plasma shutter showing the path of the laser beam on its way from the last laser disk amplified to the target chamber. The pinhole of the last spatial filter is located just upstream from the plasma shutter as shown in the enlarged view of the nozzle region. The electrical circuit is triggered slightly before the pulse passes through the pinhole on its way to the target chamber. After 340 ns the reflected light returns from the target chamber and is blocked by the plasma streaming from the exploding aluminum foil.

the aperture of the spatial filter lens. The Shiva laser was used because of its high output energy capability and the relative ease of mounting the plasma shutter into one of the output spatial filters. The plasma shutter as it was installed for testing is shown in Fig. 6. The shutter was configured to block outward-propagating pulses rather than pulses reflected from the target so that the entire laser arm output could be focused onto the plasma. The focused intensity exceeded 1000 TW/cm^2 over a 100-μm-diam spot. This is the same intensity that Nova will impose upon the plasma, but over a much larger diameter than could be simulated with Nova.

The aluminum foil that forms the plasma is vacuum-deposited onto an alumina substrate and is housed in a block of Lexan. This foil-holding chip is shown in Fig. 7, and because it is partially destroyed during firing it is automatically replaced after each shot. The chip itself will be an injection-molded part costing only a few dollars.

During the Shiva testing of the plasma shutter, two measurements were of primary concern: When, after triggering the pulser circuit, does any attenuating plasma emanate from the foil, and how much pulse attenuation can be expected 300 ns after the plasma starts moving? Initial beam attenuation was determined by probing the area above the

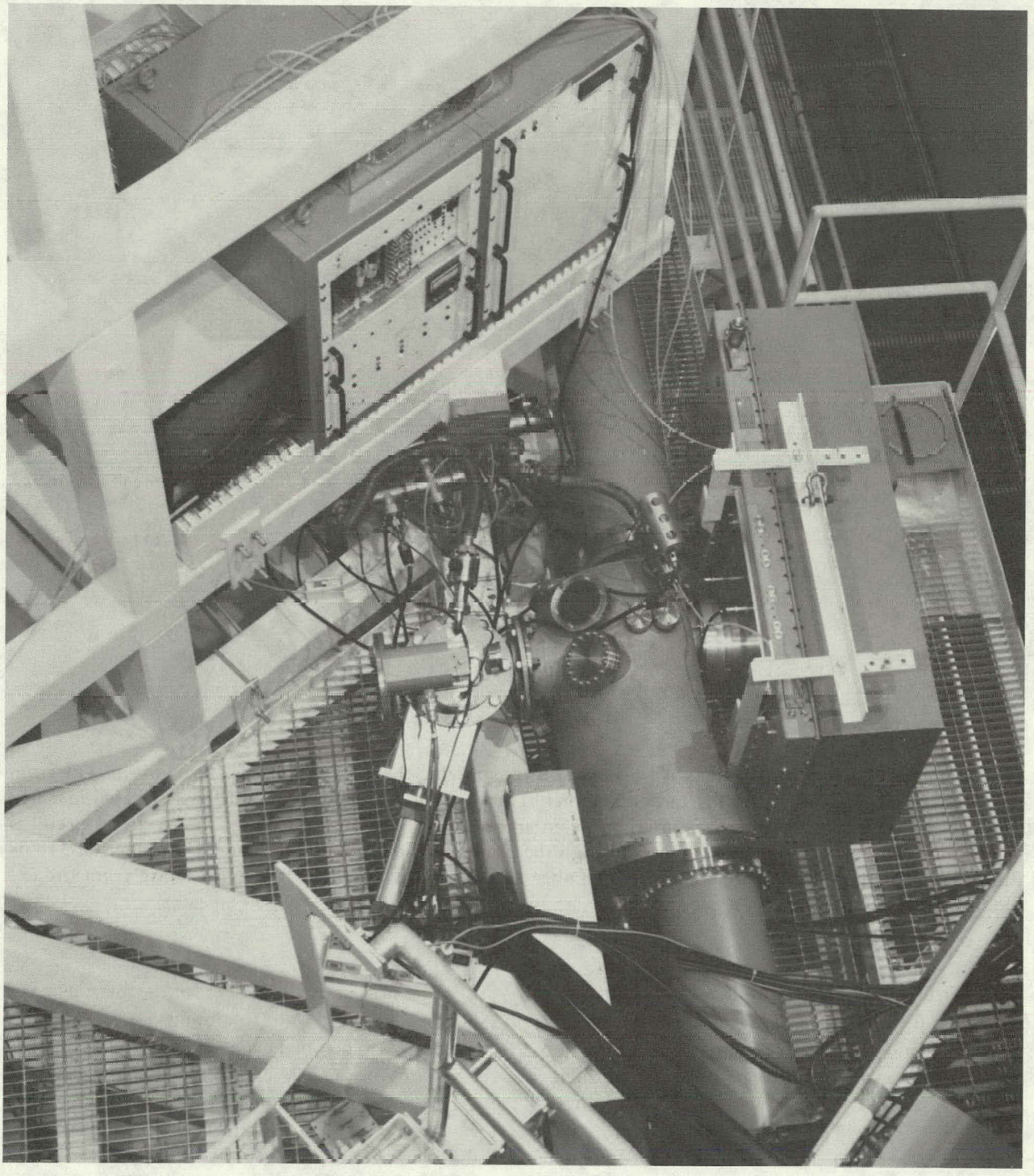

FIG. 6. The plasma shutter module as installed into the output spatial filter on the Shiva laser system. The charging power supply and diagnostic electronics are mounted above the shutter and the high-current-switch unit is mounted onto the right side of the evacuated chamber, which is in turn mounted at the center of the spatial filter. In this configuration the full output of one arm of Shiva can be used to simulate the energy that will be reflected back from a Nova target.

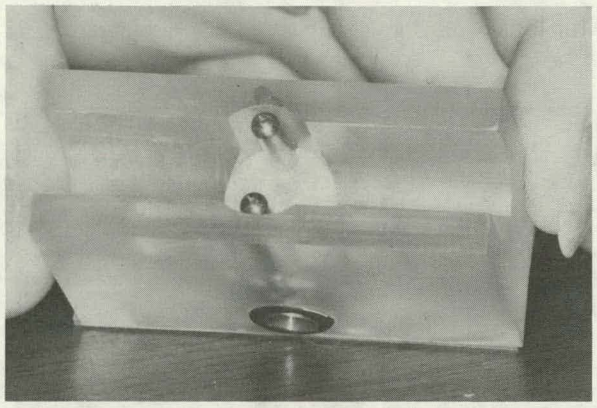

FIG. 7. This Lexan foil-holding "chip" forms the electrical contact and insulating dielectric block that sits across the 35-kV power supply. The exploding foil, in this case made of aluminum, rests on an alumina disk and explodes to form a dense plasma when 600 kA flows through the wire. The copper electrodes extend the electrical circuit and continue the electrical discharge above the alumina disk and into the volume through which the laser beam passes.

exploding foil and watching for initial signs of plasma leaving the heated foil. A typical sequence of beam photos is shown in Fig. 8 where the plasma does not leave the foil until at least 100 ns after triggering the high-voltage pulser. To measure attenuation of a full Shiva system shot, one calorimeter was mounted looking through a beam splitter at the input beam, and another full-aperture calorimeter was mounted looking at the exit of the spatial filter. The ratio of these two calorimeters was used as a measure of plasma transmission. When chips were used similar to that shown in Fig. 7 and timed to probe the plasma when the reflected light would be returning from the target chamber, the typical transmission was 0.01 to 0.002. This is sufficiently low to prevent damage to optical components in the laser chain.

(For further information, contact I. Stowers, Ext. 2-0407.)

Novette, a Two-Beam Laser System, Is Scheduled for Completion This Year

Installation of Novette, a two-beam laser system under construction in Building 381 at LLNL's former Argus site, was planned for December 1981; completion of construction is scheduled for the fall of 1982. Novette is a two-wavelength (1.05-μm and 0.53-μm) irradiation facility with projected performance to exceed the 20-beam Shiva system.

The ambitious Novette schedule is driven by the need to have in operation an experimental facility at shorter wavelengths before the huge Nova facility comes on line, which will be in 1983 for Phase I or 1984 for Phase II.

The two Novette beams will be identical to the Nova beams except that they will be folded differently, allowing the machine to fit into the Argus building. Figure 9 shows this configuration. The final amplifier stage will be the 46-cm aperture box amplifier followed by a spatial filter that expands the beam to a final aperture of 74 cm.

To convert from 1.05-to-0.53-μm wavelength, a frequency conversion crystal of potassium dihydrogen phosphate (KDP) will be installed in the beam line close to the focusing optics at 74-cm clear aperture. Focusing optics (f/2) will then focus the beam on the target. The energy per arm will be 10 to 15 kJ at 1.05 μm and 7 to 9 kJ at 0.53 μm. The pulse length will be 100 ps to 5 ns.

The chains consist of a driver section through the 20.8-cm amplifiers, followed by the 31.5- and 46-cm stages. This hardware was described in an article on Nova[3] in the last issue of the Technical Review. The driver section is Shiva hardware retrofitted with phosphate glass (Shiva has silicate glass). Space is provided for additional amplifiers in the power stage (31.5 to 46 cm) for future upgrades. Following the last stage, two mirrors are required in one arm and three in the other to direct the beams, in an east-west irradiation to an elevated target chamber.

Both chains will be driven by a common oscillator and preamplifier section located in one of the wing rooms. A four-part spaceframe will support the machine above the concrete floor slab. Spaceframe design follows philosophies used on Shiva and Nova for thermal and vibrational stability.

Hardware has been ordered for 10 beams of Nova, with deliveries for two beams scheduled early enough for Novette. All hardware except short lead-time components is in fabrication.

Many of the system requirements for Nova, such as clean room modifications and assembly

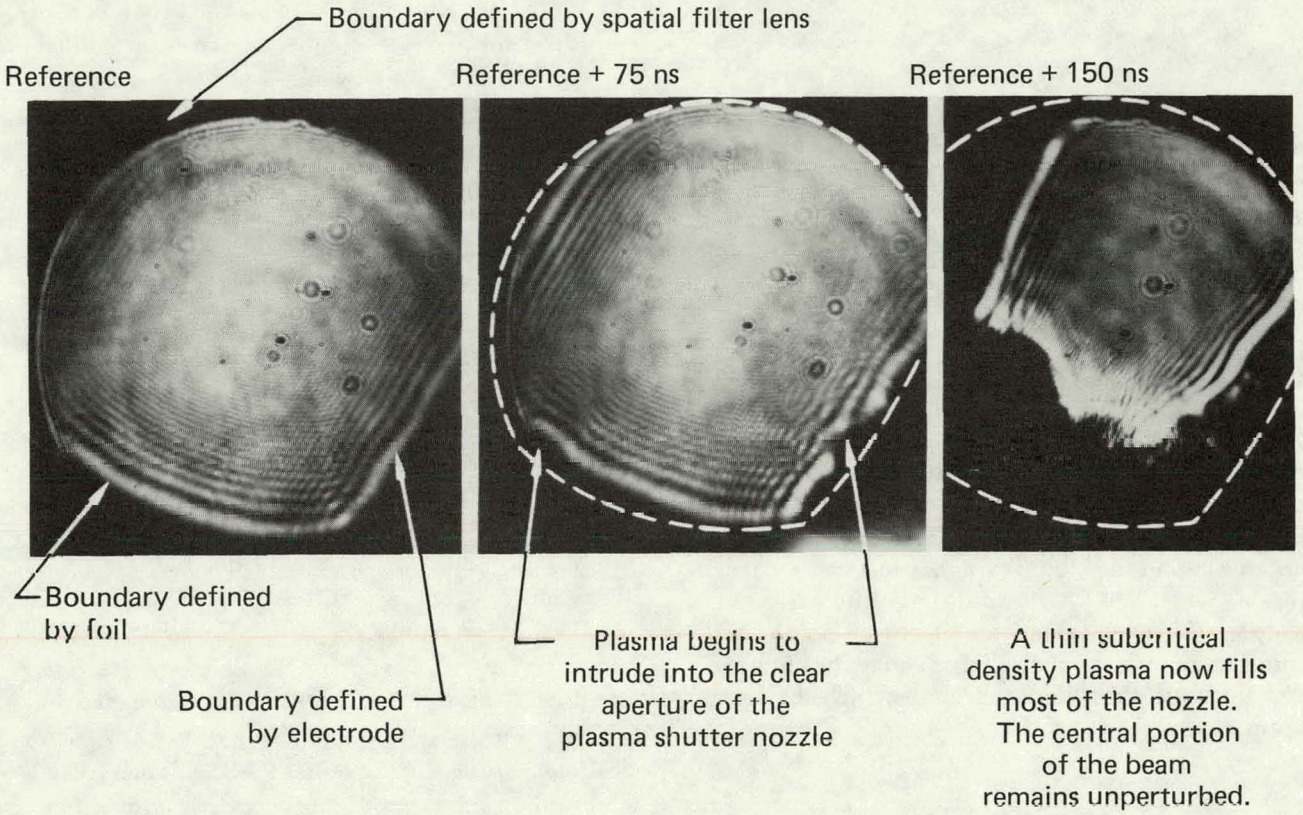

FIG. 8. Far-field diffraction pattern of the exploding-foil nozzle. The photos are arranged to show a series of time-lapse snapshots taken 0, +75, and +150 ns after triggering the shutter. During the first 100 ns, the spark-gap switches fire and current begins to flow through the foil. After 150 ns, resistive heating leads to sublimation of the aluminum foil, which streams out into the nozzle and begins to block the 5-ns-long laser pulse. After 200 ns the plasma front has moved more than halfway across the nozzle. The undistorted diffraction pattern at the top of the +75-ns picture clearly shows that no plasma has yet reached that portion of the nozzle.

facilities, are also in progress to accommodate the Novette schedule.

(For further information, contact C.A. Hurley, Ext. 2-0681.)

Fabrication of High-Precision Optical Components from Crystalline Materials

A cooperative effort between the Energy Systems Engineering Division and the Materials Fabrication Division has resulted in the technology to produce optical components with tight mechanical tolerances (±1 μm) and precision orientation of the crystalline axis (±30 μrad) from potassium dihydrogen phosphate (KDP) crystals. These components will be used to generate the second (0.532 μm) and third (0.355 μm) harmonics of the laser output of the Nova and Novette lasers currently under construction.

The KDP crystals have a number of properties that require special handling, fabrication, and measurement techniques. The crystals are:

- Hygroscopic.
- Brittle, soft, with low strength.
- High, nonisotropic thermal expansion (> aluminum).
- Low, nonisotropic thermal conductivity (≈ ceramics).
- Temperature-dependent optical properties.
- Stress-dependent optical properties.

Oversize slabs of KDP are cut from boules grown by commercial vendors. Then, operating in a fly-cut mode, we produce an optically flat surface

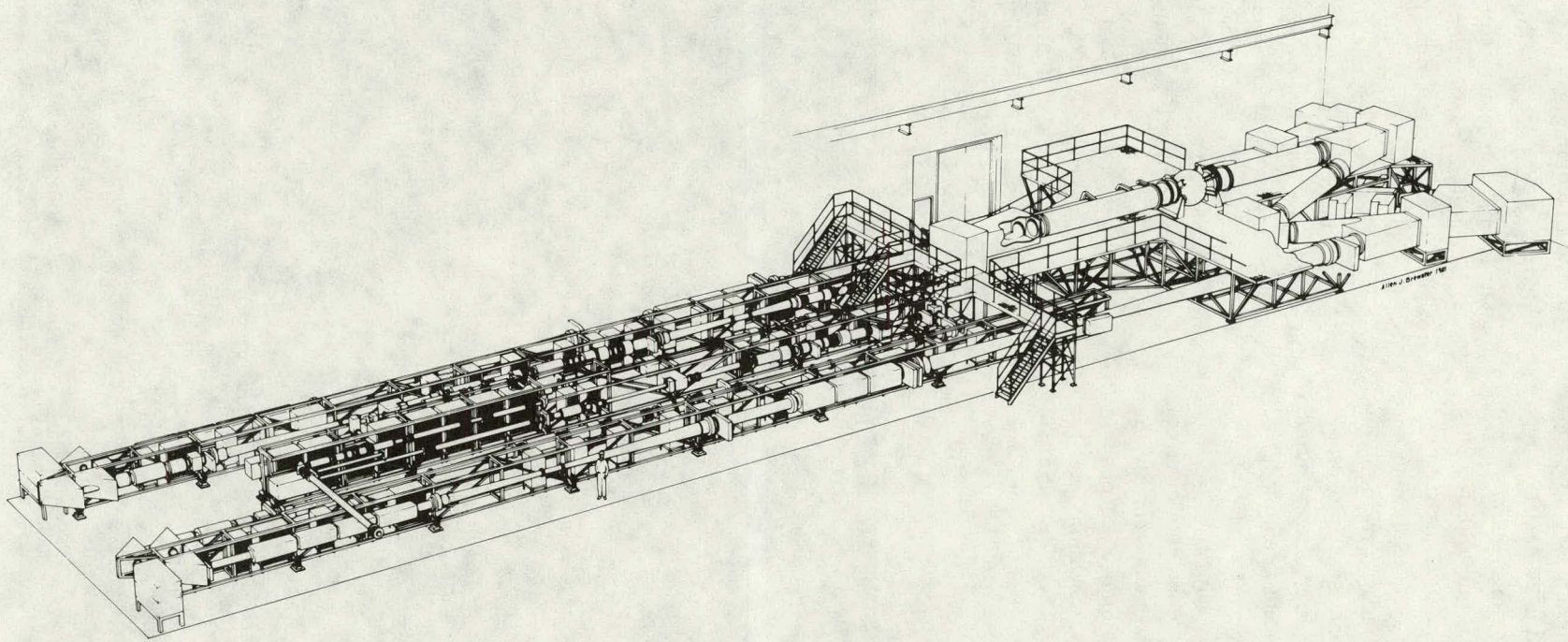

FIG. 9. Novette is a short wavelength, multikilojoule target irradiation facility.

on each slab by using the single-point diamond turning machine (DL-1) in Building 131. The temperature of the crystals is held to 20 ±0.01°C during this operation. Next, the crystals are transferred to Building 391 where a temperature- and humidity-controlled measuring instrument precisely locates the crystal axis, relative to the diamond-cut surface. The angular corrections required to bring the dimensional axes into proper relation with the crystal axes are then measured, again at 20°C. The crystal slabs are transferred back to DL-1, which cuts these corrections into the part, and final dimensions are achieved.

In order to minimize the probability of errors in the transfer of critical angular measurements, the 3-axis manipulating mechanisms used to position the crystals for both diamond machining and for axis measurement are nearly identical, and are maintained at equal temperatures.

Design of Tooling for Diamond Machining

We designed a three-rotational-axis manipulator (using a vacuum chuck to support the crystals) for use in conjunction with the x-y motion available on DL-1. The primary (z-axis) rotary motion is provided by a precision rotary table, with a wobble plate giving the other two axes of rotation. An aluminum vacuum chuck, with small pitch (2.5 mm) between supports, and a high percentage (90%) of unsupported area holds the crystals in a very repeatable and secure manner. This tooling is shown in Fig. 10.

The machining conditions were:

Tool back rake,	−45°.
Cutting speed,	2000 ft/min.
Feed rate,	0.5 in./min (rough),
	0.080 in./min (finish).

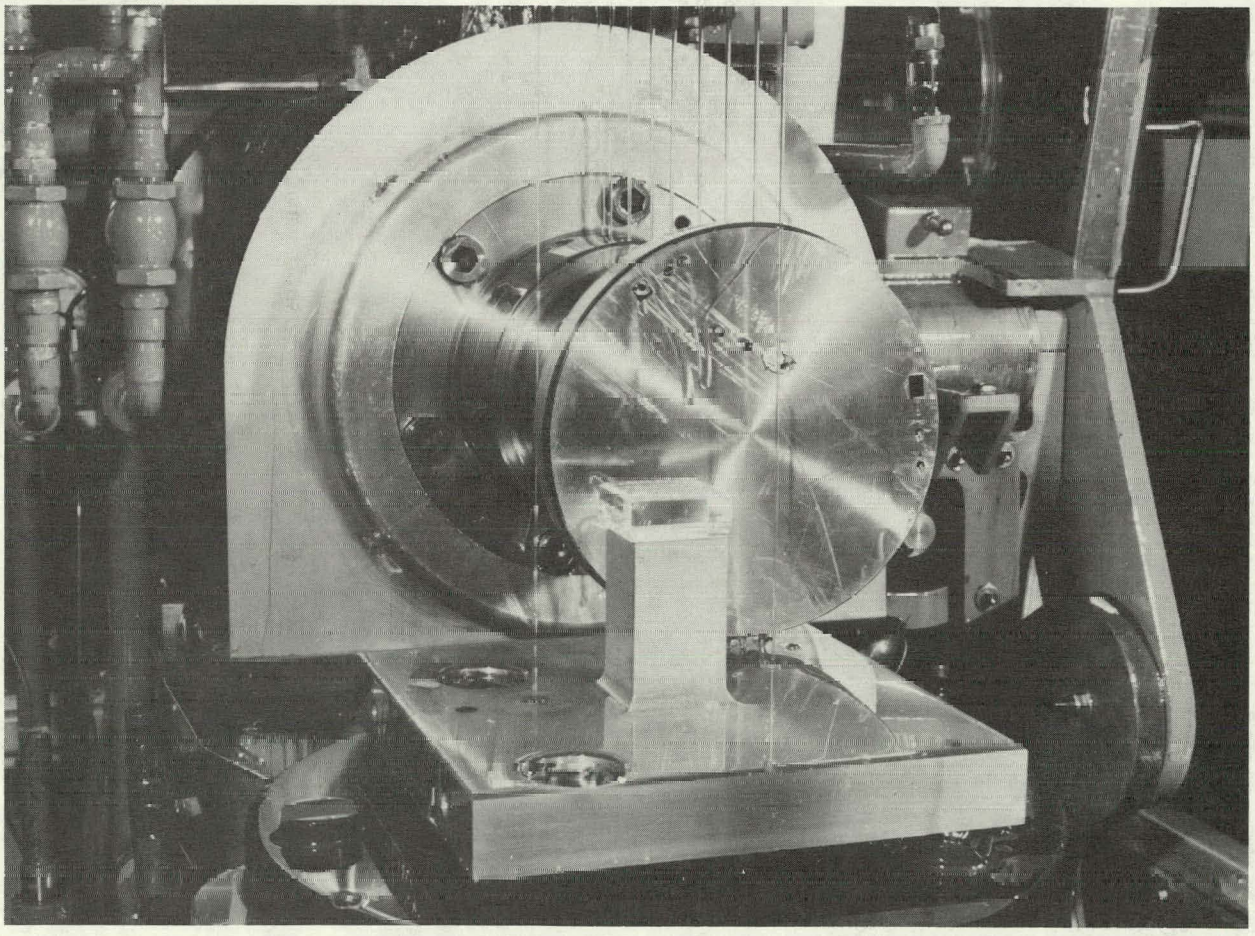

FIG. 10. A KDP crystal being machined on the diamond turning machine (DL-1).

Cutting depth, 0.001 in. (rough), 20 μin. (finish).

The negative tool back rake causes the material to be removed by compressive forces, rather than the tensile forces of a conventional metal cutting tool.

Design of Crystal-Axis Measuring Equipment

A duplicate rotary table, wobble plate and vacuum chuck assembly were installed in a temperature- and humidity-controlled enclosure we designed. Temperature is maintained by a recirculating air shower system with 1000 cfm of air blown through electric heater coils, bucking a water-cooled, finned radiator. The radiator is held to approximately ±0.25°C by a commercially available refrigeration system. The heating coils are proportionally driven by a thermistor controller that senses the air temperature near the crystal being measured. This "bucking" of a large cooling sink and a small heating source allows precise temperature control (±0.01°C at the crystal) from standard commercial equipment; it also allows rapid recovery when the enclosure is opened for crystal changes. Humidity is kept to less than 35% by purging the enclosure with dry nitrogen as necessary. This purge is controlled by a humidity sensor installed in the enclosure. This enclosure is shown in Fig. 11.

(For further information, contact J.D. Williams, Ext. 2-5943, S.E. Mayo, Ext. 2-5959, or F.T. Marchi, Ext. 2-5948.)

Ultraclean Room Required for Expensive Nova Amplifiers

The 335-m^2 Class 100 clean room (see Fig. 12) in Building 391 provides the ultraclean area required for cleaning, assembling, and inspecting the rod and disk amplifiers in LLNL's laser fusion system.

The critical components in these amplifiers are the neodymium-doped glass elements. These elements are subjected to the incoming beam energy plus the energy associated with the various arrays

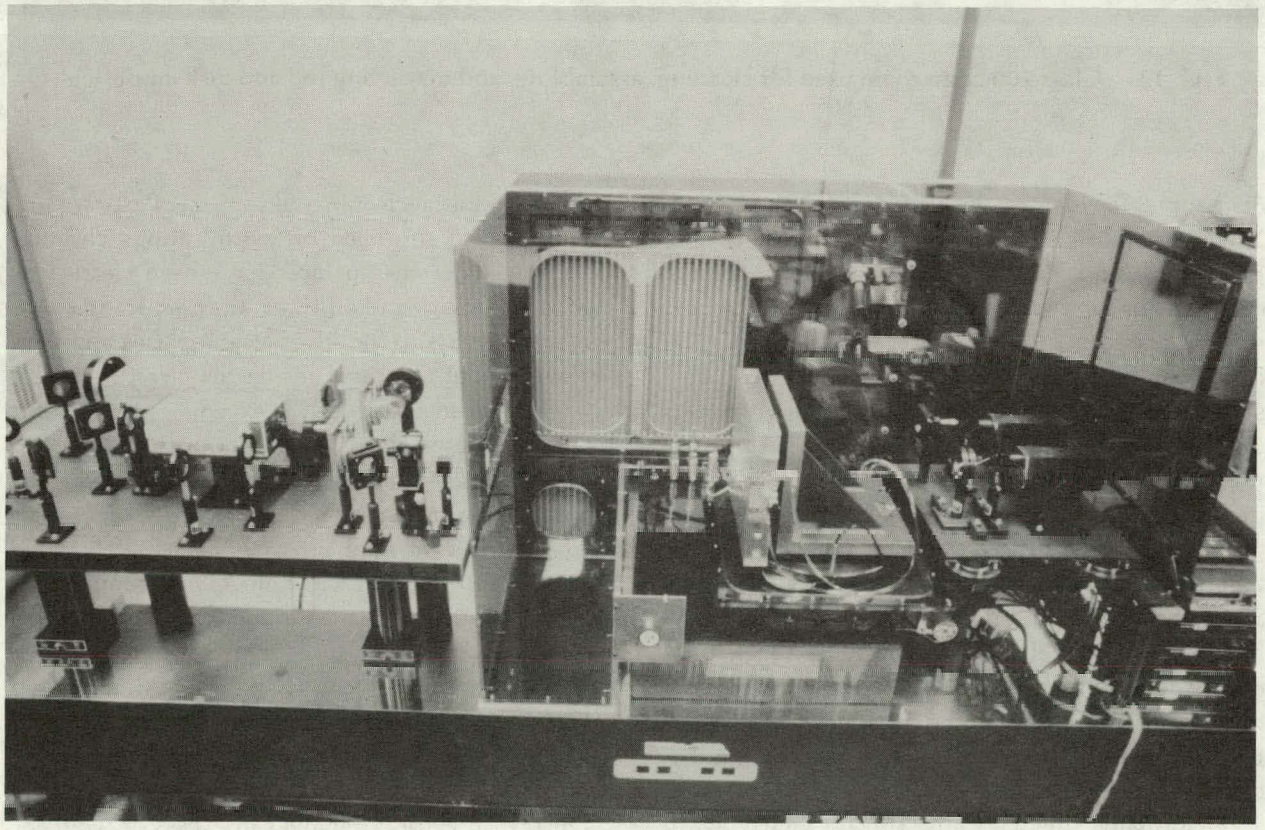

FIG. 11. Temperature- and humidity-controlled enclosure for measurement of KDP crystal properties.

FIG. 12. Class 100 clean room used for cleaning, assembling, and inspecting rod and disk amplifiers.

of xenon flashlamps located inside all Nova/Novette amplifiers. This combined fluence of the flashlamps and the beam causes contaminants, such as dirt or films on the glass surface, to be rapidly heated and in many cases to evaporate. This can cause severe damage to the surface. Any absorbing particle resting on a glass surface will either locally melt the glass or thermally stress it during the heating and cooling pulse. This repeated stressing causes fragments of glass to break out. These glass fragments themselves can then become contaminants, thus escalating this destructive process. Since the cost of these large-size disks can be as high as $50 000 each, every effort is being taken to ensure that contaminants are held to an absolute minimum. The cleaning, assembling, and inspection of these vital elements must be done using the cleanest means possible.

Normally, the cleaning process starts with equipment being delivered into the preclean room where the initial cleaning takes place. Parts are unwrapped and scrubbed off with various cleaning solvents. Once the surfaces have been cleaned of foreign particles and oil films, they are transported on special carts to the silver cleaning area and then to spray booths located inside the clean room.

The clean room itself is exceptionally clean. It is rated at better than Class 100 (no more than 100 particles larger than 5 $\mu m/ft^3$). Room air is forced through 0.3-μm air filters to provide a vertical air velocity of 30 m/min, filtering the air at a change rate of 400 times each hour. Dirty equipment therefore must be cleaned immediately upon entering the clean room.

A cleaning solvent (trichlorotrifluoroethane) at 6.9 MPa (1000 psi) is used in two spray booths to strip the contaminants from the surface of all components except for the glass rods and disks. This high pressure spray removes in excess of 99.9% of 5 μm and larger particles in a matter of a few

seconds. After spraying, the solvent is recycled through filters and a distiller to maintain the highest level of cleanliness.

Surface cleanliness is verified by examining a membrane filter located in the solvent return line. The filter is examined microscopically, and a statistical sample of the particles is counted. From this, the total particles removed per unit area is calculated. No more than two particles/cm^2 of surface area greater than 5 μm is usually considered as clean.

The glass components, disks, and rods are so delicate that an entirely separate cleaning procedure must be used. This procedure requires special fixturing and cleaning techniques, including some archaic methods such as cleaning with electronic-grade acetone and ethanol, along with innovative techniques such as a final rinsing with distilled pressurized water while spinning the disk at high speed.

The xenon flashlamps also require special attention. These subassemblies are assembled on special carts and transported to another room next to the clean room. Here they are repeatedly tested with 30 kV of electricity in a special nitrogen-filled enclosure to ensure flashlamp reliability. They are then transported back to the clean room where they are given a final cleaning using a high pressure solvent spray.

At this time, the amplifiers are ready for assembly and are extremely vulnerable to contamination. Clean surfaces can be grossly recontaminated if they are touched by a bare hand or even by a glove if it has been contaminated.

Threaded fasteners have also been "designed-out" of the assembly of the amplifier and special handling equipment because particles can be dislodged as the fasteners are put into place.

For assembling the larger components and, in particular, the larger disks and flashlamp assemblies, two special "clean" boom cranes were designed. To keep fragments from falling onto these assemblies, all moving parts of the crane are covered with bellows or are positioned many feet away from the amplifiers.

The assembly sequence is not over until the components have been inspected. Assembly of the optical elements could cause wavefront distortion or strain birefringence; therefore, inspection equipment includes an interferometer and a polariscope, both of which have been combined into one piece of equipment located in the east corner of the clean room.

With the larger components needed for Nova/Novette, cleanliness is imperative. The critical nature of these amplifiers makes them especially sensitive to contamination; the Building 391 clean room and associated equipment should provide for this high level of cleanliness.

(For further information, contact C.R. McKee, Ext. 2-6124.)

References

1. J. Miller, "XeCl Laser Development/Closed-Cycle Test Bed Experiments," *Selected Highlights: Advanced Isotope Separation Program*, Lawrence Livermore National Laboratory, Livermore, CA, UCRL-50021-79 (1979).
2. J.M. Davin and J.W. Dickie, "Designing a Rare-Gas Halide Laser Flow Loop," *Mechanical Engineering Department Quarterly Review*, Lawrence Livermore National Laboratory, Livermore, CA, UCRL-50016-78-4 (1978).
3. C. A. Hurley, "New Mechanical Technology Marks Design of the Nova Laser System," *Mechanical Engineering Department Technical Review*, Lawrence Livermore National Laboratory, Livermore, CA, UCRL-50016-81-2 (1981), pp. 34–38.

ENGINEERING SCIENCES DIVISION

The Engineering Sciences Division (ESD) provides complete technical services to LLNL programs for materials characterization, engineering measurements, nondestructive evaluation, and mechanical systems design and evaluation. The Division has more than 20 separate laboratories and facilities that are organized into sections responsible for specific technological areas.

The Materials Test and Evaluation Section provides mechanical testing, such as ASTM standard tests and special tests tailored to individual customer requirements. Developments are carried out in the fields of acoustic emission, fracture mechanics, high-rate material response, and composite materials in order to characterize and improve engineering designs.

The Engineering Measurements Section is engaged in work ranging from the design of a single transducer to the fielding of complete measurements systems. Service for the calibration and installation of transducers and accelerometers is also available.

The Nondestructive Evaluation Section provides inspection and diagnostic testing services to LLNL programs. X-ray and gamma source radiography, radiation gauging, ultrasonics, eddy current, dye penetrant, magnetic particle, and holographic techniques are available.

The Engineering Design Section performs design, analysis, and mechanical fabrication in support of the Chemistry and Materials Science Department and many ESD projects. The section is particularly experienced in automated machine design, composites processing and fabrication, tritium handling, mass spectrometry, and high explosives technology.

The Life Sciences Section provides mechanical engineering support for Biomed and Environmental Research, Hazards Control, and Toxic Waste Management programs. Examples of developments to meet the varied requirements of these groups include a cell sorter in Biomed, personnel dosimetry equipment in Hazards Control, and storage and/or burial containers for toxic wastes.

The LLNL Plutonium Facility is managed by the Chemistry and Materials Science Department with operational support provided in part by ESD. The Plutonium Engineering Section in ESD provides engineering design, fabrication, and testing services for the Facility and its users.

The Transportation Systems Research Section participates in research projects for the Department of Energy, Department of Transportation, and other agencies. Projects range from metal-air batteries and powered roadways to the engineering evaluation of various transportation technologies and their impact on the nation's transportation.

(For further information, contact R.W. Werne, Ext. 2-8360.)

Analysis Under Way to Reduce Pad Failures of Tank Tracks

U. S. Army tanks have rubber pads on the bottom of the track to support the weight of the vehicle, and to reduce vibration, noise, and damage on roadways. However, for vehicles weighing over 100 000 pounds (primarily the M60 and M1 tanks) pad failures are a primary factor in high track repair and replacement costs that amount to $150 million per year. Lawrence Livermore National Laboratory is involved in a multidisciplinary study of this problem for the U. S. Army Tank-Automotive Command. This summary deals with ESD's analysis of the thermal and mechanical response of the pad to the operation of the vehicle.

Figure 1 is a photograph and drawing in cross section of the T142 track (used on the M60 series tanks). The thermal analysis work was done using a thermal model representing a cross section of track and the LLNL code TACO. Specifying thermal boundary conditions was a very important yet very difficult part of this problem. For the case of a moving tank, the pads are primarily cooled by conduction when they are in contact with the ground and by convection when the pads are off the ground. In addition, the heat transfer problem is affected by films on the pad (such as dirt), pad condition, air movement, etc. For this problem, convective boundary conditions were used. The heat transfer coefficient was selected on the basis of surface temperature-time measurements that were made in the field on an operating M60 tank. Material properties were incorporated as a function of temperature.

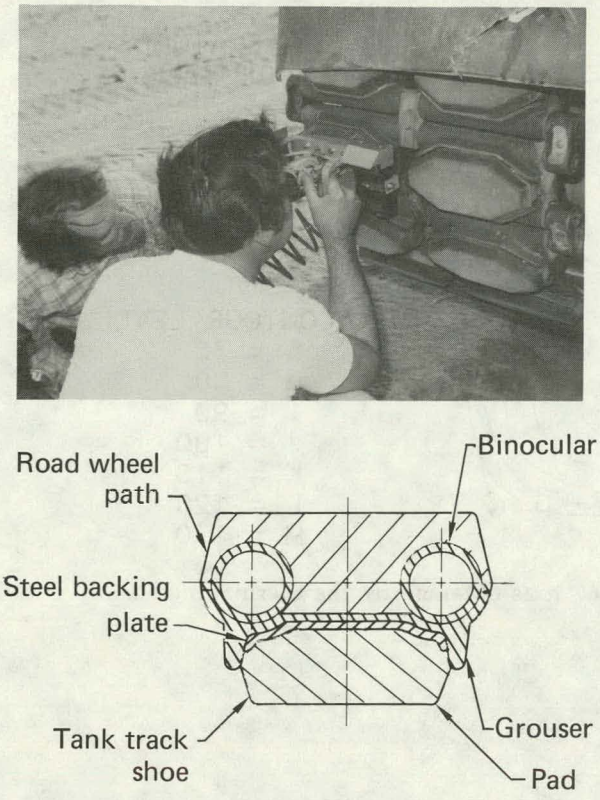

FIG. 1. A T142 track on an M60 tank, and a cross-section drawing of the track. Thermal and mechanical models are based on this cross section.

The temperature-time response predicted by the thermal model shows excellent agreement with the actual temperature-time response measured in the field on an M60 tank. The information is plotted in Fig. 2. The maximum deviation between computer calculations and the field data is about 6°C.

Constant temperature contours after 1.67 h of operation are shown in Fig. 3. Notice that the maximum pad temperature (at the pad center) is over 130°C. This temperature is not hot enough to produce bulk chemical changes (a result confirmed by independent chemical analyses). However, the high temperature adversely affects the mechanical properties of the rubber. Data are limited on the rubber used in track pads (SBR reinforced with ~35% carbon black). However, for similar synthetic elastomers one can see a decrease in toughness of over 85% at a temperature of 130°C as compared to ambient temperature. Thus, a decrease in the operating temperature of the pads would clearly improve life.

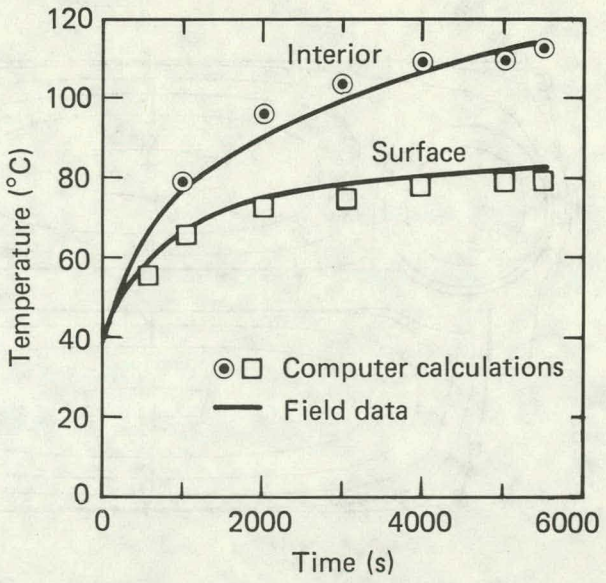

FIG. 2. Temperature-time response for a point 16 mm below the surface of a track pad as predicted by the thermal model. Agreement with experimental data is good.

The mechanical model of the T142 track shown in Fig. 4 was studied using the NIKE2D code. Extensive use was made of the slide-line capability in the code. The influence of the roadwheel moving over a section of track was incorporated by displacing the roadwheel downward until the weight of the vehicle was supported and then sliding the wheel horizontally across the roadwheel path. The slide-lines also allowed us to apply frictional loads at the interface between the pad and its supporting surface. In addition, the tension applied by the track was incorporated as shown in Fig. 4. Two of the operating scenarios that we have considered are shown in Figs. 5 and 6.

In Fig. 5 the track pad is supported on a flat surface with nominal and high applied vehicle loads. The stresses experienced by the track pad are almost entirely compressive. The σ_{zz} stress is shown in Fig. 5. In Fig. 6 the track pad has contacted a rigid obstacle representative of the localized loadings that a pad might encounter in cross-country terrain. Significant tensile stresses can be produced in this operating scenario. These are important since the propagation of flaws in rubber occurs primarily in response to tensile stresses. Figure 6 shows that there is a region of local tensile stress developing ahead of the obstacle. However, we believe the stresses are of insufficient

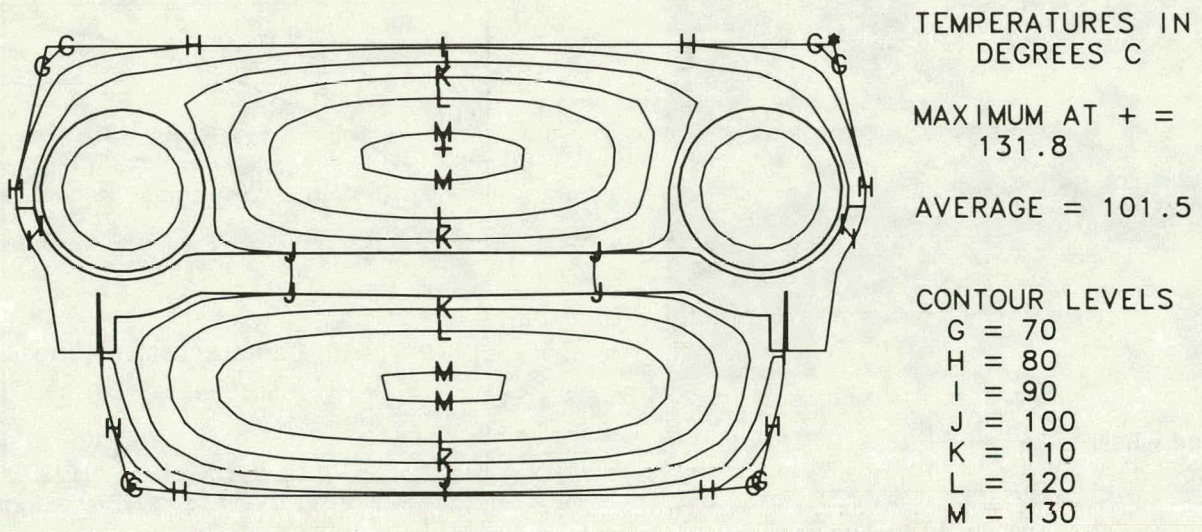

FIG. 3. Constant-temperature contours after 1.67 h as obtained by the thermal model.

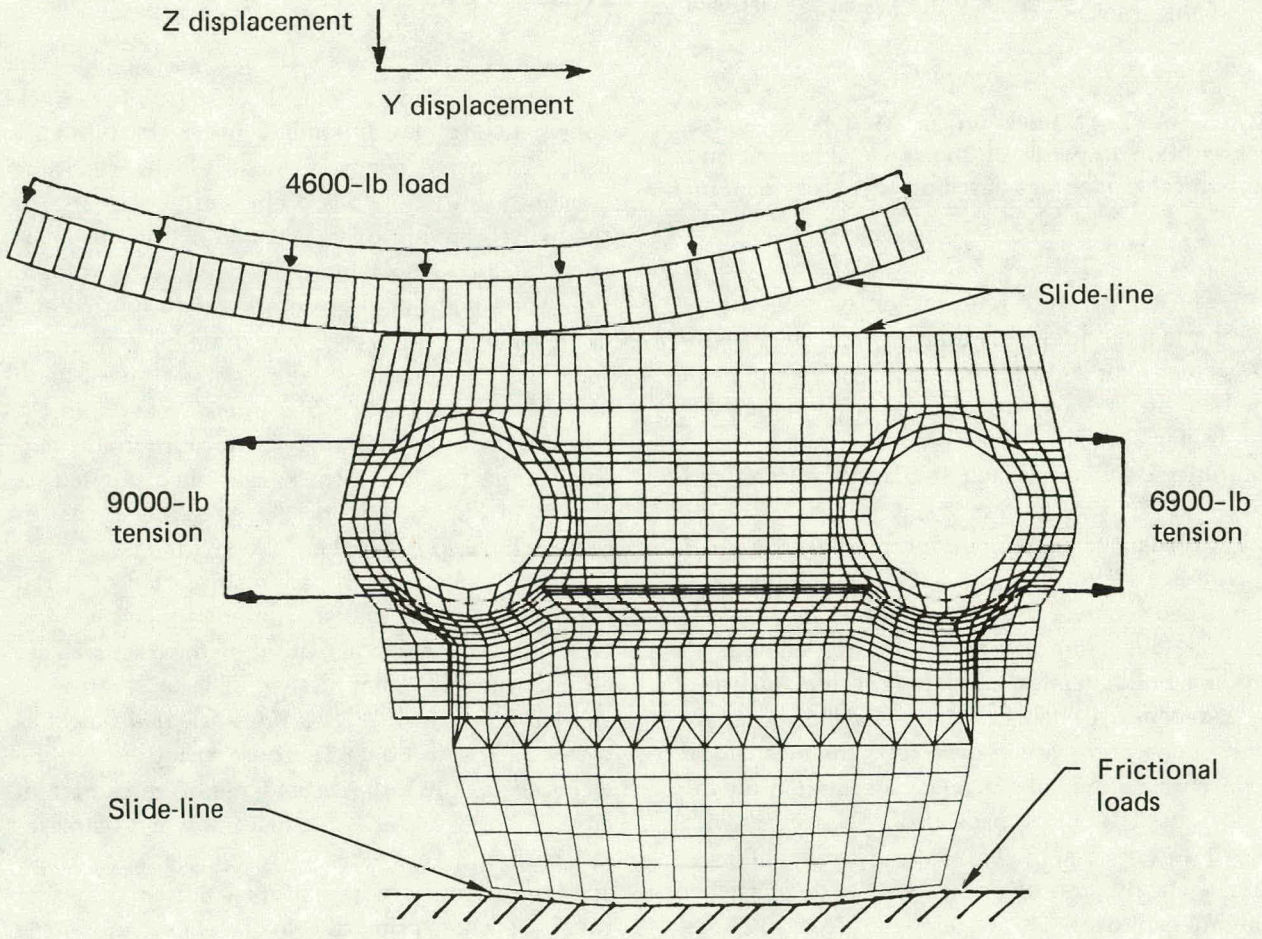

FIG. 4. Mechanical model of the T142 track. Applied loads and slide-lines are indicated. The roadwheel was displaced downward and then horizontally across the track.

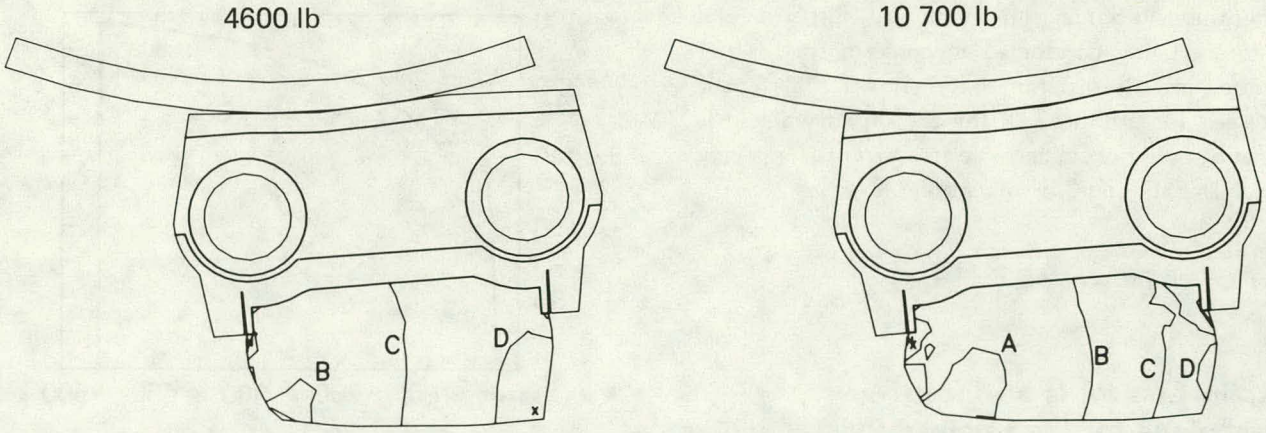

Contour levels - megapascals

A = -3
B = -2
C = -1
D = 0

FIG. 5. Contours of constant normal stress σ_{zz} for track sections that have experienced nominal and high vehicle loads.

Maximum principal stress

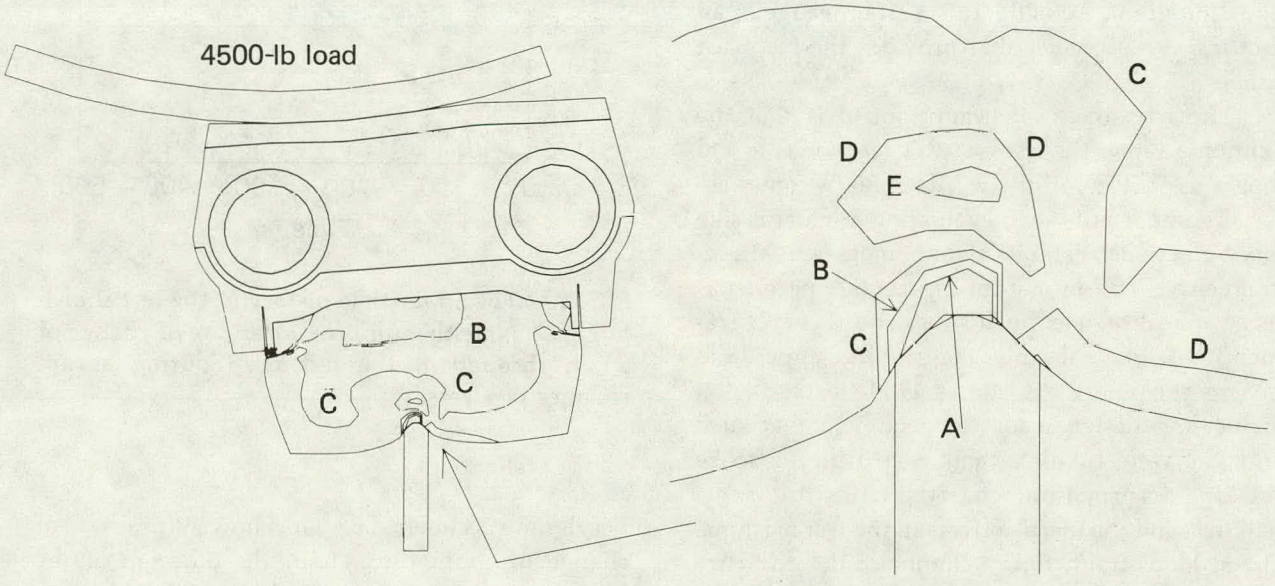

Stress contour levels — megapascals

A = -1.0
B = -0.5
C = 0.0
D = 0.5
E = 1.0

FIG. 6. Contours of maximum principal stress σ_{zz} for track sections in which the pad has encountered a rigid obstacle.

magnitude to damage the track pad. Experimental tests are being conducted to confirm this. Other studies in this program have shown that tensile stresses are produced in the track pad when it is scrubbed over obstacles. We are currently applying the NIKE2D code to this situation.

(For further information, contact D.R. Lesuer, Ext. 2-9633, or R.H. Cornell, Ext. 2-6933.)

Strain Control Is an Effective Technique for the Comparative Evaluation of the Mechanical Properties of Beryllium

Strain control is a control mode available in many servo-controlled, closed-loop engineering materials testing systems. It offers a very appealing testing concept to the experienced materials engineers because it essentially eliminates the interaction of test machine characteristics and material behavior under changing stress. In a broad sense, the test specimen becomes the feedback transducer whose output insures that the test is progressing exactly as prescribed by a predetermined program. Actually, it is a strain gauge or an electrical extensometer that provides the feedback signal.

The advantage of strain control is that the technique allows the test system's reaction frame to appear as if it is infinitely stiff. This becomes especially important when evaluating a material like beryllium, which exhibits a nonhomogenous stress-strain curve if at the start of the test the specimen is in the annealed state. Such stress-strain curves frequently display sharply contrasting upper and lower yield points. As late as 1964, textbooks on engineering design made the argument that such contrasts were fictitious and were believed to be due to deformation characteristics of some materials and the inertia effects in the test machine. Closed-loop strain control eliminates the influence of machine inertia on the test by including it in the control loop.

Figure 7 is the stress-time history of a test on a beryllium specimen. Conspicuously, the upper yield point and the lower yield point are sharply contrasted. Figure 8 is the strain-time history for the same test. These data are from an electrical extensometer monitoring the gauge length of the

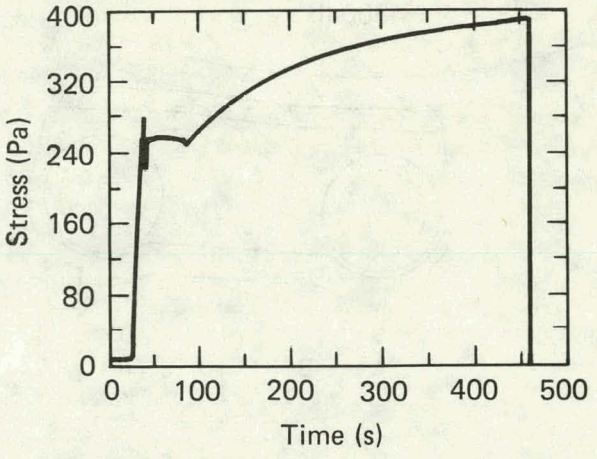

FIG. 7. The stress-time history of a test on a beryllium specimen being loaded at a constant strain rate.

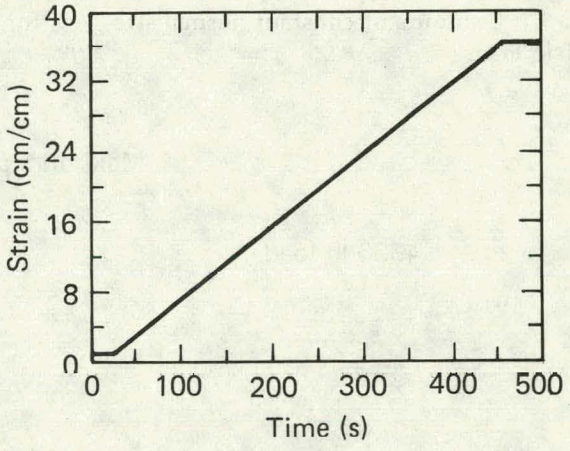

FIG. 8. The strain-time history of the test shown in Fig. 7. Note the uniform linear rate of change of strain throughout the test even during abrupt changes of stress.

beryllium specimen. The data show a linear rate of change in strain throughout the duration of the test, even at the same time the load-time history shows abrupt changes. Any extraneous uncontrolled test system influence on the test would have caused the strain-time history to become nonlinear at the instances the stress-time history was showing abrupt changes.

This strain control testing technique has been exploited in comparing the beryllium metal product

produced by two vendors. The technique can differentiate subtle variations in mechanical properties; e.g., one product when compared with the other exhibited a more abrupt deformation process as the material was strained through the initial or upper yield point. The ability to observe even the most subtle differences in the deformation process of competing candidate materials is important to the materials engineer in making the final selection.

(For further information, contact R.G. Scott, Ext. 2-7161.)

Determining the Strength Distribution of High Strength Fibers in a Bundle

One problem we are attempting to solve is how to determine the strength distribution of the individual filaments within a yarn of many filaments. The statistical distribution of fiber strengths is an important first step in understanding the failure processes and the reliability of composite material structures.

One approach in determining the characteristic strength distribution of the fibers is to separate single fibers from a piece of roving (or yarn) cut from a spool. Since the filaments are on the order of micrometres in diameter, they are very difficult to extract, mount, and test without accidentally damaging them. This process is very time-consuming and requires special equipment.

Our method to determine the strength distribution of the filaments does not involve testing individual fibers. We test a complete bundle. A load versus deformation curve is produced by testing the bundle in an Instron machine. This curve is then analyzed through comparison with a theoretical load versus deformation curve, which is a function of the parameters of the strength distribution of the fibers (see Fig. 9).

The present problem with our method is that friction and filament entanglement are not included in our multifilament model. These problems make accurate parameter estimates more difficult.

An effort is now being made to correctly model these problems. If successful, the cost of determining the strength parameters of individual filaments will be greatly reduced.

(For further information, contact J.C. Trinkle, Ext. 2-0723).

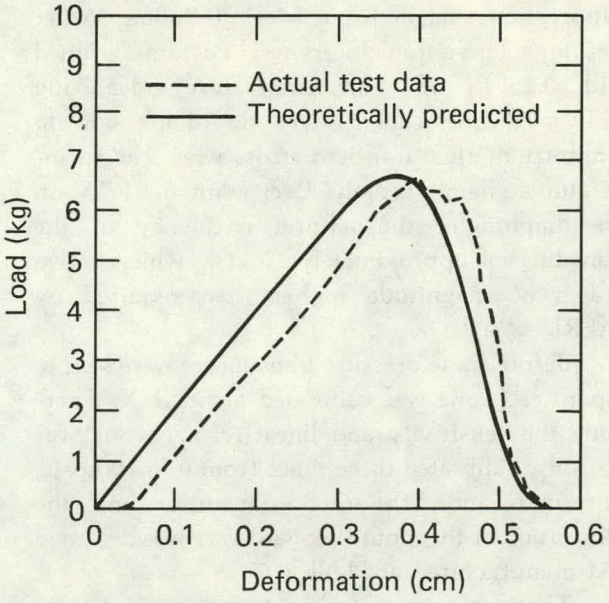

FIG. 9. Typical load-deformation curves for a bundle of 267 fibers tested at a constant rate of deformation.

Engineering Measurements Assistance Provided for the Japan Atomic Energy Research Institute

An experimental program on a full-scale multivent pressure-suppression system is in progress in Japan at the Tokai-Mura establishment of the Japan Atomic Energy Research Institute (JAERI). The results of this test program, which began in March 1979, are of interest to the U.S. Nuclear Regulatory Commission (NRC) in the areas of analytical model development and licensing of the U.S. Boiling Water Reactor using the Mark II containment design.

As part of the continuing technical liaison to the JAERI containment research testing (CRT) program for the NRC, the Engineering Measurements Section of the Engineering Sciences Division developed an assistance plan that provided 30 flush-diaphragm pressure transducers with complete mounting hardware for enhancement of the existing CRT wetwell measurement system.

The pressure transducers, which have a range of 0 to 100 psia, were manufactured by Senso-Metrics, Inc. These pressure transducers were designed by LLNL in 1976 for the 1/5-scale experiment we conducted for the NRC on the pressure

suppression system for a Mark I Boiling Water Reactor.[1] These transducers were custom-designed with 0.25 in. of room temperature vulcanizing (RTV) silicone rubber over the diaphragm to minimize thermal transient errors when fluid temperatures change rapidly. Even with the RTV on the diaphragm, the natural frequency of the transducer is approximately 15 kHz, which is two orders of magnitude higher than required by JAERI.

Before these pressure transducers were sent to Japan, each one was calibrated at LLNL to determine the sensitivity and linearity. Each one was statically calibrated three times from 0 to 100 psia. The installation for each transducer and the fabrication of the mounting hardware was designed and manufactured at LLNL.

These pressure transducers were not originally designed to be installed underwater as was necessary inside the wetwell. A special piece with a tube fitting welded to it was also designed and fabricated at LLNL. This piece was attached to the back of the transducer to seal out any water. The integral cable from the transducer ran through copper tubing attached to the tube fitting. The copper tubing from the pressure transducer terminated at junction boxes designed by the staff at JAERI, making a complete waterproof system.

Following delivery and installation of 25 pressure transducers in this system at JAERI by its staff, ESD personnel and E. W. McCauley of the Nuclear Test Engineering Division went to Tokai-Mura for the final installation and an end-to-end (ETE) *in-situ* calibration of the pressure transducers, which was completed in June 1981.

When experimental data are recorded, the accuracy is always in question; therefore, an ETE calibration is what all measurements engineers hope they can do for each test. The true error for a field test can't be specified by using the manufacturer's error for transducers and data acquisition systems, but must be determined from an ETE calibration. To perform an ETE calibration, the complete experiment is subjected to accurately known measurands, the data from each transducer are recorded, and the data are reduced from each transducer just as if it were an actual test. The complete instrumentation system from the transducer to the data acquisition system is used for this type of calibration. By comparing the data reduced from an ETE calibration to the accuracy of the known measurand, the accuracy of the experimental data can be determined.

The ETE calibration was done with approximately 23 ft of water in the wetwell. The suppression system was pressurized to a nominal 50 psi in 7 psi steps, both increasing and decreasing pressure. Data were recorded for each pressure step.

The accuracy of ETE calibrations depends on the accuracy of the instrument measuring the known input. For this calibration a pressure gauge, furnished by the staff at JAERI, was used. Its reported accuracy was ±0.15% of the full-scale reading, which is 72 psi.

The nonlinearity of the transducers from the ETE calibration was generally less than ±0.5% of full scale, and only three transducers had nonlinearities exceeding 1% or more. The sensitivities from the ETE calibration also compared very well with the sensitivities determined by LLNL. The average deviation in sensitivity between JAERI and the LLNL was only ±0.31% for all but three transducers, which had deviations greater than 1%.

We are pleased to have participated in a venture such as this. Measurements engineers the world over are confronted with the problem of determining the accuracy of experimental data. For most experiments it is not possible to perform an ETE calibration, and the accuracy must be determined by empirical methods.

By using the results of the ETE calibrations for the linearity of these 23 pressure transducers, we can state that these transducers should give valid data for JAERI.

(For further information, contact W.M. Shay, Jr., Ext. 2-7044.)

X-Ray Sensitive Vidicon Camera for Real-Time Imaging

The Nondestructive Evaluation Section (NDE) has obtained an x-ray-sensitive vidicon (XRV) camera to support weapon programs. The XRV camera is useful for radiographic inspection of small parts, with real-time display of the image on a television monitor. The x-ray-sensitive area is 9.5 by 12.5 mm. This results in a considerable magnification when the image is viewed on a 135-by-180-mm (9-in. diagonal) or larger television screen.

The XRV cameras are made by changing the light-sensitive vidicon tubes in the camera to an x-ray-sensitive type. The differences in the tube design are the use of a relatively thick lead oxide target in the x-ray-sensitive tube and a beryllium face plate to allow low energy x rays to enter. The NDE unit uses a Westinghouse tube in a Sierra Scientific two-piece vidicon camera. The two-piece camera design allows controls for focus, gain, gamma, pedestal, and polarity to be at the operator location. These cameras typically can resolve 15-μm gold wires in electronic parts. They do require a high input intensity of 100 R/min and are not usually used above 250 kVp.

To take advantage of the fine resolution of the XRV camera, the unit has been combined with a remote-control manipulator. The three-axis manipulator has left-right, up-down, and rotation stages. The two translating stages are accurate to 13 μm with 150 mm of total movement. The rotating stage is accurate to 0.01 deg. This stage mechanism allows the operator to scan over an entire part. With the rotating system, the part is observed at all angles. Where alignment along cracks is critical, the ability to rotate through all angles is an important advantage. Even with the good resolution of the XRV camera, there are cases where even a greater resolution, better contrast sensitivity, or a permanent record is desired. The XRV camera is then used to align the part in the ideal orientation and a film radiograph is taken. The use of the XRV camera saves considerable operating time and prevents wasted film.

The XRV camera, remote control stage, lead collimator, and a 150 kV_p x-ray head are shown in Fig. 10. The control console is shown in Fig. 11.

(For further information contact R.H. Bossi, Ext. 2-0431.)

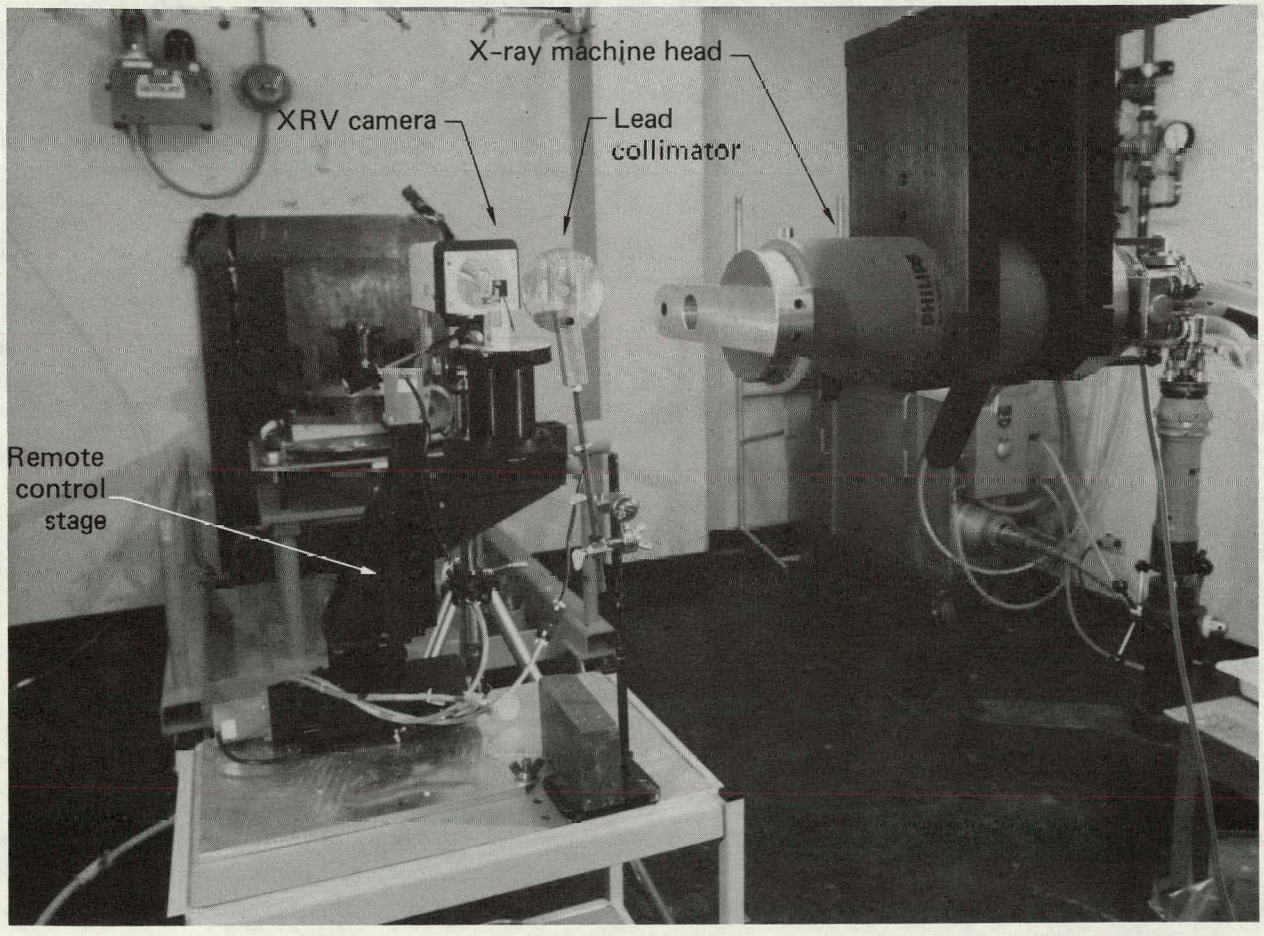

FIG. 10. The XRV camera, remote control stage, lead collimator, and 150-kV_p x-ray head inside the radiography cell.

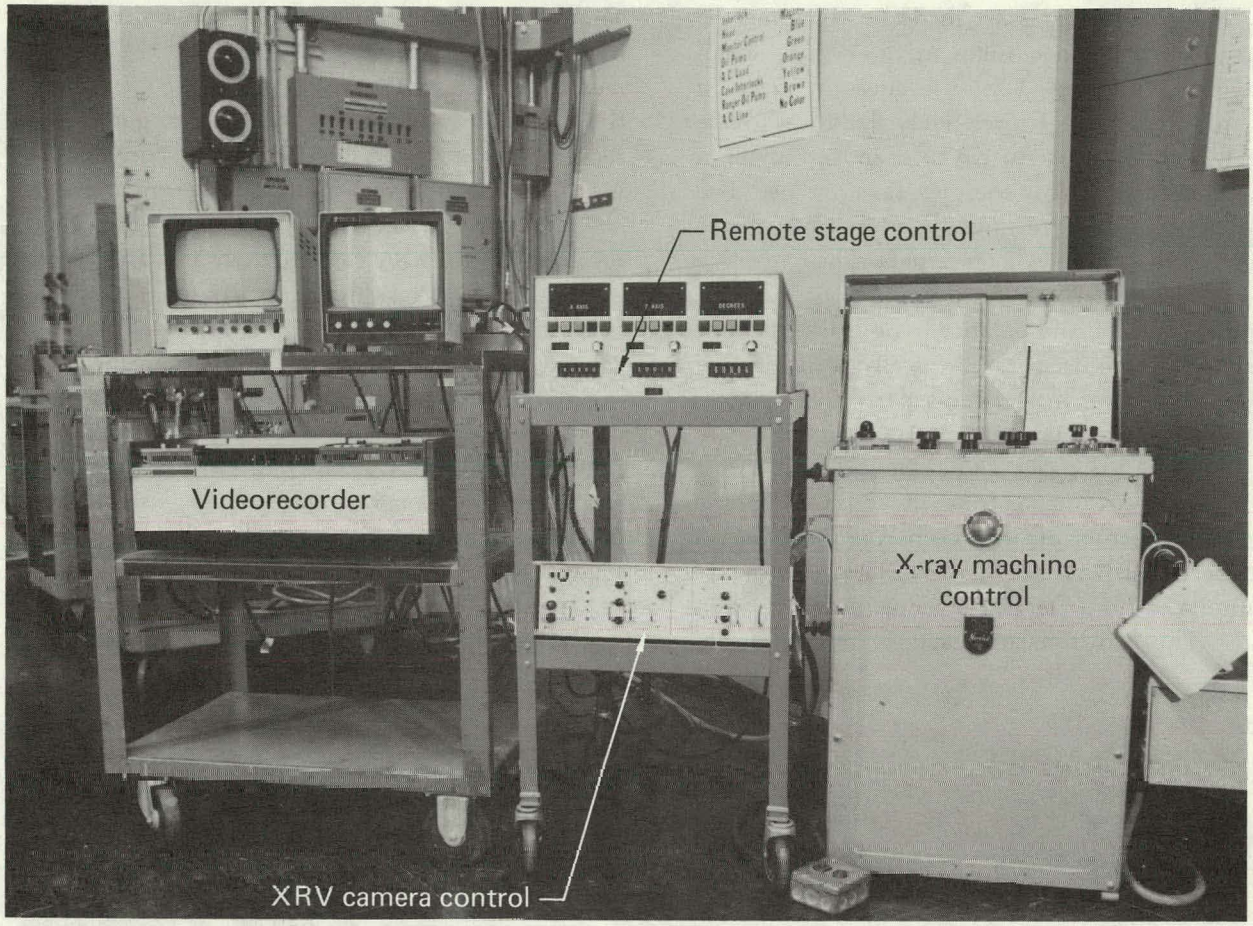

FIG. 11. Control consoles and video equipment outside the radiography cell.

Holographic Interferometry Used to Make Thermal Expansion Measurements of Detonators

Holographic interferometry (HI) is being used as part of the evaluation program on exploding bridge wire detonators. There are two objectives in the HI evaluation. The first is to measure the permanent displacement of the detonators after subjecting the part to a thermal cycle. The second objective is to measure the thermal expansion of the detonators.

Thermal testing of the live detonators was performed in the nondestructive evaluation laser laboratory. Figure 12 shows the optical arrangement and the mounting fixture used for testing the detonators. The optical arrangement allows direct viewing of the aluminum cup of the detonator through the window in an oven. The oven provides a ±0.2°C temperature control for both hot and cold (LN_2 supply) cycling.

To ensure that uniform heating is obtained, four thermocouples are used. One thermocouple monitors the temperature of the aluminum cup of the detonator, other thermocouples monitor the quartz rod, the aluminum shield, and the air. When a holographic exposure is made, all four thermocouples agree within 0.2°C of each other.

Double-exposure holography is used to record the displacement of the detonator. The permanent displacement is measured by taking the first exposure at 20°C and then thermal cycling the detonator to 70° for 10 min, then to −30°C for 10 min, and back to 20°C. The second exposure is then made. Any permanent displacement will be recorded as a fringe pattern. In order to measure the thermal expansion of the detonator, a double-exposure technique is used in which each exposure

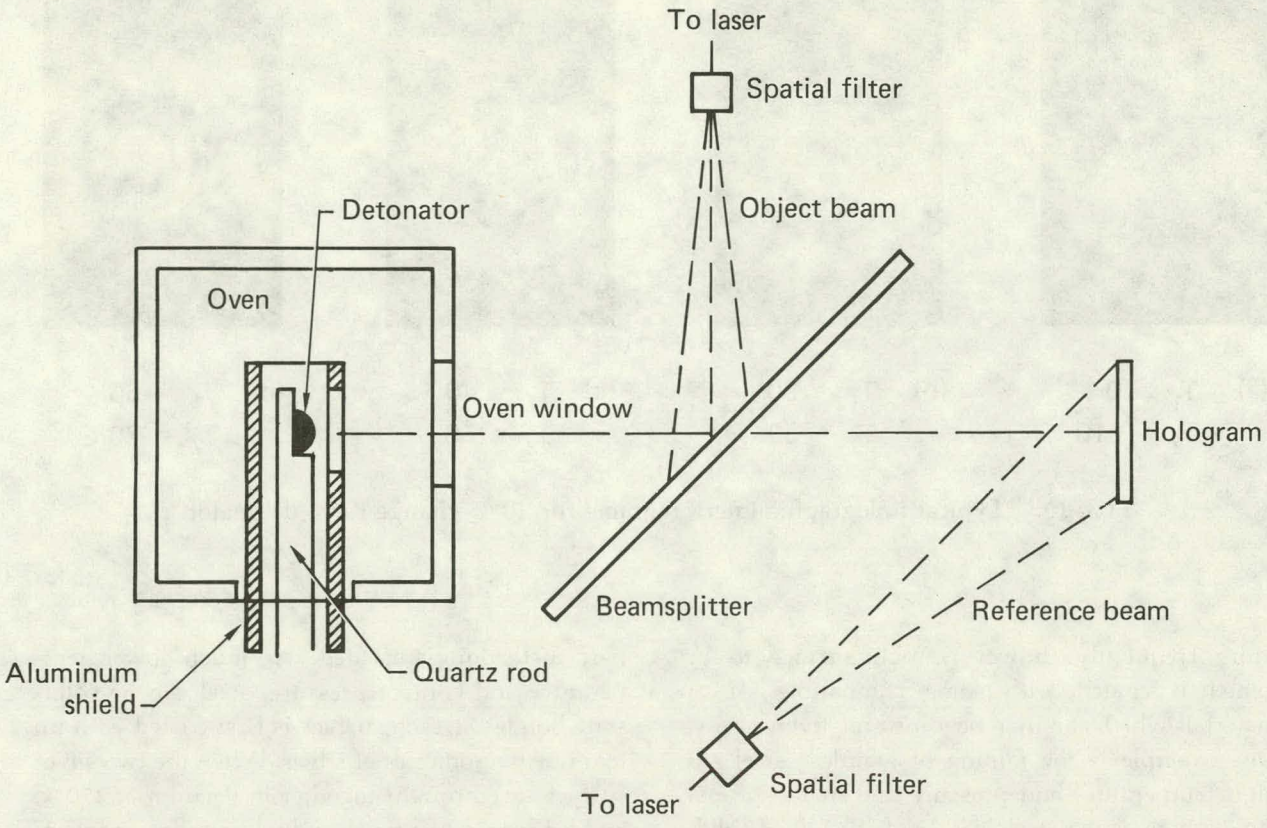

FIG. 12. Optical arrangement used for holographic testing of detonators.

is made at a different temperature. A 10° difference is used for these detonators.

In order to measure the accuracy of this system, a brass hemisphere was tested. The resulting displacement for a 5 and 10°C change was within 0.26×10^{-6} m (5×10^{-6} in.) of the calculated displacement using a handbook value for the coefficient of thermal expansion of brass.

Three detonators have been evaluated using the holographic procedure. The permanent displacement holography results indicated no permanent displacement has occurred.

Thermal expansion tests were run on the three parts from –30 to 70°C with 10-degree increments. Figure 13 shows typical holographic interferograms for one of the detonators. The results showed that for the temperature range between –30 and 30°C the fringe patterns were uniform [bull's-eye pattern, Fig. 13 (a) and (b)] and averaged five fringes or 1.28×10^{-6} m (50×10^{-6} in.) of displacement. Above 30°C the fringe patterns become nonsymmetric as indicated in Fig. 13, (c) and (d). Quantitative displacement of the detonator pole was determined from each of the holograms and is plotted on Fig. 14. The results of the holography measurements were compared with numerical calculations performed at LLNL by Art Shapiro, and with contact displacement measurements performed at Mound Laboratory. Figure 15 is a plot showing the results for the three measurements. Future work should be done to resolve the discrepancy between the measurement techniques.

(For further information, contact D.M. Boyd, Ext. 2-7971 or L.O. Hester, Ext. 2-7941.)

An Acoustic Microscope for Surface Characterization

Solid-state bonding is becoming an increasingly important joining technology. Some metals can be joined directly under the appropriate temperature, load, and atmospheric conditions.

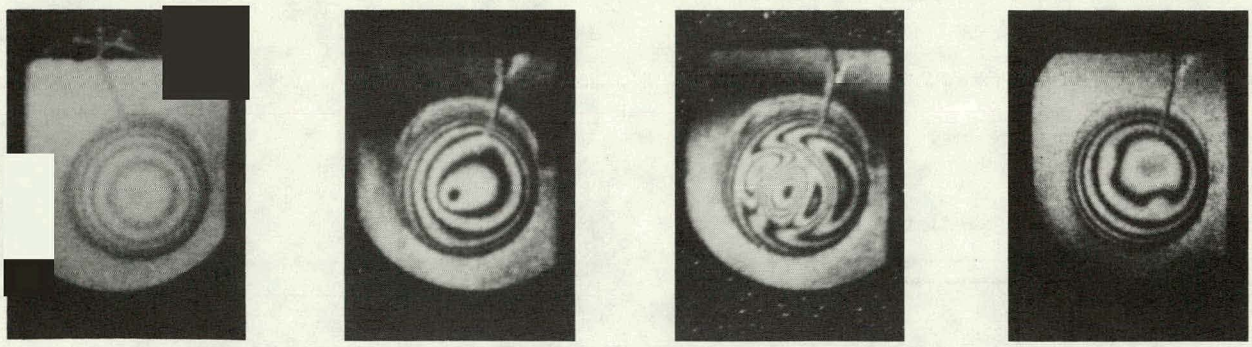

(a) $T_1 = 0$, $T_2 = -10$ (b) $T_1 = 20$, $T_2 = 30$ (c) $T_1 = 40$, $T_2 = 50$ (d) $T_1 = 60$, $T_2 = 70$

FIG. 13. Typical holographic interferograms for 10°C change for a detonator.

More frequently, however, each surface to be joined is coated with some compatible set of materials which can then be joined relatively easily. One example is the joining of stainless steel. At high temperature and pressure and in the proper atmosphere, some steels can be diffusion or solid-state bonded directly, that is, with neither surface coated. In order to obtain a strong bond, significant part distortion is needed. At much lower temperature and contact pressure, steel can be solid-state bonded if each surface is first coated with up to a few micrometres of silver. When the two silver surfaces are brought together in vacuum at 250°C and loaded up to a few hundred pounds per square inch, a joint having a strength up to 100 000 psi can be realized. Joint strength depends upon the

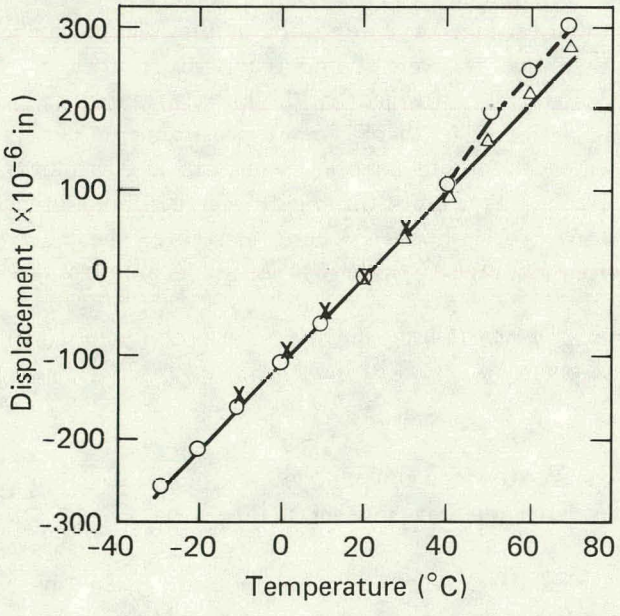

FIG. 14. Displacement vs temperature of pole for three detonators.

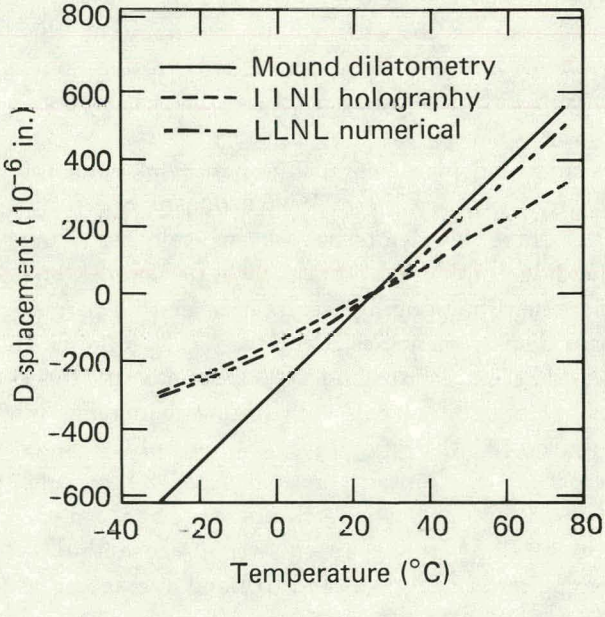

FIG. 15. Comparison of displacement measurement of the exploding bridge wire detonators.

coating thickness, coating uniformity, and the microscopic nature of the coating adhesion to the steel surfaces. Hence, it is important to have a nondestructive tool for the rapid microscopic characterization of coated surfaces.

In another area, precision machining technology using diamond and cubic boron nitride cutting elements can now produce machined surfaces of optical quality (a surface finish better than one-tenth wavelength of visible light can be achieved). At this level of surface quality, it becomes difficult to characterize these machined surfaces using visible light. Parameters of interest such as surface damage and texture must be inferred indirectly from optical measurements. Elastic waves provide subsurface as well as surface information and, hence, should be a valuable aid in quantitative machining diagnostics. One very promising method for achieving these surface characterization goals is wide-angle, focused-beam acoustic microscopy which utilizes both bulk and surface waves. Laboratory microscopes have been constructed elsewhere that operate in the transmission mode at frequencies up to 3 GHz where surface resolution comparable with optical microscopy has been obtained. At 400 MHz, by using a reflection microscope, it has been demonstrated that coating thickness and surface elastic properties, including residual stress, can be measured on both curved and flat surfaces. Problems of surface nondestructive evaluation are not very adaptable to the transmission mode, especially if one envisions the eventual rapid scanning of large areas. Consequently, we have chosen to develop reflection acoustic microscopy for use as a surface characterization tool. The coating thicknesses encountered in typical solid-state bonding operations dictate working in the frequency range of 5 to 200 MHz, while machined surface characterization will probably require frequencies in the range of 400 to 4000 MHz. Our initial developmental efforts have centered around establishing the capability to characterize metallic coatings up to 15-μm thick on metal substrates. This requires frequencies in the 5-to-50-MHz range.

Our initial thrust has been to explore materials and surface coating by means of the acoustic material signature (AMS) mode of the acoustic microscope. It has been shown that, through this technique, film thickness measurements may be performed nondestructively in a layered composite,[2] and it has been suggested that the texture of materials may be characterized in this way.[3] The aims of our program are to carry this technique to the point where on-line measurements may be made routinely, to explore the limits of the characterization mode and, in that pursuit, to develop a means of characterizing bond strength between layer and substrate. In this initial effort, measurements of dispersive surface acoustic wave (SAW) velocities were made and compared with the computed dispersion curves of several layered metal composites.

Actual computed dispersion curves are shown in Fig. 16. For an aluminum layer on beryllium, for example, the surface acoustic wave propagates initially ($h = 0$) at its predicted Rayleigh velocity. As the layer thickness increases, this velocity decreases asymptotically toward the aluminum Rayleigh velocity. Between these end points, the detailed variation in velocity depends on a number of physical and elastic parameters. These may be divided into three categories, the first of which relates to the bulk properties of the materials involved. Other factors depend on the manner in which the layers are fabricated or deposited, e.g., differential interface stress may be introduced. Finally, subsequent adhesion-related phenomena that affect bond strength may play a separate and distinct role in determining the precise shape of the dispersion curve. One of these combinations was experimentally investigated and is discussed in greater detail.

To obtain dispersive SAW velocity data, a series of beryllium disks were metallized on one half of each face with aluminum films of thickness 1, 2, 4, 7, 8.31, 9.29, 10, and 12.9 μm. The metal deposition was accomplished by electron-beam vacuum evaporation, and the film thickness was ascertained by a quartz frequency monitor as well as by weight determination. The corresponding SAW velocity results from these specimens are shown in Fig. 17, superimposed on the predicted curve that was computed from the known property values.

The differences between computed and measured Rayleigh velocities as well as the SAW velocity dispersion are quite small. Though gratifying, this agreement is surprising in view of both the widely varying experimental conditions (between

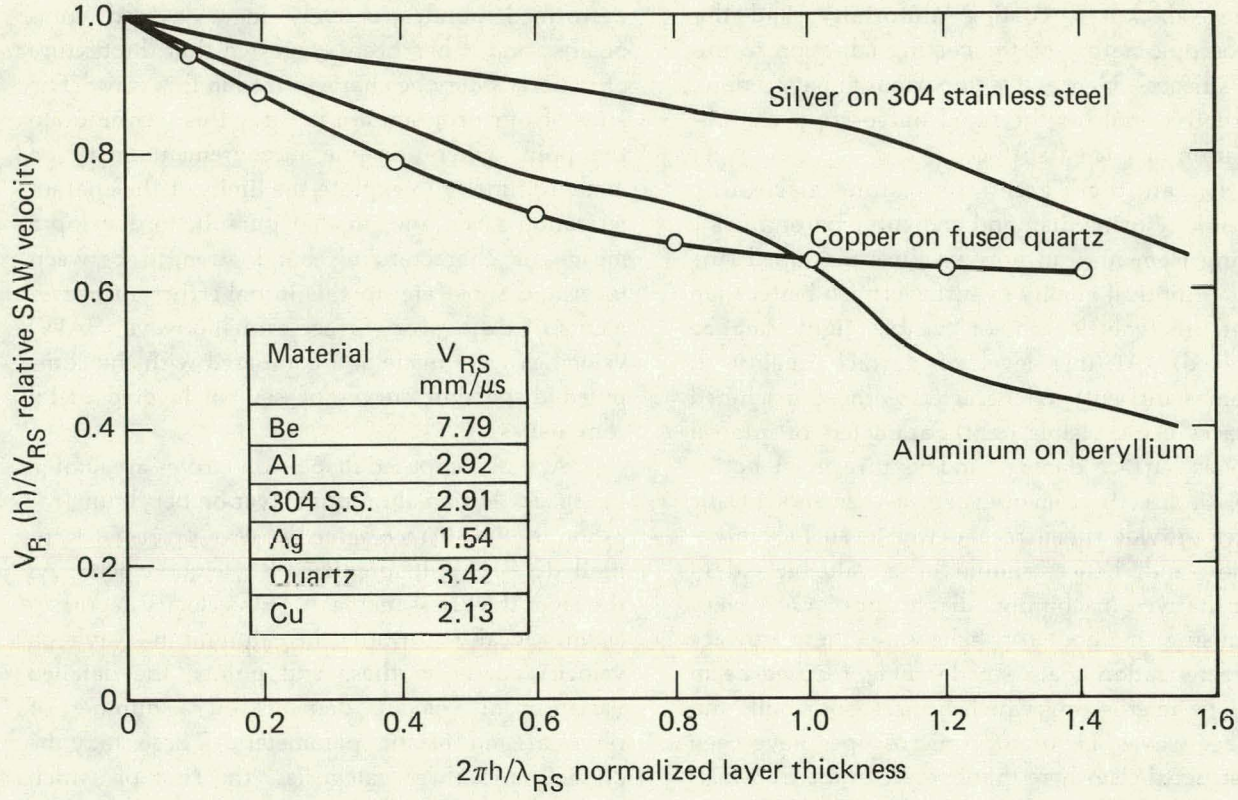

FIG. 16. Normalized SAW velocity dispersion curves for several layered systems computed using known constants.

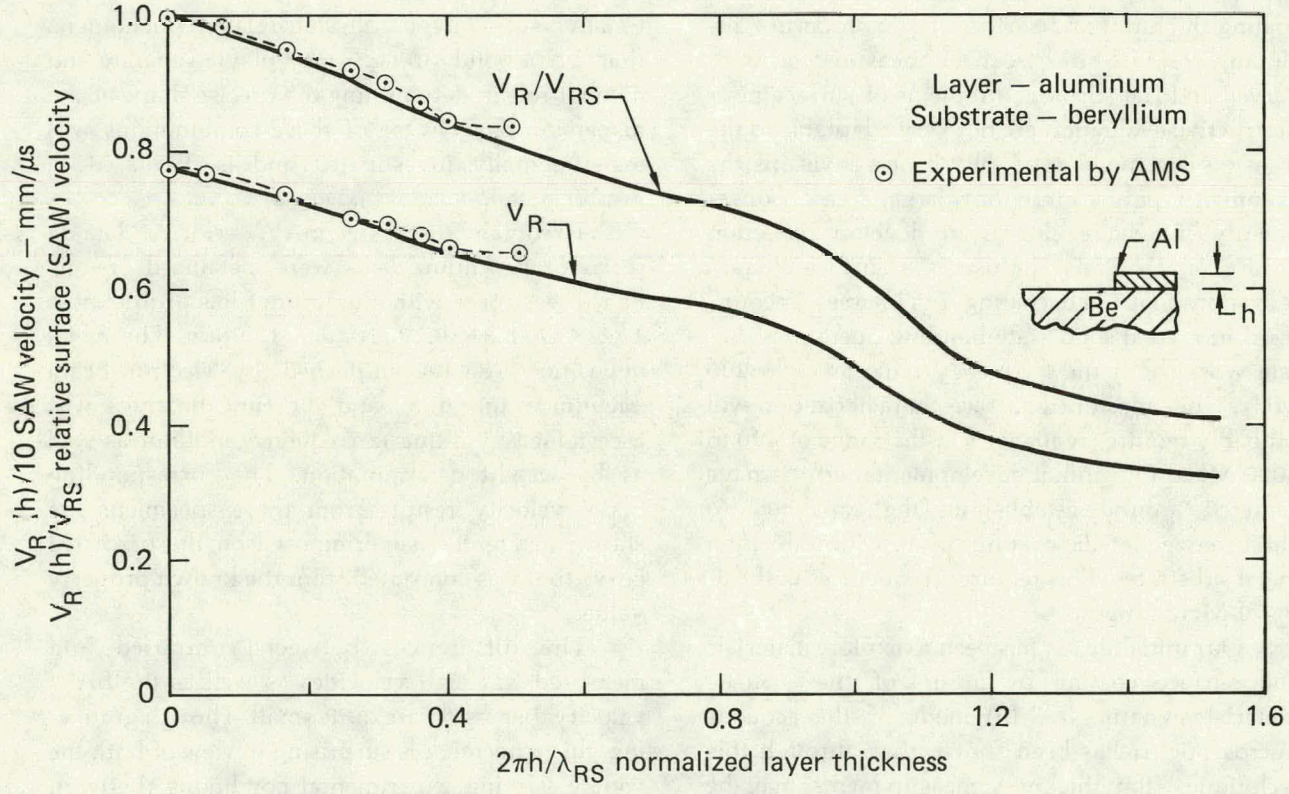

FIG. 17. Dispersive SAW velocity for an aluminum layer on beryllium substrate: a comparison between computed and experimental results.

this and the prior work)[3] and the simple ray model that forms the basis for the AMS measurement interpretation.

Although these results are preliminary, they seem to suggest that the AMS technique and, therefore, the model are both frequency-independent and lens-geometry invariant. Hence, the recently suggested effects of large convergence angles appear to pertain primarily to the near focal-zone behavior.[4]

(For further information, contact B.W. Maxfield, at Ext. 2-7969.)

New Filament Winding Machine Begins Production

A new precision filament winding machine has been brought on line for the production of spherical test vessels. Parts ranging from less than 75 mm (3 in.) to 4 mm (15 in.) in diameter and weighing as much as 45 kg (100 lb) can be handled by the machine, which is sturdily constructed. The ability of the machine to locate fiber to within 0.05 mm (0.002 in.) of true position on a helical path whose pitch may be from 0.025 mm (0.001 in.) to 13 mm (0.500 in.) per turn is nearly an order of magnitude improvement on standard filament winding machines. Designed to be operated by an LSI-11 microcomputer supervisor, the machine also has extensive manual input controls.

Difficulties encountered by the manufacturer in meeting specifications required a team of LLNL engineers and technicians to assist in the design and qualification of this state-of-the-art machine. The most severe difficulties arose in the area of control. The specifications called for a stand-alone machine with microprocessor supervision; however, problems associated with the proper correlation of sphere movements forced early control fixes to require increased interaction of the LSI-11 system in the control process.

As a result of interactions with the LLNL team, the machine was reduced in complexity, both mechanically and electronically. The number of circuit boards in the controller was reduced by a factor of 5. Upon delivery of the machine, Ken Waltjen and Dave Conrad of the Electronics Engineering Department took responsibility for setting up a functional, high-precision control system that used the existing display drivers and interface circuits supplied by the manufacturer. Bob Sherry and Leon Newton of the Mechanical Engineering Department then aligned the machine axes to within 0.13 mm (0.005 in.) of their theoretical spherical locations, removed all lost motion in the drive trains, and checked out the positional accuracy and repeatability of the complete machine and controller. The success of the LLNL control system allowed the LSI-11 computer to assume a supervisory role once again.

The prove-in consisted of a number of successful attempts to make a spherical vessel with a winding pattern that was sensitive to positional errors as small as 0.05 mm (0.002 in.) Over 80 attempts were made, and many subtle problems in the mechanism, the controls, or in the computer program were solved. Initial runs were made with dry fiber on dummy mandrels to ease the problem of recovery of the mandrels without damage. After basic positional problems were settled with the dry fiber, wet winding was begun, using an LLNL-designed meter-mix resin delivery system to accurately control the amount of resin applied to the fiber. Forty-one parts were wet wound and evaluated before the process was proved in late August 1981.

Production of test vessels to date on the new filament winding machine (shown in Fig. 18) has shown good control of the processing parameters, better than that observed in the past. With the type of control observed, it will be possible to do a much better job of making precision test specimens that will lead to a better understanding of fiber composite structures.

As understanding of the materials science aspects of composites increases, light-weight pressure vessels with remarkable strength and durability may come into routine usage. Research on the interface properties of various fiber/matrix combinations, the fracture mechanics of composites, and computer code development of optimized winding patterns for various applications will be key elements in the realization of increased performance in these materials.

(For further information, contact R.J. Sherry, Ext. 2-8129.)

FIG. 18. The new sphere winder with sphere arm and spindle at right, resin mix and filament delivery system in background, and control system at left. Participants in development of the machine are (left to right) Dennis Silva and Ken Waltjen, both of the Electronics Engineering Department, and Leon Newton and Bob Sherry, both of the Mechanical Engineering Department.

Precision Machining of Plutonium Parts

During the course of weapon design and development, several underground shots may be required to test design concepts and weaponization features. One of the several missions of LLNL's Plutonium Facility is to cast, machine, inspect, and assemble plutonium components for downhole testing at the Nevada Test Site. To more effectively machine the close-tolerance parts required in most of the devices, the Plutonium Facility acquired an Excello 905 numerically controlled lathe that had survived the 1969 fire at the Rocky Flats Plant. It had been used at Rocky Flats for machining plutonium parts and was, therefore, highly contaminated with plutonium oxide dust. Appropriate packaging and transportation from Rocky Flats to LLNL proved to be a meticulous task. Setting the machine up in the new addition to the Plutonium Facility was similarly difficult in that the lathe and glovebox enclosure are large and were highly contaminated.

Materials Fabrication Division (MFD) personnel calibrated and tuned the Excello to where it would reliably machine plutonium parts to tolerances of ±25 μm (0.001 in.). Since its installation in the Plutonium Facility in 1978, it has been used to machine several plutonium device components often to tolerances approaching ±12 μm (0.0005 in.).

The FY82 nuclear test schedule is planned to test concepts and devices that will require some plutonium components machined to tolerances of

±6 μm (0.00025 in.). That kind of tolerance in the size of plutonium parts being considered has been beyond the capability of the B332 Excello (and, in fact, not easily achieved by any Department of Energy machining facilities for plutonium). The B332 Excello has been carefully and thoroughly cleaned, calibrated, and "tuned" (again by MFD personnel) to where it is now repeatable to ±0.50 μm (0.000020 in.) on a 130-mm (5-in.) disk check. Incorporating a means of computer correction to subtract repeatable errors will then allow the B332 Excello to produce parts to the required accuracies. Although the B332 Excello is an old machine and should be replaced before too long with newer state-of-the-art equipment, it appears it will indeed be reliably able to meet the ±6-μm (0.00025 in.) tolerance parts required to meet the FY82 nuclear test schedule.

(For further information, contact W. Haslam, Ext. 3-1745.)

Route Profile Analysis to Determine Suitability of Electric Postal Delivery Vehicles

An instrumentation system and computer program were developed that allow the U.S. Postal Service to determine which postal routes are suitable for electric delivery vehicles. The instrumentation system provides the route data. The route data and electric vehicle characteristics are used in the computer program to calculate the energy and power requirements for the particular route. The performance characteristics of electric vehicles are contained in an input data file to the computer program. At present two electric vehicles, American Motors DJ5E and DJ5E(GE), are included.

The instrumentation system is designed for use during normal mail delivery with gasoline powered vehicles. This system is powered by the vehicle battery. Minimum operator interaction and inexpensive maintenance-free sensors are featured in the design. Route grade is determined from a gravity-sensitive sensor (pendulum) measurement corrected for vehicle acceleration by differentiating a measurement of the distance traveled. The value of road grade obtained in this manner is in excellent agreement with civil survey data. The distance transducer utilizes an electro-optical sensor and a rotating disk driven by the speedometer gear to provide a resolution of 3 mm. A microprocessor provides timing and data management. Data are recorded on a cassette tape. Pendulum data are sampled once a second. Distance data are sampled once a quarter second. The use of complementary metal oxide semiconductor electronics avoids difficulties created by the high electrical noise environment in the vehicle.

The instrumentation system is compact and readily installed or removed in a "survey" delivery vehicle. Calibration requirements are minimal. The only requirement is to enter a distance pulse count number (obtained by driving the survey vehicle over a short measured distance). The calibration number is valid until the instrumentation system is removed and installed in another vehicle. Since postal delivery routes are closed, i.e., they begin and end at the same location (elevation), any bias error in initial orientation of the pendulum can be reduced to zero during data reduction. After the tape is inserted by the operator at the beginning of a run, and identification information is keyed in, data are automatically recorded in 50-s blocks. If the vehicle is not in motion during a data block period, no data are recorded for that period. On completion of the route, the tape is sent to a central computer (PDP-11) where it is read in as input to the electric vehicle simulation program CARA.

Route data on the cassette tape are reduced in subroutine CARAIN which converts the binary data to engineering plots of time, speed, acceleration, road grade, and elevation vs distance. Output plots of speed and elevation vs distance for a surveyed mail route are illustrated in Figs. 19 and 20. Despite the nonuniform speed in this example, the correct elevation profile was obtained.

The program CARA determines whether a specific electric vehicle can complete the route, subject to energy and power limitations. Output plots of battery-power and battery state of charge vs time are provided. If battery power or motor torque limitations are exceeded, this fact is noted, but otherwise disregarded, as the calculation proceeds to the end of the route or to a set minimum value of battery state of charge. Battery state of charge is determined by a first-order-system method developed at Purdue University; the results compare well with battery test data. The predicted battery state of charge for the American Motors DJ5E

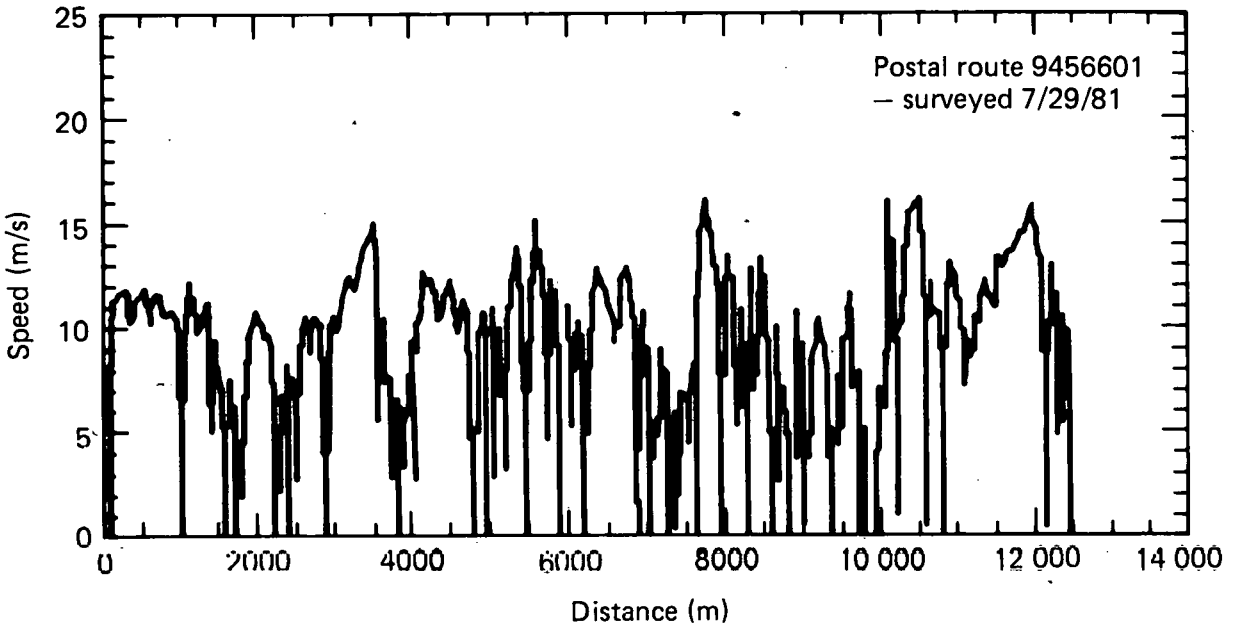

FIG. 19. Speed vs distance as determined with the instrumentation system for Postal Route 9456601.

vehicle is shown in Fig. 21 for the route previously mentioned.

The simulation program CARA was validated by comparing performance predictions with test data obtained with the DJ5E electric postal delivery vehicle. Acceptance test results indicate that a useful route profile analysis system has been developed. The system appears to be versatile and adaptable to other vehicle instrumentation applications.

(For further information, contact C.E. Walter, Ext. 2-1777, or M.K. Kong, Ext. 2-6425.)

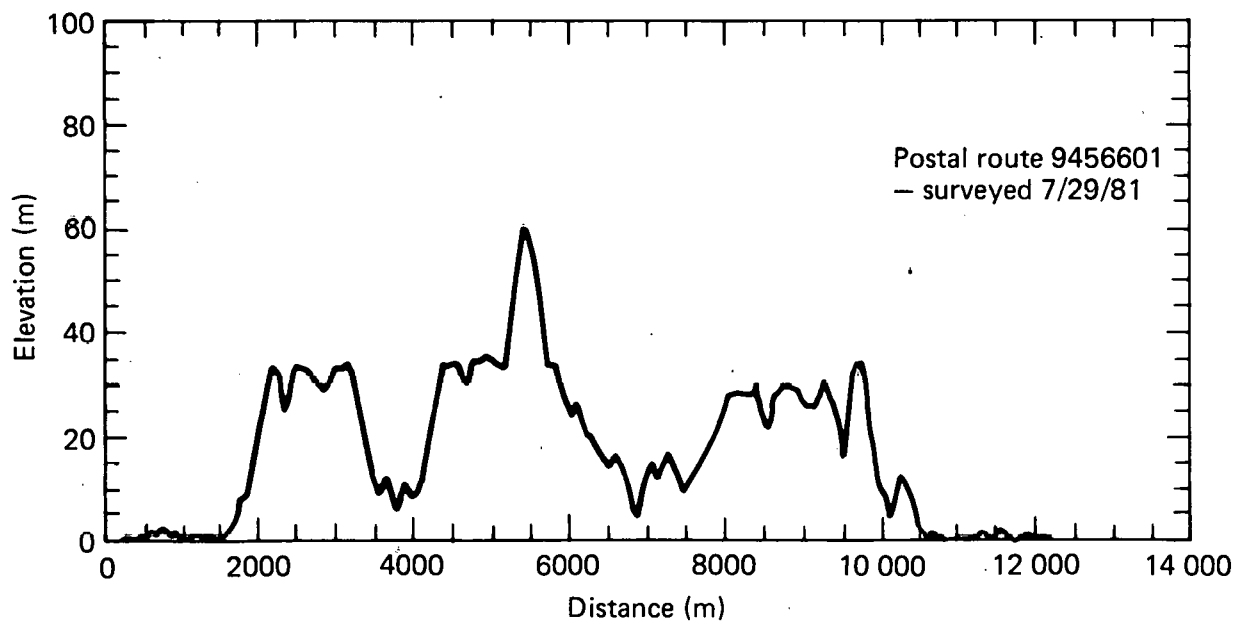

FIG. 20. Elevation vs distance for Postal Route 9456601 calculated from pendulum and distance data recorded by the instrumentation system.

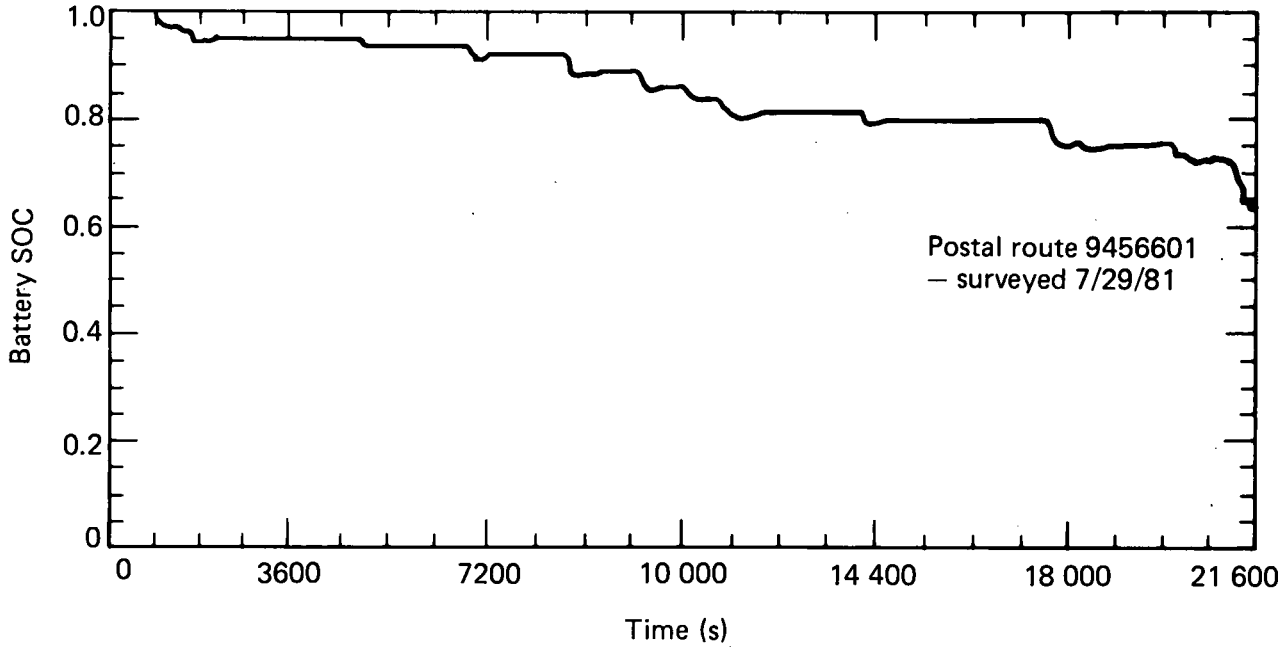

FIG. 21. Battery state of charge (SOC) predicted by CARA for Postal Route 9456601 if the American Motors DJ5E electric vehicle was used.

References

1. W. M. Shay, W. G. Brough, T. B. Miller, *Instrumenting a Pressure Suppression Experiment for a Mark I Boiling Water Reactor—Another Measurements Engineering Challenge,* Lawrence Livermore Laboratory, UCRL-52314 (1977).
2. R. D. Weglein, "Acoustic Microscopy Applied to SAW Dispersion and Film Thickness Measurement," *IEEE Transactions on Sonics and Ultrasonics,* **SU-27**, No. 2, March 1980, pp. 82–86.
3. R. D. Weglein, "Metrology and Imaging in the Acoustic Microscope," *Scanned Image Microscopy,* E. A. Ash, Ed. (Academic Press, London, 1980), pp. 127–136.
4. C. J. R. Sheppard and T. Wilson, "Effects of High Angles of Convergence on V(z) in the Scanning Acoustic Microscope," *Appl. Phys. Lett.* **38**, No. 11, June 1981, pp. 858–859.

MAGNETIC FUSION ENGINEERING DIVISION

The Magnetic Fusion Engineering Division (MFED) supports the LLNL physics programs in four principal areas:

- Magnetic fusion energy (MFE) confinement experiments.
- MFE development and technology.
- Particle beam development.
- High energy physics.

The four areas share a common technological base, although their individual goals differ greatly. Each area requires support from essentially all mechanical engineering disciplines and from specialists in normal and superconducting magnetics, cryogenic systems, vacuum systems, high-voltage components, and nucleonics.

Our role in the MFE confinement experiments is to provide systems engineering and to design and fabricate mechanical hardware. The research in magnetic mirror confinement of nuclear fusion reactions is expected to lead to utilizing deuterium, an isotope of hydrogen present in sea water, as a nearly inexhaustible energy source. The major confinement experiments are the Tandem Mirror Experiment (TMX), Beta II (formerly 2XIIB), and the Mirror Fusion Test Facility (MFTF).

In MFE development and technology, our mission is to develop the technical base and engineering skills necessary to meet future needs of magnetic confinement systems. Our active programs are the development of a multifilamentary Nb_3Sn superconductor, high-vacuum technology, and fusion reactor studies. Basic research and development are emphasized to lay the groundwork for future fusion experiments.

The particle beam development program, funded by the Defense Advanced Research Projects Agency (DARPA), involves building high-current, high-voltage, electron accelerators. Such accelerators are of interest for basic physics research and in the weapons community. The present program calls for developing two accelerators, the Experimental Test Accelerator (ETA) and the Advanced Test Accelerator (ATA). The ETA program is the predecessor to the ATA, and it will generate the technology data base to build the 10-kA, 50-MeV ATA machine.

Our role in high energy physics is to provide tools with which to pursue fundamental understanding of energy and matter. Technical support is provided for experiments performed at the 100-MeV electron linear accelerator (Linac)—three 400-keV dc high-current accelerators, a 3-MeV electrostatic accelerator, a 6-MeV tandem electrostatic accelerator, and a 76-cm cyclotron.

The MFED consists of seven project groups plus a division office. Current work and recent accomplishments of some of these groups are summarized in the following pages.

(For further information, contact D.K. Fisher, Ext. 2-6750.)

First Pair of MFTF Magnet Coils Nearing Completion

The mission of the Magnet Systems group for the Mirror Fusion Test Facility (MFTF) is to design, fabricate, and test 22 large superconducting coils. There are two A-cell coils, two Yin-Yang coil pairs, two transition coils, and 14 solenoid coils. When completed, these coils will constitute the world's largest collection of superconducting coils. The Convair Division of General Dynamics is the subcontractor for design and fabrication of the A-cell and the transition and solenoid coils.

Our most recent project, now nearing completion, includes installing the first pair of Yin-Yang coils in its vacuum vessel and making fluid and electrical hookups for it. This pair of Yin-Yang coils can be used to test the design of the magnets before they are actually built. Testing is scheduled before the end of 1981 during the technology demonstration of the MFTF project. The final phase, now in progress, includes checking out the instrumentation and looking for possible helium leaks in the piping and thermal radiation shields. The radiation shields consist of over 300 stainless steel panels that have liquid nitrogen flowing through them. Technicians in the Magnet Systems Group will install the panels on the outside of the structural case.

(For further information, contact T.A. Kozman, Ext. 3-0312.)

Engineering and Construction of the Advanced Test Accelerator Is on Schedule

Members of the Advanced Test Accelerator (ATA) project are responsible for designing and constructing a linear induction accelerator. Electron beam propagation will be studied and the existing theory of beam propagation tested using this accelerator. Critical experiments will be conducted in a variety of gases and in air to determine what beam parameters lead to stable and controllable self-focused propagation. The accelerator performance characteristics required to conduct these experiments are:

- Current 10 kA
- Energy 50 MeV
- Pulse length 70 ns, FWHM (50 ns flattop)
- Repetition rate 1000 pps maximum for a 10-pulse burst every 2 s

The accelerator consists of a 2.5-MeV injector and 190 accelerator units. Each unit adds 250 keV of energy to the beam and has its own pulse power system, accelerator cavity, and magnet system. Timing and control are critical issues for successful operation.

The ATA project is a vital part of the LLNL Charged Particle Beam Program supported by the Defense Advanced Research Projects Agency through the Naval Surface Weapons Center under the Chair Heritage Program in the U.S. Department of Defense.

The ATA project is just ending its third year and is progressing as originally projected. The main building at Site 300 was fully occupied by December 1981. Assembly lines for the pulse power units were established at a 20 000-ft^2 facility being leased on Vasco Road just south of LLNL, and the electronic switch chassis, power supplies, and racks are being preassembled in Building 438 prior to being shipped to Site 300.

All the accelerator components are in various phases of assembly or installation. The prototype test stand is still in operation and provides final information on materials in the pulse power chain, which will improve system lifetime under high electrical stresses. Testing has demonstrated reliability of all components in the power conditioning chain and in the accelerator by accumulating over 7 million pulses at varying repetition rates. ATA has achieved the following parameters:

- Full voltage for each 250-kV module having 10^5 pulses at 350 kV.
- Pulse risetime less than 20 ns.
- Voltage flattop of 50 ns.
- Pulse width at FWHM of 70 ns.
- Spark-gap jitter less than 1 ns.
- Repetition rate greater than 1000 pps.

These data make us very confident that the requisite performance characteristics for the critical experiments will be achieved, and there will be sufficient flexibility in much of the system to operate it at higher levels.

(For further information, contact L.W. Pollard, Ext. 2-1474.)

Reactor Studies

The primary goal of the magnetic fusion program at LLNL is to develop magnetic mirror devices for the economical production of power. In addition, production of fissile fuel and synfuel is being investigated. Although at this stage in the program our experimental devices operate only for short pulses and consume more energy than they produce, we are beginning to design commercial power-and-fuel-producing reactors. We study these future machines for two reasons. One, we can judge how close we are to the goal and, thus, give guidance to our current experimental program. Two, we can identify critically needed technological systems (superconducting magnets, for example).

To achieve high power density in a tandem mirror fusion reactor (TMR), we must obtain stable confinement of a high-density central cell plasma. The end plugs used in the Tandem Mirror Experiment (TMX) generated the necessary electrostatic fields to confine central cell plasma by increasing the plug plasma density, but for reactors this strategy is impractical. For TMRs, the confining potential must be enhanced by heating plug electrons that are insulated from the electrons in the central cell by a thermal barrier. The thermal barrier is a region of reduced magnetic field, plasma density, and plasma potential between the central cell and the end plug.

During 1981, a major effort in designing a magnetic fusion reactor at LLNL was devoted to

comparatively evaluating end plug configurations for TMRs with thermal barriers. Three different configurations—A-cell, modified-cusp, and axi-cell—were considered. In each case we designed the end plug magnets, assessed their physics performance (MHD stability, adiabaticity, etc.), and estimated their cost. We coupled each end plug with a 150-m-long central cell producing 3500 MW of fusion power at a first-wall neutron loading of about 2.3 MW/m^2. We used zero-dimensional fluid models of the tandem mirror plasma to determine the plasma parameters and the end plug power requirements [neutral beams and electron cyclotron resonance heating (ECRH)]. Cost estimates were made for the neutral beams, ECRH, central cell, end-leakage direct converter, reactor building, and balance-of-plant (BOP). A power balance analysis yielded the gross electrical output and the net electrical output for each case. Finally, the cost of power (dollars per kilowatt) was calculated for each case by dividing the total direct capital cost by the net electrical output.

In addition to the cost of power, several more subjective figures of merit were considered in our comparative evaluation. These included the degree of dependence on undeveloped technologies and on uncertain physics and of the relation of the concept to the ongoing tandem mirror program. These considerations led us to select one of the end plug configurations, the axi-cell, for further study.

Major studies are also under way on fissile (fusion breeder) and hydrogen (synfuels) production applications of fission. In the fusion breeder project, we are concentrating on fission suppressed blankets that produce fissile fuel (^{233}U or ^{239}Pu) while minimizing *in situ* fission. In the synfuels project, we are studying thermochemical systems. Both the fusion breeder and synfuel projects are joint efforts. For example, other organizations participating in the fusion breeder project are: TRW, Westinghouse, General Atomics, and Oak Ridge National Laboratory.

(For further information, contact G.A. Carlson, Ext. 2-6728.)

Superconducting Magnet Development

A study of the overall concept of the Tandem Mirror Next Step (TMNS) was reported in the July 1, 1981 edition of the Mechanical Engineering Department Technical Review. We anticipated that it would be possible to use a Nb_3Sn superconductor for the large Yin-Yang magnets, and the maximum field would be about 12 tesla. The dimensions of the magnet, its total current, and its field strength are all much higher than those of the Mirror Fusion Test Facility (MFTF) magnets, resulting in very much larger electromagnetic forces and stresses. In view of this and the fact that Nb_3Sn is a brittle material with limited strain performance, a more detailed study of the winding itself was undertaken. The work was carried out in conjunction with the Convair Division of General Dynamics.

If the winding is considered as a single section, the cumulative transverse magnetic-pressure buildup, as each turn presses against its neighbor, is approximately six times that encountered on the MFTF Yin-Yang magnet. In addition to this, the longitudinal or tensile force in the conductor is also very much higher. In the case of MFTF, the pressure is just about at the acceptable limit; beyond this, the insulation between turns of the coils would begin to produce indentations in the annealed copper of the conductor. Therefore, we are making two major modifications in the design for the TMNS magnet to overcome this problem. These are:

- The stabilizer, into which the superconducting core is being soldered, is cold-worked to increase its yield strength by a factor of 4.
- Steel structure is being incorporated in the winding itself to limit the maximum transverse pressure to an acceptable value. In effect, the Yin-Yang coil pair is made up of a set of four separately wound sections assembled in a common structural case. This results in an assembly of nested coils (see Fig. 1).

The operating current of the conductor is 15.6 kA. This current is considerably larger than that in MFTF; however, the design prevents the conductor from being damaged during a quench when the large amount of stored magnetic energy, 1.3×10^{10} J, is discharged. The rectangular conductor (1.656 × 2.791 cm) has no internal cooling channels. Consequently, manufacture is simplified and maximum strength can be achieved. However, some means of improving the heat-transfer characteristics to the liquid helium is necessary to obtain cryostatic stability, and we propose to cool this magnet in superfluid helium at 1.8 K and 1.2 atm. To operate superconducting magnets under these

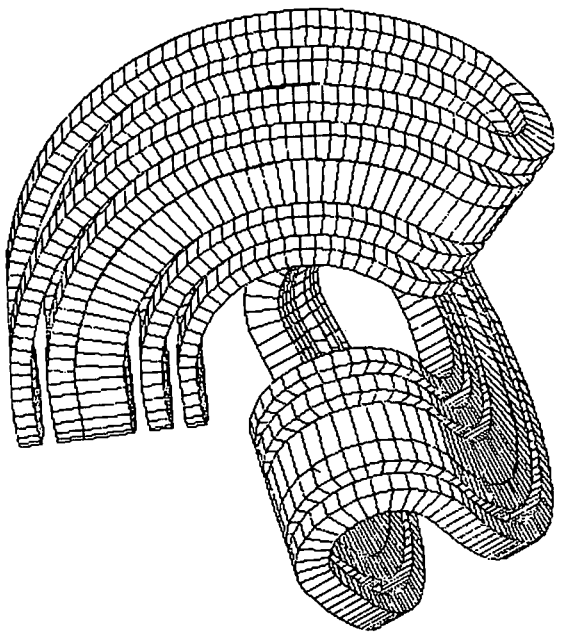

FIG. 1. Schematic of the nested Yin-Yang coils of the TMNS.

conditions is a relatively new development, but the method shows great promise and enables us to use higher heat-transfer rates. In this instance, the heat-transfer rate is 0.8 $W \cdot cm^{-2}$, compared to 0.18 in the MFTF Yin-Yang coils.

Overall, we can conclude from this design study that it should be possible to design and build the larger 12-tesla Yin-Yang coil system envisaged for TMNS using a strengthened conductor, additional substructure in the winding, and subcooled superfluid helium.

(For further information, contact D.N. Cornish, Ext. 2-6718.)

Plasma Diagnostics for the Mirror Fusion Test Facility Are in the Conceptual Design Stage

The mission of the Plasma Diagnostics group of the Mirror Fusion Test Facility (MFTF) is to plan, design, and fabricate the plasma diagnostics for the facility. Our efforts, at the physics level, to finish the MFTF requirements proceed concurrently with our efforts to work out conceptual designs. In addition, we started to generate detailed cost estimations.

Twelve types of instruments for diagnostics are currently envisioned for the MFTF startup operations. The total instrument system can grow and incorporate the anticipated 23 types (called the "basic set") needed to achieve all the MFTF goals for plasma diagnostics measurement.

(For further information, contact S.R. Thomas, Ext. 2-5250.)

Accomplishments Reported for Mechanical Systems of the Mirror Fusion Test Facility-B

The Mechanical Systems Group reports that construction is progressing on schedule for the Mirror Fusion Test Facility (MFTF-B). The group has completed the acceptance test for the east helium refrigerator and has succeeded in testing the east vacuum vessel and vacuum system to 10^{-7} Torr. The east helium refrigeration capacity is 3075 W and the helium liquefaction rate is 600 l/h. When completed, the total MFTF-B helium refrigeration capacity will be 11 075 W and have a liquefaction rate of 2300 l/h.

Overall responsibilities of the Mechanical Systems Group for the MFTF-B cover the cryogenic system, the vacuum vessel system, external and internal vacuum systems, and the long-pulse 30-s neutral beamline system.

(For further information, contact W.H. Sterbentz, Ext. 2-1494.)

Analysis of Neutron and Gamma-Ray Effects in the Mirror Fusion Test Facility-B

The Tandem Mirror Test Facility being constructed at LLNL is expected to produce 2.3×10^{16} D-D fusion neutrons (at 2.5 MeV) per second while operating (Fig. 2). According to design specifications, the facility should produce plasma for an average of 3000 s per week during each 13-wk experimental period. The effects of the neutrons on the experimental apparatus (i.e., heating, displacement damage, and radioactivation) were predicted using a three-dimensional computer model of the

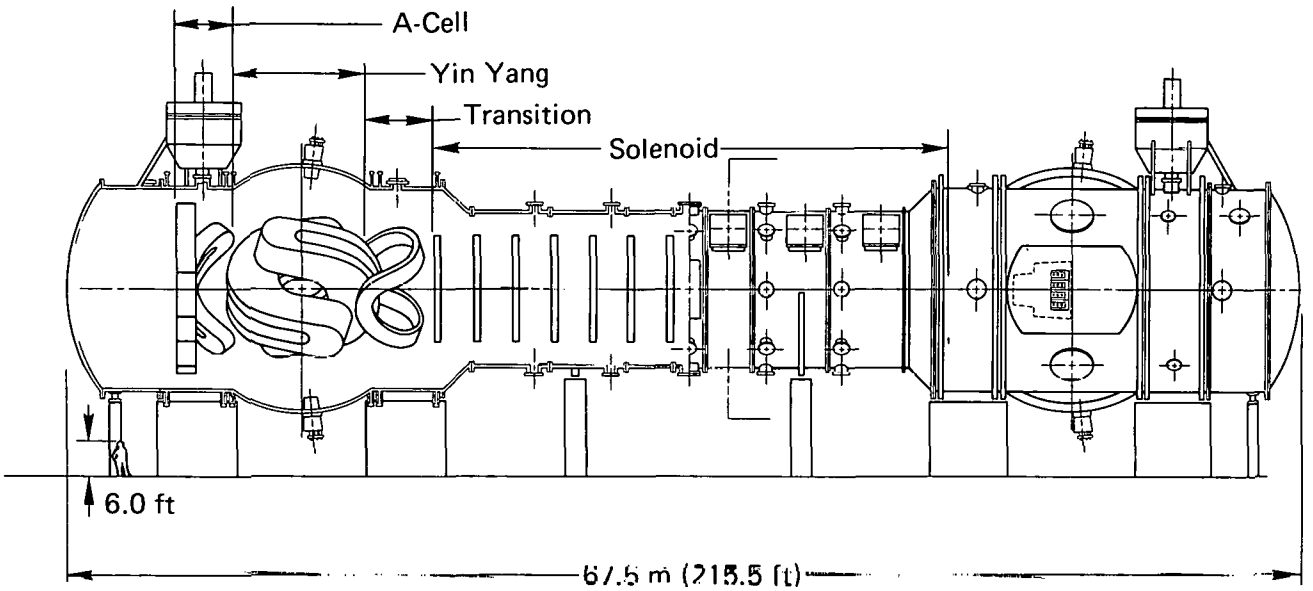

FIG. 2. Cutaway diagram of the MFTF-B.

facility and a Monte Carlo particle transport code. A summary of the results of these analyses follows.

The computer model was developed for the particle code and includes the 22 magnet coils and their cases, the cryopanels, the vacuum vessel, and the concrete vault. Distinct volumes and materials are treated separately and modeled as homogeneous mixtures. Composite cross-sectional data regarding transport, activation, heat deposition, and gamma production were calculated for each mixture using available data for the individual atomic species making up each mixture.[1] The model includes 14 such mixtures formed from 24 elements.

The source of the neutrons is modeled after the shape of the fusion plasma and consists of five basic regions. The plasma model in the central solenoid region is a cylinder, 118 cm in diameter by 26-m long. Enclosed by each Yin-Yang set is a plasma cylinder, 1.0-m long and 80 cm in diameter. The Yin-Yang plasmas, whose centers are separated by 40 m, are joined to the central cylinder by transition plasmas that flair out to elliptical cross sections when they pass through the inboard Yin-Yang coils and neck back down to the circular central solenoid. The number of neutrons generated within a given plasma volume is based on the expected local plasma density and temperature. All neutrons are generated at 2.5 MeV and have random initial directions.

The transport of the neutrons and gammas is calculated by the Monte Carlo code MORSE, written for LLNL by Thomas P. Wilcox,[2] and runs on a CDC 7600 computer. The code combines the energies of the particles into groups and treats the particles within each group as if they have the average energy of that group. The cross-sectional data are also averaged into the same energy groups. The analysis described here uses 17 neutron groups from 10^{-4} eV to 2.5 MeV and 15 gamma groups from 500 keV to 10 MeV.

The results of a series of Monte Carlo calculations to determine the neutron and gamma heating of liquid helium cooled components of the MFTF are summarized in Table 1. The specific heating of the superconducting magnets is below the design level to maintain cryostability, while the total heat load is within the design capacity allocation of the refrigeration system.

The neutron and subsequent gamma fluxes generated by the Mirror Fusion Test Facility-B (MFTF-B) fusion plasma will have a degrading effect on the superconducting magnets. The flux data generated by the Monte Carlo analysis, reported here, were related to the experimental analyses of other investigators[3–10] to estimate the magnitude of the effect. Because current plans call for periodically warming the magnets to room temperature (every 18 wk), most of the metallic defects

TABLE 1. Neutron and gamma heating of MFTF-B cryogenic components.

Component	Component part	Total heating,[a] J/plasma-s	Peak-specific heating,[a] J/plasma-s/cm^3
Yin Yang	Coils	3191	3.1×10^{-4}
	Jackets	4958	3.4×10^{-4}
Solenoid	Coils	870	6.7×10^{-5}
	Jackets	385	8.6×10^{-5}
A-cell	Coils	219	4.7×10^{-5}
	Jackets	184	
Transition	Coils	249	
	Jackets	172	
Cryopanels	End dome	30	
	Beam dome	72	
Total		10330	

[a]Data based on 2.3×10^{16} neutrons/plasma-s generated at 2.5 MeV.

will be annealed. Over the 10-yr lifetime of the facility, we expect to see a decrease in the critical current of the Yin-Yang coils of less than 0.5% and a negligible effect in the Nb-Ti of the other coils. The magnetoresistance of the copper stabilizer in the Yin-Yang coils will rise less than 8%, in the other coils less than 3%, during the 10-yr period.

Some organic insulating materials used in the construction of the Yin-Yang coils (such as Mylar and Dacron) may be damaged by radiation during their lifetime, but these materials are not critical to the operation of the magnets. The function of more important insulators, NEMA G-11 laminates and Kapton strips, are not expected to be affected. The radiation fluxes are also well below the thresholds for structural degradation of the stainless steel jackets and supports.

Besides energy deposition and radiation degradation, the plasma neutrons will also be absorbed and will transmute several chemical elements into radioactive isotopes. The decay of some of the isotopes may cause a biological hazard within the MFTF. Based in part on prior work by Lee,[11] the elements listed in Table 2 were selected for Monte Carlo activation evaluation using MORSE76L and an LLNL activation library.[12,13]

The small amounts of ^{14}C and ^{41}Ar produced in the vault air will be vented to and diluted by the atmosphere before personnel are permitted access. The practical maximum operation of the facility is production of plasma for 3000 s per day. This will generate 130 μCi of ^{14}C per day, all of which will be vented. The amount of ^{41}Ar released to the atmosphere, however, depends on how long the air is held before venting, since ^{41}Ar has a half-life less than 2 h. Plasma generation for 3000 s per day will produce 7.8 Ci of ^{41}Ar. If the vault is continuously vented, this will all be released. If the vault is sealed until the end of the experimental day, only 1.3 Ci of ^{41}Ar would remain to be vented. In any case, the biologic inactivity of argon coupled with the short half-life of ^{41}Ar should prove to be a minimal hazard to employees and to the general public. The amount of ^{14}C produced and vented is virtually negligible.

The other activation reactions occur within fixed structures and if not mitigated, could be hazardous to personnel entering the vault. The reaction products can be divided into three categories depending on radioisotope half-life. Short half-life isotopes (e.g., ^{56}Mn) contribute dosages that depend only on operation the previous day. Medium-lived products (e.g., ^{24}Na, ^{64}Cu) are important on a week-by-week basis, but they decay away over a weekend. Radiation levels of isotopes with long half-lives reflect the entire operational history of the facility and must also be considered long after the facility has completed its purpose. In Table 3 are the total doses each isotope will contribute inside and outside the MFTF-B vessel for each second plasma is generated. The dose rate at any location within the vault is dependent on prior

TABLE 2. MFTF-B radioactivation reactions.

Radioisotope	Parent reaction	Location	Half-life
^{14}C	^{14}N (n,p)	Air	5730 yr
^{24}Na	^{23}Na (n,γ)	Concrete	14.96 h
^{41}Ar	^{40}Ar (n,γ)	Air	1.82 h
^{54}Mn	^{54}Fe (n,p)	Stainless steel, concrete	312 d
^{56}Mn	^{55}Mn (n,γ)	Stainless steel	2.576 h
^{58}Co	^{58}Ni (n,p)	Stainless steel	71.3 d
^{59}Fe	^{58}Fe (n,γ)	Stainless steel, concrete	45.6 d
^{60}Co	^{59}Co (n,γ)	Stainless steel	5.26 yr
^{60}Co	^{60}Ni (n,p)	Stainless steel	5.26 yr
^{60}Co	^{61}Ni (n,pn)	Stainless steel	5.26 yr
^{64}Cu	^{63}Cu (n,γ)	Magnet coils	12.8 h
^{64}Cu	^{65}Cu (n, 2n)	Magnet coils	12.8 h

TABLE 3. MFTF-B activation dosage.

Isotope	Half-life	Dose, mrem/plasma-s	
		Inside vessel	Outside vessel
^{56}Mn	2.6 h	24[a]	0.9
^{24}Na	15 h	—	1.0
^{64}Cu	13 h	0.2[a]	0.002
^{54}Mn	303 d	2.0	0.1
^{58}Co	71 d	7.0	0.3
^{59}Fe	46 d	0.1	0.004
^{60}Co	5.3 yr	3.0	0.1

[a]Will be 0.0 by the time personnel can enter.

operational history, the half-life of each isotope, and local shielding and shadowing. The complex issues involved are beyond the scope of this summary. Although high enough to be of concern, the hazards from activation reactions in MFTF can be mitigated by limited vault access, careful radiation monitoring, and selective experimental schedules.

(For further information, contact S.A. Muelder, Ext. 2-0220 or J.D. Lee, Ext. 2-6734.)

References

1. T. P. Wilcox, *MORSE Cross Section Library Tapes*, Lawrence Livermore National Laboratory, Livermore, CA, UCID-16683 (1973).
2. T. P. Wilcox, *MORSE-L, A Special Version of the MORSE Program Designed to Solve Neutron, Gamma and Coupled Neutron-Gamma Penetration Problems*, Lawrence Livermore National Laboratory, Livermore, CA, UCID-16680 (1972).
3. R. A. Van Konynenburg, *Relative Radiation Sensitivity of Insulators, Stabilizers, and Superconductors*, Lawrence Livermore National Laboratory, Livermore, CA, UCRL-85438 (1980).
4. J. B. Roberto, C. E. Klabunde, J. M. Williams, and R. R. Coltman, Jr., "Damage Production by High-Energy d-Be Neutrons in Cu, Nb, and Pt at 4.2°K," *Appl. Phys. Lett.* 30, 509 (1977).
5. J. M. Williams, C. E. Klabunde, J. K. Redman, R. R. Coltman, Jr., and R. L. Chaplin, "The Effects of Irradiation on the Copper Normal Metal of a Composite Superconductor," *IEEE Trans. Magnetics*, **Mag-15**, 731 (1979).

6. R. H. Kernohan, C. J. Long, and R. R. Coltman, Jr., "Cryogenic Radiation Effects on Electric Insulators," *J. Nucl. Mater.* **85–86**, 379 (1979).
7. S. Takamura and T. Kato, "Effect of Low Temperature Irradiation on Organic Insulators in Superconducting Magnets," in *Nonmetallic Materials and Composites at Low Temperatures (Proc. ICMC Symp.)*, A. F. Clark, R. P. Reed, and G. Hartwig, Eds. (Plenum, New York, 1979), p. 155.
8. J. F. Kircher and R. E. Bowman, *Effects of Radiation on Materials and Components* (Reinhold, New York, 1964).
9. C. J. Long, R. R. Coltman, Jr., C. E. Klabunde, and R. H. Kernohan, "Effects of Radiation at 5 K on Organic Insulators for Superconducting Magnets," in *Special Purpose Materials Annual Progress Report*, U.S. Dept. of Energy, DOE/ER-0048/1 (1980), p. 73.
10. S. Takamura and T. Kato, "Effect of Low Temperature Irradiation on the Mechanical Strength of Organic Insulators for Superconducting Magnets," *Cryogenics* **20**, 441 (1980).
11. F. H. Coensgen, *MX Major Project Proposal*, Lawrence Livermore National Laboratory, Livermore, CA, LLL-Prop-142 (1976), Appendix E.
12. T. P. Wilcox, *Neutron Activation Cross Section Library*, Lawrence Livermore National Laboratory, Livermore, CA, MOR-17 (1974).
13. M. A. Gardner and R. J. Howerton, *ACTL-Evaluated Neutron Activation Cross Section Library—Evaluation Techniques and Reaction Index*, Lawrence Livermore National Laboratory, Livermore, CA, UCRL-50400-18 (1978).

MATERIALS FABRICATION DIVISION

The Materials Fabrication Division, a multidisciplinary organization in the Mechanical Engineering Department, provides services that are not available from commercial sources. The number and diversity of LLNL research efforts make this division one of the Laboratory's largest. We have about 450 highly skilled persons and more than 3,700 pieces of equipment in our inventory.

With these facilities and the special capabilities of our staff we provide services in the fields of optics, welding, vacuum process, glass, plastics, sheet metal, metal finishing, metrology, pressing, inspection and assembly, as well as conventional and numerically controlled machining of metals, high explosives, and ceramics.

In-house fabrication services are available for all LLNL programs when requirements call for:

- Fabrication capabilities not readily available elsewhere.
- Rapid turnaround time.
- Handling of materials that are toxic, radioactive, or classified.

In addition, the Division's facilities are used to develop improved manufacturing techniques and to advance machine tool research. Our operating philosophy is to satisfy the mechanical fabrication need of the programs, consistent with priorities set by those programs.

(For further information, contact R.A. Berg, Ext. 2-7643.)

A Third Diamond Lathe Is Completed

A small diamond lathe that is comparable in accuracy to larger machines is now in production operation in the Materials Fabrication Division. The Baby Optics Diamond Turning Machine (Fig. 1), built because of rapidly increasing demand for time on our other two high-accuracy lathes, was constructed and tested within 3 weeks by over 40 people from our Machine Tool Development and Machine Control Groups. The BODTM is a two-axis, numerically controlled lathe with a diamond cutting tool which produces aspheric parts with demonstrated accuracy of 10 μin. (size and contour band), and with surface finish of 1-1.5 μin. rms. Part-size capacity on this new machine is limited to parts of less than 4 in. in diameter. Two other diamond turning machines, DTM-1 and DTM-2, have been in operation here for about 10 yr, producing optical components and metal parts of high surface accuracy. Both lathes are three-axis numerically controlled machines with a maximum size capacity of approximately 30 in. A third large machine, DTM-3, which will have a maximum swing of 84 in. and allow contour grinding, is now under construction with an expected completion date of January 1984.

Planning for the Baby Optics Diamond Turning Machine first began in January 1981, when the demands of several Laboratory programs required that a third machine capable of handling a wide variety of small parts be placed in service in as short a time as possible. Although several U.S. manufacturers could have met the performance requirements set, we constructed the machine in-house because of the need to expand our production capability within a few weeks of the request. This time constraint precluded the purchase or fabrication of any major components and did not allow the completion of a formal design cycle prior to assembly.

The fabrication groups established design criteria as follows:

- Minimization of sources of nonrepeatable errors, such as those arising from thermal effects.
- Minimization of sources of spindle random motion, such as vibrations from the spindle drive motor.

The effort to reduce both of these sources of error led to the construction of a smaller size machine. The design criteria also permitted use of commercially produced parts that were available onsite at the time of construction. The components of the Baby Optics Diamond Turning Machine are:

- *Slides*: crossed roller slides with 6 in. of travel. The straightness of travel for the X slide, 2 in. above the slide surface, is 45 μin. over 4 in. The straightness of travel of the Z slide was 70 μin. over 4 in.; rework by MFD reduced this figure to 40 μin.
- *Spindle*: an air-bearing spindle with average radial and axial motion values of less than 1 μin.
- *Spindle drive motor*: a dc servo-drive motor. With the LLNL-supplied electronics

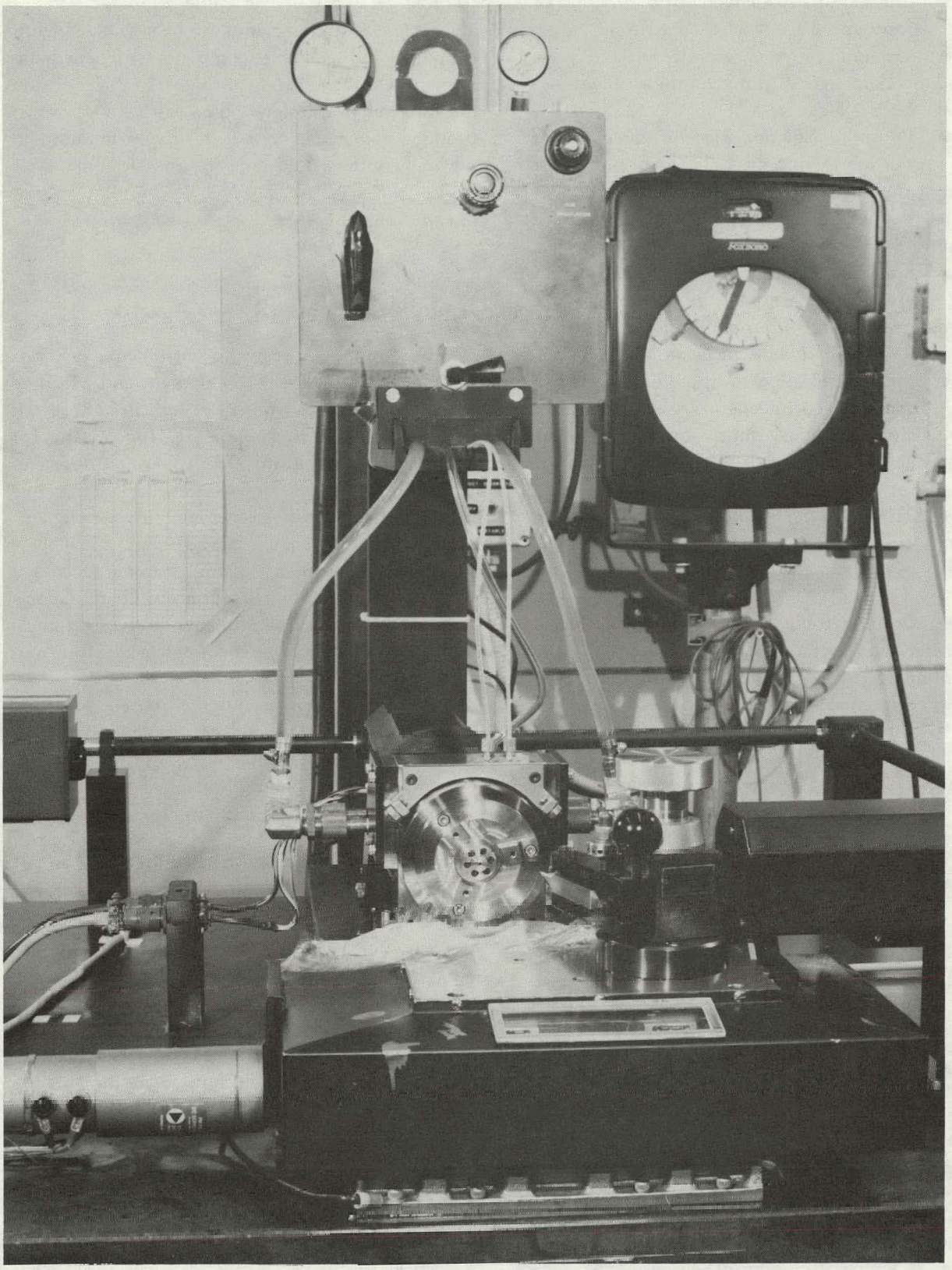

FIG. 1. The Baby Optics Diamond Turning Machine, now boosting part production in the Materials Fabrication Division.

package, the motor can deliver up to 10 in.-lb of torque at any speed from 50 to 2000 rpm.

- *Machine base*: a granite surface plate lapped to a flatness of 20 μin. over the area to be occupied by the slides.
- *Vibration isolation system*: three rubber pads supporting the granite base. This method for isolating the machine from vibrations was chosen because we did not have self-leveling pneumatic isolators of an appropriate size.
- *Spindle temperature control system*: approximately 5 gpm of temperature-controlled water is circulated through the spindle motor housing. The entire machine is located in an area with air-temperature control good to approximately 68 ± 0.2°F; thermal effects in general are reduced by our minimization of critical dimensions, such as the distance between the X-axis interferometer and the tool post.
- *Tool holder*: a holder for the diamond cutting tool. Slight modification of a commercial holder was made to allow improved tool-height adjustment.
- *Position-feedback system*: a laser interferometer and interface package operating at 1 μin. resolution to provide position feedback information to the computer numerical controller.
- *Computer numerical controller*: a commercial controller that was already on hand to be used on DTM–3, and that was already configured to interface with the position-feedback system.
- *Servo-amplifiers*: high-performance linear amplifiers to power the dc torque motors. Since none were commercially available in the time required, we constructed servo-amplifiers similar to those used on our larger diamond-turning machines.

The assembly of the machine was completed with its first contoured part cut two weeks (and one man-year) after the initial request was made. The third week of the project was devoted to establishing the machine geometry and proving it capable of turning parts to the required tolerances.

If more time had been available, we would probably have implemented a more conservative design—possibly a larger machine incorporating air bearing slides, improved leadscrews, a more elaborate temperature-control system, and self-leveling pneumatic vibration isolators. Our success with a more modest approach shows us that the design of diamond turning machines is a mature technology, and that a machine comparable in accuracy to existing machines can be assembled from commercially available components if adequate human resources are available. The size of the machine and our design criteria worked together to produce a machine that is relatively immune to vibration sources and temperature variations.

(For further information, contact D.C. Thompson, Ext. 2-1915.)

Compuron Wins IR–100 Award

A roundness-measuring instrument developed by the Machine Tool Development and Machine Control Groups has won one of *Industrial Research and Development* magazine's "IR–100" awards for 1981. The "Compuron" (Fig. 2), which measures the out-of-roundness of axisymmetric parts, is one of 100 developments selected annually for recognition as unique industrial advances. The new measuring system maintains extreme accuracy through the use of high-accuracy mechanical components, specially designed low-noise electronics, and use of a minicomputer for data acquisition and reduction.

The exceptional machining accuracy provided by the diamond turning process has created a serious need for comparable improvements in measurement accuracy. The Compuron provides the accuracy necessary to assess the roundness of diamond-turned parts over a wide range of sizes. First developed between November 1979 and August 1980, the Compuron measures part roundness to an accuracy of 0.1 μin. (25 Å), with a resolution of 0.01 μin. (2.5 Å). It maintains this accuracy over a large range of frequencies, preserving 0.1 μin. (p–v) accuracy up to 50 undulations per revolution (UPR).

The mechanical portion of the system features an air bearing rotary table supporting the part being measured, an air-isolated granite plate upon which the mechanical components are mounted, and a gaging framework that has fine adjustments with which to locate the gagehead. The gagehead itself is an air bearing linear-variable differential transformer (LVDT) with a stylus force of 0.1 g.

In the electronics portion, a direct-drive rotary encoder signals the microcomputer to read the LVDT output signal. The operator may select the number of revolutions desired for data collection,

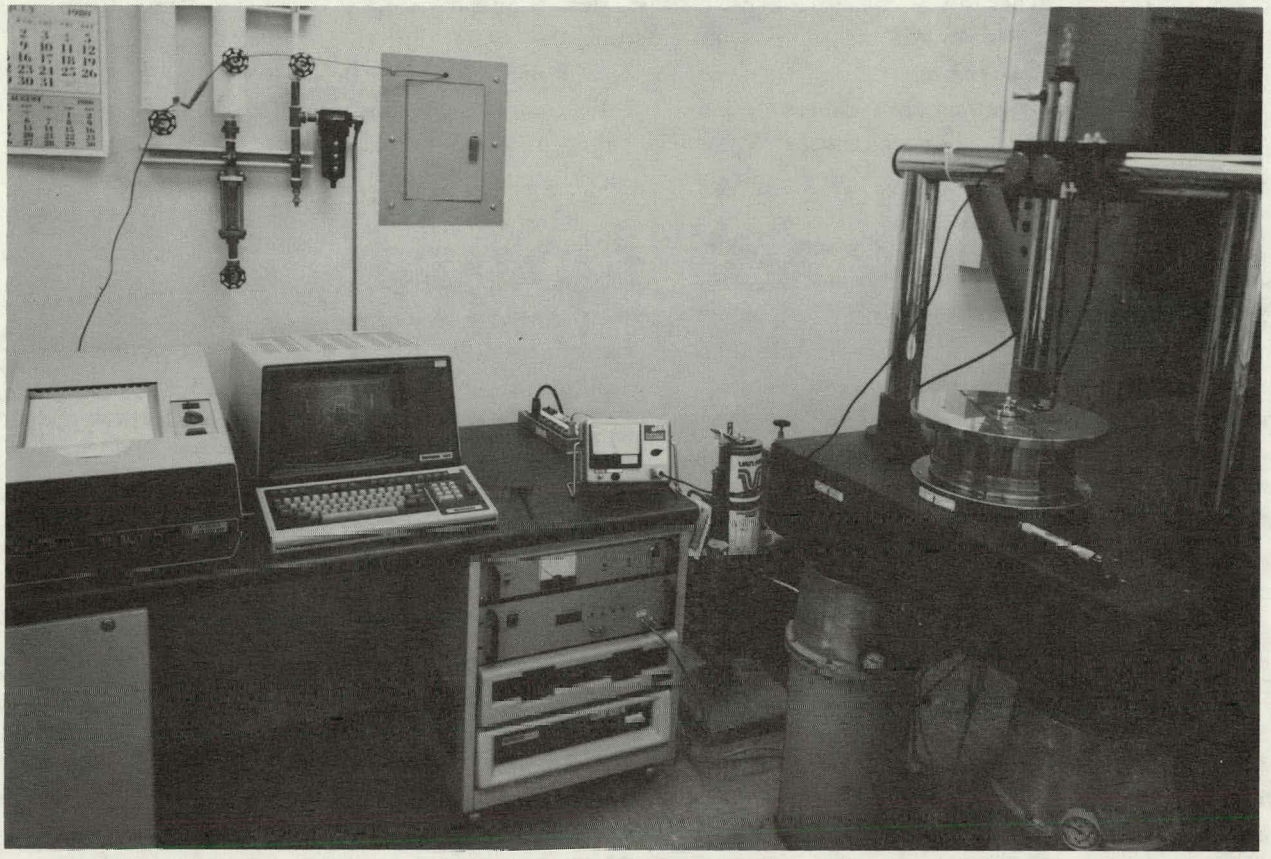

FIG. 2. The Compuron, currently the world's most accurate system for measuring the out-of-roundness of axisymmetric parts.

and then the data is averaged, with the system subtracting residual part-centering error and the repeatable spindle error. It then calculates part-roundness error by the method of least squares. The system produces polar plots of part roundness with magnification of up to 10^7 (at which 1 in. equals 0.1 μin.) and plots of the roundness spectra in the frequency domain, with both plots having selectable levels of digital filtering.

(For further information, contact D.C. Thompson, Ext. 2-1915.)

Plating on Stainless Steel Alloys

Our continuing joint effort with Sandia National Laboratories in obtaining adhesion data for electroplated stainless steel-type alloys has been summarized for a presentation planned for the American Electroplaters' Society Second Symposium on Plating on Difficult to Plate Metals, St. Louis, 1982.[1] This article presents the major conclusions of that summary.

Although plating has been successfully performed on stainless steels for many years, special activating steps are required prior to plating to ensure adequate adhesion of the coating. These steps remove stainless steel's thin, protective film of chromium and/or nickel oxide and keep the film from reforming until the surface is covered with an electrodeposit. In assessing the bond strength of coatings applied to various stainless steels, we have obtained data that show excellent adhesion is obtained when an adherent thin deposit of nickel is applied to the stainless steel substrate prior to plating. This deposit, which may be either a Wood's nickel strike or a sulfamate nickel strike (both are described below), allows excellent adhesion of the plating material. We noted even better

adhesion properties when an anodic treatment in sulfuric acid was used prior to Wood's nickel striking. We have found that the alternate methods of immersion or cathodic treatment of stainless steel in hydrochloric acid result in bond strengths of less than half those obtained with a Wood's nickel strike.

To obtain such data, we have pioneered the use of the "ring shear test." For this test, a cylindrical rod is coated with machined, electrodeposited rings of a premeasured width. The rod is then forced through a hardened steel die having a hole of greater diameter than that of the rod but less than that of the rod and coating combined. The load required for material failure is measured, and, considering also the area of the test specimen, we obtain shear strength data for the adhesion. The American Society of Testing and Materials is now recommending use of the ring shear test as a method of obtaining quantitative data for the bond strength of coated parts.

Many procedures have been suggested for activating stainless steels prior to plating.[2] These include immersion in acids, simultaneous activation-plating treatments such as the Wood's nickel strike,[3] anodic treatment in various solutions, and a combination of anodic and cathodic treatment in highly acidified solutions. The Wood's strike—probably the most common method used today—contains about 240 g/l nickel chloride and 125 ml/l hydrochloric acid (37 wt%) and is operated with nickel anodes. Table 1 shows the varying bonding strengths obtained in gold plating on 410 stainless steel for immersion, cathodic treatment, and for Wood's nickel strike. This data shows the intermediate adhesion obtained after immersion or cathodic treatment in hydrochloric acid, with the failure consistently occurring at the electrodeposit/substrate interface. Even though the best results among these three were obtained with cathodic treatment in hydrochloric acid, their bond strengths were still less than that seen with Wood's nickel strike.

In a further refinement, Seegmiller of Los Alamos suggested that a combination of anodic treatment in sulfuric acid followed by cathodic treatment in a Wood's strike may be necessary for a high degree of adhesion.[5] Table 2 shows the data we have obtained during exploration of this idea, and we see that the shear strength for 17–4 PH stainless steel given only a Wood's nickel strike was lower than that for an anodic treatment in sulfuric acid followed by a Wood's nickel strike.

For most stainless steels, the ring shear test does not provide discrimination between Wood's nickel alone and the additional sulfuric acid treatment, as prior failure typically occurs in the electrodeposit for both procedures. For these cases, the "flyer plate test" can measure differences. In this second type of test, thin, flat flyer plates are accelerated against the substrate by means of magnetic repulsion. The flyer travels at speeds of approximately 0.07 cm/μs (1550 mph), and the impact induces a compressive wave in the specimen. As this compressive wave reaches the rear surface of the sample, it is reflected as a tensile wave that propagates back through the specimen. This tensile wave, combined with rarefaction waves from the impedance mismatch at the interface between the substrate and the coating subjects the interface to dynamic tensile stresses. Interface damage can then be assessed by visual and metallographic inspection. We have used the flyer plate test to illustrate an approximately 50% improvement in bond

TABLE 1. Shear strength of adhesion bond of gold plating on 410 stainless steel for four different activation treatments.[4] The shear strength was measured by means of the "ring shear test."

Activation treatment	Bond shear strength, MN/m^2 (psi)	Location of failure
Immersion in 6 wt% HCl	5 (700)	Gold/stainless-steel interface
Cathodic treatment in 6 wt% HCl at 968 A/m^2 for 2 min	15 (2,200)	Gold/stainless-steel interface
Cathodic treatment in 37 wt% HCl at 968 A/m^2 for 2 min	66 (9,600)	Gold/stainless-steel interface
Cathodic treatment in Wood's nickel strike solution at 108 A/m^2 for 2 min	152 (22,000)	Within gold deposit

TABLE 2. Shear strength for nickel-plated 17-4 PH stainless steel[a] prepared by Wood's strike alone, and by anodic treatment in sulfuric acid plus a Wood's strike.[6] The shear strength was measured by the ring shear test.

Cleaning/activating cycle[b]	Shear strength, MN/m^2 (psi)
Clean, HCl pickle, Wood's nickel strike at 268 A/m^2 for 5 min, sulfamate nickel plate	195 (28,200)
Clean, HCl pickle, anodic treatment in 70 wt% H_2SO_4 at 1070 A/m^2 for 3 min, Wood's nickel strike at 268 A/m^2 for 5 min, sulfamate nickel plate	472 (68,300)

[a]The composition of 17-4 PH stainless steel is (all wt%) 0.04 carbon, 0.40 manganese, 0.50 silicon, 126.5 chromium, 4.25 nickel, 0.25 iridium, 3.6 copper, and the remainder is iron.
[b]The cleaning step in all cases included degreasing followed by anodic and cathodic treatment in hot alkaline cleaner. The HCl pickle was 30 wt%.

strength for activation with sulfuric acid prior to Wood's striking.[7]

Often the electroplater must activate stainless steel in the presence of other metals which may be attacked by the chloride ions in the Wood's nickel strike solution, e.g., a composite substrate containing stainless steel, nickel, and aluminum. To overcome this difficulty, we developed a sulfamate nickel strike which allowed excellent adhesion to both 405 stainless steel and nickel and did not attack the aluminum. The sulfamate nickel strike composition is 80 g/l nickel as nickel sulfamate, and 150 g/l sulfamic acid used at 50°C with electroformed nickel sheets as anodes.

(For further information, contact J.W. Dini, Ext. 2-8342.)

References

1. J. W. Dini and H. R. Johnson, *Plating on Stainless Steel Alloys*, Lawrence Livermore National Laboratory, Livermore, CA, UCRL-86673 (1981).
2. *Preparation of and Plating on Stainless Steel*, American Society of Testing and Materials, Philadelphia, PA, ASTM B254-70 (1970).
3. D. Wood, "A Simple Method of Plating Nickel on Stainless Steel," *Metal Industry* **36**, 330 (1938).
4. J. W. Dini and J. R. Helms, "Electroplating Gold on Stainless Steel," *Plating* **57**, 906 (1970).
5. R. Seegmiller, Los Alamos National Laboratory, private communication.
6. J. W. Dini and H. R. Johnson, "Preparation of Metals for Plating: Ring Shear Tests," *Surface Technology* **5**, 405 (1977).
7. J. W. Dini, H. R. Johnson, and R. S. Jacobson, "A Test for Quantitatively Measuring the Adhesion of Plated Coatings Under Dynamic Loading Conditions," in: *Properties of Electrodeposits, Their Measurement and Significance*, Ed. by R. Sard *et al.*, The Electrochemical Society, Princeton, NJ, pp. 307-318 (1975).

PUBLICATION ABSTRACTS*

C. M. Bacigalupi and W. A. Burton, *Model Testing of a 10-kg High Explosive Blast Attenuation Maze,* Lawrence Livermore National Laboratory, Livermore, CA, UCRL-53160 (1981).

The basement area of the proposed High Explosive Applications Facility (HEAF) at the Lawrence Livermore National Laboratory includes 10-kg HE assembly and process cells, and a 10-kg corridor for the transport of up to 10 kg of HE from the receiving dock to the cells and to the experimental firing tanks. Previous model experiments developed a process cell-maze configuration that attenuated the effects of an accidental 10-kg detonation to acceptable levels (maximum of 10 to 11 psi reflected). This document reports 1/8-scale model test conducted to confirm the maze design and to determine the blast pressures in adjacent areas in the final HEAF building configuration. In addition, pressure/time information was obtained at selected points in the model expansion chamber to provide the architect-engineer with information for structural design.

N. H. Beachley and D. R. Otis, *A Study of Accumulator Passenger Cars Based on the Ifield Hydrostatic Pump/Motor Unit,* Lawrence Livermore National Laboratory, Livermore, CA, UCRL-15390 (1981).

The use of hydraulic accumulators for energy storage in passenger automobiles has the theoretical potential of providing a significant improvement in fuel economy under urban driving conditions. Until now, however, the concept has suffered from the unavailability of hydrostatic variable-displacement pump/motor units with satisfactory efficiency characteristics. A new design recently developed by Ifield Engineering Pty. Ltd., of Dural, N.S.W., Australia, has significantly higher efficiencies than any other known units, and has the potential to make high-mileage accumulator vehicles a practical reality.

We have done a preliminary study to determine: (1) the potential fuel economy improvement of an Ifield accumulator vehicle, and (2) whether or not additional research and development work in this area is justified. The study was based on efficiency data in equation form provided by Ifield. The calculated results are quite promising, indicating mileage on the order of 60 mpg for a 3000-lb vehicle over the Federal Urban Driving Cycle (FUDC), and mileage on the order of 85 mpg for the New York City Cycle. These figures appear to be feasible not only on a system with two pump/motor units, but on one with a single pump/motor unit as well. The latter apears attractive because of price considerations. Fuel economy figures compare favorably with those of a comparable flywheel energy-storage vehicle.

The above figures are based on the use of accumulators with plastic foam as a heat sink to provide nearly isothermal operation with correspondingly low thermodynamic losses. With a conventional accumulator, the fuel mileage calculated for the FUDC drops approximately 9%. The required accumulator weight has been calculated to be about 100 lb, using state-of-the-art composite construction. Foam, if used, would add approximately 30% to the weight.

Donald M. Boyd, *A Review of Holographic Nondestructive Evaluation at Lawrence Livermore National Laboratory,* Lawrence Livermore National Laboratory, Livermore, CA, UCRL-96788 (1981).

At Lawrence Livermore National Laboratory two holographic facilities have been established for the technology transfer of holographic interferometry. This report is a review of the principles of holographic interferometry (HI) and the application of this technique to nondestructive evalution. Simplified quantitative analysis using a coincident viewing and illumination optical arrangement will be described.

A. L. Brooks and R. S. Hawke, *The Electromagnetic Launcher: A New Weapon?* Lawrence Livermore

*The abstracts are arranged alphabetically by first author's name.

National Laboratory, Livermore, CA, UCRL-85877 (1981). Prepared for the 6th Intern. Symp. on Ballistics, Orlando, FL, October 22–24, 1981.

Using electromagnetic (EM) forces to accelerate projectiles is not a new idea; it dates back to the first part of this century. The idea has been revitalized, however, by some recent work done in this area.

There are two basic types of electromagnetic accelerator: those that rely on induced currents to provide the Lorentz force that accelerates the projectile (ac), and those that rely on direct current (dc). The ac accelerators are characterized by the potential for very high electrical to mechanical (kinetic energy) conversion efficiencies and relatively low accelerating forces. The dc accelerators produce much higher acceleration, but with lower efficiency. This is the type of interest for weapons applications. The higher accelerations will permit much shorter barrel lengths, minimizing pointing and tracking difficulties.

There are several perceived advantages to using EM launching for weapons applications. Higher muzzle velocities than can be achieved with conventional ordnance will minimize the projectile time-of-flight to the target; this is of particular interest for air-defense applications against maneuvering targets and for penetrator launching. The potential for precise current (hence acceleration) control promises lower peak accelerations that the projectile must withstand, and much more precise muzzle velocity control, permitting the use of "smart" projectiles and continuous zoning for artillery applications.

This paper will discuss the principles behind EM accelerators, particularly dc accelerators (railguns), the recent history of their development, their advantages for weapons applications, the general requirements, potential problem areas that must be faced by designers, and the work that has been done by researchers at Livermore and Los Alamos National Laboratories in accelerating 3-g projectiles to 10 km/s, and larger masses to lower velocities.

Norman J. Brown, Phillip C. Baker, and Richard T. Maney, *The Optical Polishing of Metals,* Lawrence Livermore National Laboratory, Livermore, CA, UCRL-86514 (1981). Prepared for the Society of Photo-Optical Instrumentation Engineer's 25th Annual Intern. Technical Symp., San Diego, CA, August 24–28, 1981.

A polishing model and a fixed charge lap model are presented. Optical polishing data is presented for 11 metals partially supporting the models.

Norman J. Brown and Phillip C. Baker (both LLNL), **and Robert E. Parks** (University of Arizona), *The Polishing-to-Figuring Transition in Turned Optics,* Lawrence Livermore National Laboratory, Livermore, CA, UCRL-86513 (1981). Prepared for the Society of Photo-Optical Instrumentation Engineer's 25th Annual Intern. Technical Symp., San Diego, CA, August 24–28, 1981.

The spatial frequency response of elastic backed flexible lapping belts is examined. The transition from planing off to propagating sinusoidal ripple is shown to be extremely sensitive to ripple frequency.

Gustav A. Carlson and William L. Barr, *The Effect of Non-Adiabaticity of Alpha Particles in the Axisymmetric Cusp TMR,* Lawrence Livermore National Laboratory, Livermore, CA, UCID-19150 (1981).

One of the end plug configurations we have investigated for use in a tandem mirror reactor is the axisymmetric cusp. We show that because of non-adiabaticity, the containment of 3.5 MeV alpha particles in this configuration is insufficient for the attainment of acceptable plasma performance.

G. A. Carlson, W. L. Barr, B. M. Boghosian, R. S. Devoto, J. N. Doggett, G. W. Hamilton, B. M. Johnston, J. D. Lee, B. G. Logan, R. W. Moir, W. S. Neef (all LLNL), **and R. B. Campbell** (TRW, Inc.), *Designs of Tandem Mirror Fusion Reactors.* Prepared for 3rd Technical Committee and Workshop on Fusion Reactor Design and Techn., Intern. Atomic Energy Agency, Tokyo, Japan, October 5–16, 1981.

We have completed a comparative evaluation of several end plug configurations for tandem mirror fusion reactors with thermal barriers. The axi-cell configuration has been selected for further study and will be the basis for a detailed conceptual design study to be carried out over the next two years. The axi-cell end plug has a simple mirror cell produced by two circular coils followed by a transition coil and a Yin-Yang pair, which provides for MHD stability.

Alan B. Casamajor, *Engineering Evaluation of Riola Containment,*. Lawrence Livermore National Laboratory, Livermore, CA, UCID-19164 (1981).

An independent review of the engineering of the Riola Event (U2eq) containment system was conducted. This review included interviews with personnel involved with the event's containment, and examination of available documentation at Lawrence Livermore National Laboratory and at the Nevada Test Site. Calculations were made to verify the adequacy of the lower coal tar epoxy plug design. All activities associated with the containment system design and installation were found to conform with established specifications and procedures. Recommendations are made regarding the need for additional engineering data on containment systems, and on the need for more complete documentation of containment system requirements.

John F. Cooper and Robert V. Homsy, *Development of the Aluminum-Air Battery for Electric Vehicle Applications,* Lawrence Livermore National Laboratory, Livermore, CA, UCRL-86560 (1981). Prepared for the EVDG 4th Intern. Conf. and Demonstration, Chiswick, London, England, September 15–16, 1981.

Current progress is reported concerning the development of hardware for the aluminum-air electric vehicle battery. The polarization curves of large-scale aluminum-air cells (0.1-m^2 anodes) have been replicated in rapidly refuelable cells of subscale size (167-cm^2) which were constructed for stacking into multicell modules. Solution-side current collection by a structure which makes point- or line contacts at the aluminum/electrolyte interface is described. The technique allows rapid anode addition, minimizes anode fabrication costs, and simplifies cell design. The possible application of solution-side current collection to wedge-shaped cells allowing continuous anode feed and full utilization is discussed. Life-cycle testing of air electrodes in candidate battery electrolytes is reported. Temperature and aluminate concentration transients are modeled using experimental rate data. Program structures, technical strategy, goals, and economic analysis are briefly discussed.

J. A. Day, *Opportunistic Replacement of Fusion Power System Parts,* Lawrence Livermore National Laboratory, Livermore, CA, UCRL-85894 (1981). Prepared for Proc. Annual Reliability and Maintainability Symp., Los Angeles, CA, January 26–28, 1982.

This paper describes a maintenance problem in a fusion power plant. The problem is to specify which life-limited parts should be replaced when there is an opportunity. The objective is to minimize the cost rate of replacement parts and of maintenance actions while satisfying a power plant availability constraint. The maintenance policy is to look ahead and replace all parts that will reach their life limits within a time called a screen. Longer screens yield greater system availabilities because more parts are replaced prior to their life limits.

J. W. Dini (LLNL) **and H. R. Johnson** (Sandia Livermore National Laboratory), *Plating on Stainless Steel Alloys,* Lawrence Livermore National Laboratory, Livermore, CA, UCRL-86673 (1981). Prepared for the American Electroplaters' Society, 2nd Symp. on Plating on Difficult to Plate Metals, St. Louis, MO, March 1982.

Quantitative adhesion data are presented for a variety of electroplated stainless steel type alloys. Results show that excellent adhesion can be obtained by using a Wood's nickel strike or a sulfamate nickel strike prior to final plating. Specimens plated after Wood's nickel striking failed in the deposit rather than at the interface between the substrate and the coating. Flyer plate

quantitative tests showed that use of anodic treatment in sulfuric acid prior to Wood's nickel striking even further improved adhesion. In contrast activation of stainless steels by immersion or cathodic treatment in hydrochloric acid resulted in very reduced bond strengths with failure always occurring at the interface between the coating and substrate.

J. N. Doggett and C. C. Damm, *Conceptual Design of a Technology Development Facility (TDF),* Lawrence Livermore National Laboratory, Livermore, CA, UCRL-85999 (1981).

We have developed a concept for employing a single-cell mirror machine in a facility for testing and developing fusion reactor materials, components, and subsystems in a fusion reactor environment. Our approach is similar to that of the 1974 FERF study, except that we have added an auxiliary thermal barrier cell at each end of the central Yin-Yang magnet. In this way, we provide for plasma microstability by confining a warm plasma component between potential peaks at each end of the device, just as in the tandem mirror with auxiliary barrier cells, while further improvement in confinement is provided by the inherent reduction in ambipolar potential drop in the central cell.

TDF is a driven D-T reactor that delivers power reactor level wall loads, has significant test space at high flux, and is based on conservative physics and engineering assumptions. While our parameter study is still evolving toward an optimized design, it is clear that we can achieve a neutron wall loading of more than 3 MW/m^2 with about 2 m^2 of high flux test area. Total fusion power is about 20 MW and the input (utility) power for the facility will be about 125 MW. Steady-state operation at this level allows the possibility of high-fluence materials testing. The two relatively large (1 m^2) high-flux test areas can accommodate component test assemblies (breeding blanket modules, shields). The facility would also provide operating experience with reactor-like subsystems, such as tritium, remote handling, neutral beams, and ECRH.

The physics connected with thermal barrier operation and microstability will be tested in the TMX-Upgrade experiment starting early in 1982. Technology for the TDF is basically that of MFTF-B (Nb-Ti magnets, 80-keV neutral beams, ECRH, and cryopumping), although the heating and pumping must be extended to steady-state operation. Thus, a good physics and engineering basis for proceeding with construction of a TDF will be available at an early date.

D. L. Ermak, B. J. Alder (both LLNL), **and L. R. Pratt** (University of California, Berkeley), *Hard Sphere Solids with One Fluid Component,* Lawrence Livermore National Laboratory, Livermore, CA, UCRL-53831 (1981). Prepared for *J. Phys. Chem.*

A perturbation calculation in the ratio of the diameter of the smaller to larger hard sphere shows that the interatomic distance in the large sphere solid phase coexisting with the fluid phase expands upon addition of a smaller component. Molecular dynamic calculations of the diffusion coefficient show that a diameter ratio no larger than 0.4 can be achieved in a fcc crystal without both components becoming either localized or fluid. Occupation of every tetrahedral interstitial site in a bcc lattice by spheres of close to the maximum possible size failed to stabilize the unstable bcc lattice of hard spheres, so that no bcc solid with a diffusing second component could be generated.

T. G. Frank and J. H. Pendergrass (Los Alamos), **D. L. Cook** (Sandia National Laboratory, Albuquerque), **and J. H. Pitts** (LLNL), *Power Plant Design for Inertial Confinement Fusion-Implications for Pellets,* Los Alamos National Laboratory, Los Alamos, NM, LA-UR-81-2545 (1981). Prepared for the 28th National Vacuum Symp., Anaheim, CA, November 3–6, 1981.

Potential commercial applications of inertial fusion include the production of electricity and fissile and chemical fuels. In all these applications, a significant amount of high-temperature heat will be produced and converted to electricity. Because most of the implications for fusion pellets are common to all applications, the emphasis in this discussion is on central station electric power plants.

In an inertial fusion electric power plant, fusion pellets containing deuterium and tritium (D-T) will be injected into one or more reaction chambers

at rates of 1 to 10 per second at high velocity where they are intercepted, in flight, by laser or particle beam driver pulses. The fusion fuel is compressed and heated to conditions necessary for fusion reactions to take place. Energy is released from the pellet as x rays, high-energy neutrons, and energetic pellet debris. The x rays and pellet debris ions deposit their energy very near surfaces of incidence, whereas neutron energy deposition occurs volumetrically in relatively thick blanket regions surrounding the reaction chambers. Special provisions are required to accommodate the x-ray and pellet-debris energy deposition without severe damage to the interior surfaces of reaction chambers of reasonable size. Pellet energy releases are converted to sensible heat in reactor structures and coolants and are transported by a flowing coolant to appropriate power conversion equipment.

The requirements and constraints on fusion pellets for power plant applications include: survivability in hostile reaction chamber environments, the ability to withstand large acceleration forces encountered in high-velocity injection, sufficiently large energy releases for economic power production, and high-rate automated manufacture at costs which are not a large fraction of the value of the fusion energy released. These requirements and their dependence on the several possible combinations of generic reactor-driver combinations are discussed in this paper.

L. L. George, *A Comparison of Some Probability Distributions of Peak Combined Responses,* Lawrence Livermore National Laboratory, Livermore, CA, UCRL-84174 (1981). Prepared for the 6th Intern. Conf. on Structural Mechanics in Reactor Technology, Paris, France, August 17–21, 1981.

The objective is to compare the exact probability distribution of the peak combined response with an approximation. The combined response is the sum of a Poisson Square wave and a Poisson shock process. The sizes of the square waves are independent and identically distributed random variables, and so are the shock sizes. The combined response models earthquake and operating load responses. The two stochastic processes are dependent because events in the processes may occur simultaneously. That is, shocks may cause changes in the square wave process, or changes in the square wave process may cause shocks.

The approximation for independent processes is accurate in the neighborhood of the peak combined load if the responses in one of the stochastic processes dominates responses in the other or if shocks are rare. The approximation is not accurate if the processes have approximately the same means and if events occur frequently in the processes. This inaccuracy is shown in one example.

L. L. George (LLNL), **E. Y. Lim and S. L. Basin** (Science Applications, Inc.), **and D. L. Eglehart** (Stanford University), *A Fracture Mechanics Evaluation of Reactor Piping Reliability II: Simulation of Pipe Fracture Probability,* Lawrence Livermore National Laboratory, Livermore, CA, UCRL-84173 Rev. 1 (1981). Prepared for the 6th Intern. Conf. on Structural Mechanics in Reactor Technology, Paris, France, August 17–21, 1981.

An objective of the Load Combination Program at the Lawrence Livermore National Laboratory is to estimate the probability of primary coolant loop pipe fracture caused directly by an earthquake. This probability will be used by the U.S. Nuclear Regulatory Commission (NRC) to help decide whether to decouple LOCA and earthquake. If the probability is small, the U.S. NRC may decouple LOCA and earthquake. The probability is in SMiRT-6 paper J 6/6.

This paper describes simulation of fatigue crack growth of fabricated cracks in welds due to transients and earthquakes and the combination of the single weld joint simulations to estimate primary coolant loop pipe fracture probability. It also gives a sensitivity measure, the derivative of the probability with respect to input variables, and constructs a confidence interval on the probability. The fatigue crack growth model is in SMiRT-6 paper M 12/2.

Deterministic computation of pipe fracture probability requires conservative assumptions. To avoid conservative assumptions, we simulated pipe fracture in welds. To obtain accurate estimates of pipe fracture probability, we used stratified sampling.

L. L. George and J. E. Wells, *The Reliability of Systems of Dependent Components,* Lawrence Livermore National Laboratory, Livermore, CA, UCRL-84154 (1980). Prepared for the ASQC Quality Congress Trans., National Meeting, San Francisco, CA, May 27–29, 1981.

We have developed a method to compute the reliability of a multiple component system. This method computes system reliability accurately because the program represents dependent component failures. Component failure occurs if the random stress applied to the component exceeds its random strength. System failure occurs if any cut set of components fails. The method also determines which components or parameters have the largest effect on system failure probability.

Inputs are the joint cumulative distribution functions (cdfs) of stress and strength for all components and the Boolean expression that defines system failure. The joint cdfs must be normal, lognormal, or mixtures of normal or lognormal cdfs. (Mixtures can fit multimodal cdfs or cdfs with positive probability on a set of measure zero.)

System failure can be defined by any Boolean expression of basic events, component failures or survivals. The Boolean expression can be reduced to the union of mutually exclusive intersections of basic events. Our method computes the probabilities of intersections of dependent basic events. It can handle up to ten dependent basic events.

The method computes the exact probability of the intersections by numerical evaluation of multivariate normal integrals. It then adds the probabilities of all mutually exclusive intersections to obtain the probability of system failure.

Sensitivity of system failure probability is its derivative with respect to component variables. Formulas are given for the derivatives of system failure probabilities with respect to component stress and strength means, variances, and covariances. They can be used to estimate the sensitivity of system failure probability to changes in component failure probabilities by the chain rule.

Alan I. Goldner and David Margolies, *Neutral-Beam Aiming and Calorimetry for MFTF-B,* Lawrence Livermore National Laboratory, Livermore, CA, UCRL-85995 (1981).

The vessel for the Tandem Mirror Fusion Test Facility (MFTF-B) will have up to eleven 0.5-s-duration neutral-beam injectors for the initial heating of the MFTF-B plasma. Knowing the exact alignment of the beams and their total power is critical to the performance of the experiment. Using prototype aiming and calorimetry systems on the High Voltage Test Stand (HVTS) at Lawrence Livermore National Laboratory (LLNL), we hope to prove our ability to obtain an aiming accuracy of ±1 cm at the plasma and a calorimetric accuracy of ±5% of the actual total beam energy.

R. S. Hawke, A. L. Brooks, and A. C. Mitchell (all LLNL), **and C. M. Fowler, D. R. Peterson, and J. W. Shaner** (all Los Alamos), *Railguns for Equation-of-State Research,* Lawrence Livermore National Laboratory, Livermore, CA, UCRL-85298 (1981). Prepared for the American Physical Society 1981 Topical Conference on Shock Waves in Condensed Matter, Menlo Park, CA, June 23–25, 1981.

It appears that a railgun can be used to accelerate an impactor plate to velocities of 10 to 40 km/s, which could generate shock pressures of 1 to 10 TPa. As a first step to determining the potential and limits of railgun accelerators for shock-wave equation-of-state research, a joint team of scientists and engineers at Los Alamos National Laboratory and Lawrence Livermore National Laboratory have initiated railgun research. We have utilized a combined capacitor bank and magnetic flux compression generator to power railguns and have demonstrated the feasibility of accelerating projectiles to ~10 km/s. This paper reports the status of experimental research directed toward launching EOS impactors and achieving higher velocities.

P. H. Y. Lee, K. G. Tirsell, G. R. Leipelt, and W. B. Laird, *Measurement of 2–5 keV X-Ray Emission from Laser-Target Interactions by Using Fluor-MCP and CsI-XRD Detectors,* Lawrence Livermore National Laboratory, Livermore, CA, UCRL-86306

(1981). Prepared for the 23rd Annual Meeting of the American Physical Society, Division of Plasma Physics, New York City, October 12–16, 1981.

For inertial confinement fusion plasma diagnostics, x-ray diode (XRD) detectors using conventional cathodes are not sensitive enough to measure x rays above ~1.5 keV. However, for laser driver fusion targets, x rays in the range of 2–5 keV are important because of their mobility in the target. We have successfully used fluor-microchannel plate (MCP) detectors to obtain absolute x-ray measurements in the 2–5 keV range. Recent data obtained from experiments on the Shiva laser system are presented. In addition, designs for a variety of channels in the range using fluor-MCP and CsI-XRDs above 1.5 keV will be discussed.

Fred R. Holdener and Serwer Sadik, *Development of a Dynamic Multiaxial Interface Bond Testing Machine,* Lawrence Livermore National Laboratory, Livermore, CA, UCID-19099 (1981).

We have developed a dynamic bond testing capability to measure the bond characteristics simulating those between Composition-B explosive and a munition case. The bond can be subjected to dynamic loads approximating those of loading the round and the subsequent launch environment of high-performance artillery projectiles. The test machine is capable of 100 000-lb compressive load and 50 000 in.-lb torsional load with a maximum torsional torque rate of 1000 in.-lb/ms. Detailed information of initial criteria and design parameters are discussed along with actual checkout test results.

Robert V. Homsy, *Temperature and Concentration Transients in the Aluminum-Air Battery,* Lawrence Livermore National Laboratory, Livermore, CA, UCRL-86648 (1981). Prepared for the Fall Meeting, Electrochemical Soc., Denver, CO, October 11–16, 1981.

Coupled conservation equations of heat and mass transfer are solved, that predict temperature and concentration of the electrolyte of an aluminum-air battery system upon startup and shutdown. Results of recent laboratory studies investigating the crystallization kinetics and solubility of the caustic-aluminate electrolyte system are used in the predictions. Temperature and concentration startup transients are short, while during standby conditions, temperature increases to a maximum and decreases slowly.

S. V. Kulkarni, K. L. Reifsnider, and D. M. Boyd, *Composite Flywheel Durability and Life Expectancy: Test Program,* Lawrence Livermore National Laboratory, Livermore, CA, UCRL-86450 (1981). Prepared for the Proc. Mechanical, Magnetic, and Underground Energy Storage Contractors' Review, Washington, D.C., August 24–26, 1981.

Under the leadership of LLNL, various industries and national laboratories have developed flywheels from composite materials that are capable of achieving significantly higher energy densities than those made from conventional metals. Recent burst tests have firmly established this fact. The only remaining major question is in regard to their durability and life expectancy. In other words, how will they perform during long-term service loading? The test program discussed in this report is being developed to answer that question.

C. M. Logan, J. W. Dini, W. D. Ludemann, B. J. Schumacher, E. N. C. Dalder W. K. Kelley, and G. A. Harter, *Development of Manufacturing Methods for 50-cm Diameter Neutron Source Targets for RTNS-II,* Lawrence Livermore National Laboratory, Livermore, CA, UCRL-85429 (1981). Prepared for the 2nd Topical Meeting on Fusion Reactor Material, Seattle, WA, August 9–12, 1981.

RTNS-II is an accelerator-driven neutron source. We attempted to produce a larger version of our current accelerator target but experienced problems in diffusion bonding and thermal stability of the copper alloy used for target fabrication. We have identified the causes of these problems and demonstrated a new technique, electroforming, for fabricating targets.

J. A. Maniscalco, D. H. Berwald, and R. B. Campbell (TRW, Inc.), **and R. W. Moir and J. D. Lee** (LLNL), "Recent Progress in Fusion-Fission

Hybrid Reactor Concepts," *Nuclear Technology*, October 1981, vol. 1, No. 4 NTFUDO 1(4), pp. 415–478.

An overview is presented of recent design trends and developments in fusion-fission hybrid reactor concepts. Emphasis is on recent progress and developments but a brief review of the evolution of the hybrid concept since 1950 is also presented. Required fusion performance and technology development issues for the fusion-fission hybrid are explored with the tandem mirror as the primary example of a fusion driver. The results show that fusion breeders, especially ones with suppressed fission blankets, have the potential to produce unprecedented quantities of fissile fuel. The resulting high light water reactor (LWR) support ratio relaxes both the fusion performance required and the economic constraints for commercial feasibility. It also enhances the fusion breeder's ability to rapidly impact our energy needs.

J. A. Monjes, B. W. Weinstein, and D. L. Willenborg, *Reflection/Transmission Phase Shift Interferometer and Viewing Optics,* Lawrence Livermore National Laboratory, Livermore, CA, UCRL-85281 (1981). Prepared for the Conf. on Laser and Electro Optics, Washington, D.C., June 10–12, 1981; and for *Applied Optics.*

The interferometer and viewing optics that are the main optical components of an Automated Surface Mapping system (ASM) used to characterize the surface topography and the wall thickness uniformity of opaque and transparent spherical shells is described.

To characterize surface finish or wall thickness of spherical shells with an accuracy of 10 nm and a resolution of 1 μm the differential phase shift between two beams of orthogonal polarizations is measured, before and after the probe beam has interacted with the test object.

M. J. Monsler and J. Hovingh (LLNL), **D. L. Cook** (Sandia National Laboratory, Albuquerque), **T. G. Frank** (Los Alamos), **and G. A. Moses** (University of Wisconsin), "An Overview of Inertial Fusion Reactor Design," *Nucl. Tech./Fusion* 1, 302 (July 1981).

Recent progress in the conceptual design of inertial fusion reaction chambers and power plants is reviewed. A discussion of expected operating parameters and a brief historical perspective are provided to organize the rich array of chamber and driver concepts. The technical feasibility of several reaction chamber concepts is discussed, along with technical issues that require future analysis, experiment, and development. Where these chambers have been integrated into a power plant design, the characteristics are described. Finally, requirements on the future development of inertial fusion reactor technology are discussed.

Lawrence G. O'Connell, *The Future Possibilities for Energy Storage Automobiles,* Lawrence Livermore National Laboratory, Livermore, CA, UCRL-85902 (1981). Presented at the 91st National Meeting, American Institute of Chemical Engineers, Detroit, MI, August 16–19, 1981.

Because of the potential theat of a future petroleum shortage, there is increased interest in developing alternative propulsion systems for automobiles, systems that will allow the nation to reduce its demand for petroleum by this part of the transportation sector. A four-year study which assessed the future of energy storage devices for use in automobile propulsion systems has been completed. Results of the energy storage device evaluation are presented. This includes projections of future device characteristics. In addition, the results of the propulsion system analysis are given. Future energy storage automobiles were conceptually designed and they are compared to each other and the baseline internal combustion engine vehicle for several levels of performance.

Lawrence G. O'Connell and L. R. Spogen, *Application Analysis of Energy Storage Systems for Transportation,* Lawrence Livermore National Laboratory, Livermore, CA, UCRL-85851 (1981). Prepared for the Technical and Economic Analysis Contractors' Meeting, Chicago, IL, April 21–22, 1981.

An application analysis study of energy storage systems for automotive propulsion was conducted over a period of four years. The purpose

was to identify the most promising energy storage devices and the vehicular missions for which the resultant propulsion systems are best suited. Projected costs of the vehicles are used to discuss the study's findings. Additionally, some preliminary findings concerning an assessment of the impact on energy storage device requirements of current transportation developments and trends are discussed.

W. C. O'Neal, G. M. Bianchini, R. E. Blocker, D. L. Hipple, W. J. Hogan, M. Ochoa, Jr., and W. Wakeman, Jr., *The 500-m^3 Liquefied Gaseous Fuels Spill Test Facility,* Lawrence Livermore National Laboratory, Livermore, CA, UCRL-85596 (1981). Prepared for *Advances in Cryogenic Engineering.*

The LGF Spill Test Facility is designed to be a safe and reliable 500 m^3 capacity facility for storing and spill-testing various liquefied gaseous fuels (LGF's) at Frenchman Flat Nevada Test Site. The LGF's currently of interest to the DOE are LNG, LNH_3, and LH_2.

John H. Pitts (LLNL) and **I. U. Ojalvo** (Perkin-Elmer), *Fluid and Structural Dynamic Design Considerations of the HYLIFE Nozzle Plate,* Lawrence Livermore National Laboratory, Livermore, CA, UCRL-84874 (1981). Prepared for 6th Intern. Conf. on Structural Mechanics in Reactor Techn., Paris, France, August 17–21, 1981.

The basic concept of the High Yield Lithium Injection Fusion Energy (HYLIFE) reaction chamber involves a falling liquid-metal (lithium) jet array that absorbs 90% of the energy released from inertial confinement fusion reactions. The key element of the chamber that produces the jet array is the nozzle plate. This paper describes the design and analysis of a nozzle plate which can withstand the structural loads and permit the fluid jet array to be reestablished for a 1-Hz fusion reaction frequency.

The shape of the nozzle plate and jet array is dictated by considerations of fluid dynamics and neutron-shielding. A vertical jet array, rather than a single annulus, is used because this design enhances fluid momentum interchange and dissipation of the kinetic energy that occurs when the jets disassemble. Less net outward-directed momentum results than with a single liquid annular flow configuration, thus producing lower stresses in the structural components.

The lithium head is established to ensure that the velocity of the free jets leaving the nozzle plate is sufficient for them to restablish themselves between fusion reactions. The jet channels have a constant cross section, arranged in a pattern that maximizes shielding uniformity. An annular weir flow over the plate's central hole provides shielding for the inner areas of the plate. Geometric perturbations at discrete locations around the circumference of the weir are intentionally introduced so that the weir flow breaks up into jets before it reaches the reaction chamber midplane.

A variable-property thick annular wedge was used to structurally model the nozzle plate. The static loads imposed were those due to the head of lithium, drag of the fluid as it entered the nozzle plate and the weight of the plate itself. Dynamic loads resulted from neutron-induced pressure above the plate, and lithium gas pressure and liquid impact pressures below the nozzle plate. An approximate Rayleigh-Ritz procedure was used in conjunction with a finite element program to obtain the stress components. It was found that the design thickness was dictated by the plate static stressed in conjunction with appropriate design stress concentration factors and fatigue considerations.

Allan Rosencwaig, *New Developments in Photoacoustics,* Lawrence Livermore National Laboratory, Livermore, CA, UCRL-86490 (1981). Prepared for the 9th Intern. Conf. on Atomic Spectroscopy, Tokyo, Japan, September 4–8, 1981.

There have been several important new developments in the fields of photoacoustics and photoacoustic spectroscopy. Photoacoustic techniques are now being used in ferromagnetic and electron spin resonance experiments, and there have been rapid advances in Fourier-transform infrared photoacoustic spectroscopy. In addition, the calorimetric aspects of photoacoustics are now being extensively exploited for phase transition studies, and to perform thermal-wave imaging and microscopy.

G. M. Sanger, *A Perspective on Precision Machining, Polishing and Optical Requirements,* Lawrence Livermore National Laboratory, Livermore, CA, UCRL-86579 (1981).

While precision machining has been applied to the manufacture of optical components for a considerable period, the process has, in general, had its thinking restricted to producing only the accurate shapes required. The purpose of this paper is to show how optical components must be considered from an optical (functional) point of view and that the manufacturing process must be selected on that basis. To fill out this perspective, simplistic examples of how optical components are specified with respect to form and finish are given, a comparison between optical polishing and precision machining is made, and some thoughts on which technique should be selected for a specific application are presented. A short discussion of future trends related to accuracy, materials, and tools is included.

J. D. Salisbury and C. E. Walter, *Projected Electrical Characteristics of the Dynamic RPEV System,* Lawrence Livermore National Laboratory, Livermore, CA, UCID-19188 (1981).

The principle of the roadway powered electric vehicle system (RPEV) is to propel a moving vehicle by the transfer of electrical power from a powered roadway. Power is transferred by electromagnetic induction. The system behaves like a transformer with an air gap. The powered roadway or energy source is the primary, the vehicle-mounted power pickup is the secondary, and the air gap permits power to be transferred without mechanical connections while the vehicle is in motion. An independent energy source for propulsion, e.g. batteries, is provided to allow operation away from the powered roadway.

Considerable data exists from test results of the RPEV system in the static mode. To determine operating characteristics of an RPEV in motion, a dynamic test system has been constructed at LLNL. This system consists of: a powered section of 50-m length plus acceleration and deceleration sections; an electrical power conditioner for the roadway; a test vehicle with power pickup, rectifier, batteries, electric motor and controller; and instruments and other ancillary equipment.

Dynamic RPEV system parameters and operating characteristics were projected by means of a computer model of the source/pickup equivalent electrical circuit and static test data suitably modified for the dynamic test system. This was the basis for system design, instrumentation, and planning for the dynamic test phase. These projections are discussed and presented in tabular and graphic form.

D. R. Speck, E. S. Bliss, J. A. Glaze,* J. W. Herris, F. W. Holloway, J. T. Hunt, B. C. Johnson, D. J. Kuizenga, R. G. Ozarski, H. G. Patton, P. R. Rupert, G. J. Suski, C. D. Swift, and C. E. Thompson, *The Shiva Laser Fusion Facility,* Lawrence Livermore National Laboratory, Livermore, CA, UCRL-85593 (1981). Prepared for the *IEEE J. of Quantum Electronics.*

The 10 kJ Shiva laser irradiation facility is the first major laser experimental facility devoted to Inertial Confinement Fusion research. It consists of: (1) a twenty beam Nd:glass laser amplifier system in which each beam has a final clear aperture of 20 cm diameter, (2) optical and alignment systems to focus the twenty beams simultaneously onto microscopic fusion targets, and (3) target diagnostics systems to measure the response of the targets to the irradiating beams. Since its activation in early 1978 Shiva has operated continuously providing up to 28 TW of 1.064 m optical power to targets. The evolution of Shiva into a reliable experimental facility required the development of engineering technology based on solid state laser concepts first introduced in the 1960's and early 1970's.

Leo R. Spogen, *The Technology Information System Description,* Lawrence Livermore National Laboratory, Livermore, CA, UCID-19087 (1981).

The Technology Information System (TIS) is a new generation, dedicated information machine with capabilities for nationwide bibliographic and

---

*Present address is Physics International Co., San Leandro, CA.

numeric database management, interactive modeling, electronic communications, and distributed networking. These capabilities are used successfully by those not intimately familiar with computers. Although many of its present databases and modeling capabilities are applicable to specific user communities, the technology employed has general applicability. This document describes the objective behind TIS development, the present system configuration, and its capabilities. It is hoped that the understanding of TIS gained from information contained herein is sufficient for potential users to realize the effectiveness of TIS in their applications.

Leo R. Spogen, Viktor E. Hampel, and John R. Raymond, *Technology Information System Review*, Lawrence Livermore National Laboratory, Livermore, CA, UCRL-85863 (1981). Prepared for the Technical and Economic Analysis Contractors' Meeting, Chicago, IL, April 21–22, 1981.

The Technology Information System (TIS) is being developed as part of the Transportation Systems Research (TSR) program at Lawrence Livermore National Laboratory (LLNL). The TIS project has for the most part been sponsored by the Technical and Economic Analysis (TEA) Branch of the U.S. Department of Energy (DOE) Office of Applied Conservation Technology (ACT). The goal of TIS is to provide ACT and its contractors the capability to readily access, develop, and utilize information needed in the R&D decision-making process and the conduct of resultant R&D projects.

C. C. Thompson, D. H. Polk, and D. J. McFarlin (United Technologies Research Center), **and R. R. Stone** (LLNL), *Heat Exchanger Concepts for Neutral Beam Calorimeters*, Lawrence Livermore National Laboratory, Livermore, CA, UCRL-85948 (1981).

Advanced cooling concepts that would permit the design of water cooled heat exchangers for use as calorimeters and beam dumps for advanced neutral beam injection systems were studied. Water cooling techniques ranging from pool boiling to high pressure, high velocity swirl flow were considered. Preliminary performance tests were carried out with copper, inconel and molybdenum tubes ranging in size from 0.19 to 0.50 in. diameter. Coolant flow configurations included (1) smooth tube/straight flow, (2) smooth tube with swirl flow created by tangential injection of the coolant, and (3) axial flow in internally finned tubes. Additionally, the effect of tube L/D was evaluated. A CO_2 laser was employed to irradiate a sector of the tube exterior wall; the laser power was incrementally increased until burnout (as evidenced by a coolant leak) occurred. Absorbed heat fluxes were calculated by dividing the measured coolant heat load by the area of the burn spot on the tube surface. Two 6 element thermopiles were used to accurately determine the coolant temperature.

J. H. VanSant and R. H. Bulmer, *Structural and Thermal Requirements for the Tandem Mirror Fusion Test Facility Magnet System*, Lawrence Livermore National Laboratory, Livermore, CA, UCRL-84904 (1981). Prepared for 6th Intern. Conf. on Structural Mechanics in Reactor Techn., Paris, France, August 17–21, 1981.

In October 1980 the United States Congress approved a budget for expansion of the Lawrence Livermore National Laboratory Mirror Fusion Test Facility (MFTF) to a tandem mirror facility designated MFTF-B. The new facility, scheduled for completion before 1985, will demonstrate energy "break even" capability (ratio of fusion energy to plasma heating energy) of mirror fusion and engineering feasibility of reactor scale machines. Twenty-two superconducting magnets contained in a 12 m diameter by 64 m long vacuum vessel will confine a fusion plasma fueled by 80 axial streaming plasma guns and over 40 radial neutral beams. Successful operation of the magnets requires thermal and structural designs to assure a stable superconducting state and to prevent unacceptable mechanical stresses.

Structural requirements for the magnet system include unique spatial constraints and materials restrictions to meet the operational needs of the unusual configuration. All of the magnets are liquid helium cooled which represents about 1500 tonnes of 4.5 K structure in the vacuum environment of the large vessel. Magnet support structures must

satisfy complex load conditions, including electromagnetic (both normal-operating and fault conditions) and seismically induced. Improved plasma confinement, characterized by long particle lifetimes, requires attention to coil alignment and field errors. Continued monitoring of field accuracy and possible adjustment during operation are contemplated.

Operating conditions for the magnet system include rapid cooldown and warm-up to minimize down time for maintenance. Also, a short-time magnet surface temperature cycle is needed during regeneration of cryopumping surfaces. The magnets must be protected from plasma radiation and beam impingements by using appropriate shields. Neutrons and gamma radiation must also be sufficiently intercepted to protect the superconductors and other sensitive materials. Liquid nitrogen barriers must shield the magnets from room temperature radiation and conduction heat sources. Adequate liquid helium flow through the magnets is required to maintain sufficient cooling of the superconductors in the presence of unavoidable heat sources. Moreover, the superconductor coil must be designed to inhibit helium vapor build-up. In the event of a magnet quench or fast dump, an adjacent magnet must withstand additional induced currents without adverse effects. Consequently, the superconductors must have properly selected materials and dimensions.

J. H. VanSant, T. A. Kozman, R. H. Bulmer, and D. S. Ng, *The Mirror Fusion Test Facility Magnet System,* Lawrence Livermore National Laboratory, Livermore, CA, UCRL-86001 (1981). Prepared for the 9th Symp. on Engineering Problems of Fusion Research, Chicago, IL, October 26–29, 1981.

In 1979, R. H. Bulmer of Lawrence Livermore National Laboratory (LLNL) discussed a proposed tandem-mirror magnet system for the Mirror Fusion Test Facility (MFTF) at the 8th Symposium on Engineering Problems in Fusion Research. Since then, Congress has voted funds for expanding LLNL's MFTF to a tandem-mirror facility (designated MFTF-B). The new facility, scheduled for completion by 1985, will seek to achieve two goals:

- Energy "break-even" capability (Q or the ratio of fusion energy to plasma heating energy = 1) of mirror fusion,
- Engineering feasibility of reactor-scale machines.

Briefly stated, 22 superconducting magnets contained in an 11-m-diam by 65-m-long vacuum vessel will confine a fusion plasma fueled by 80 axial streaming-plasma guns and over 40 radial neutral beams. We have already completed a preliminary design of this magnet system.

H. Joseph Weaver, *Modeling of Dynamic Behavior of Structural Systems,* Lawrence Livermore National Laboratory, Livermore, CA, UCRL-84177 (1981). Prepared for the 6th Intern. Conf. on Structural Mechanics in Reactor Technology, Paris, France, August 17–21 (1981).

Civil and structural engineers are often interested in constructing a mathematical model of a structure. This model is then typically used to predict response motions of the structure resulting from various loading conditions or forcing functions. When we mathematically model a structure we are, in effect, treating the structure as a system. For this system, the forcing function is considered the input, the resulting response motion is the output, and the cause-effect relationship between them is determined by the dynamic properties and geometry of the structure. In this paper, we will demonstrate that when formal systems theory techniques are applied to structures, much information concerning the physical and dynamic properties of the structure can be obtained.

R. W. Werner and M. A. Hoffman, *Optimizing the Heat Pipe for Operation in a Magnetic Field When Liquid Metal Working Fluids Are Used,* Lawrence Livermore National Laboratory, Livermore, CA, UCID-19049 (1981).

A novel method for reducing the magnetohydrodynamic (MHD) pressure drops in the liquid metal flow in a heat pipe wick is described. By flattening the heat pipe, the eddy current return path

in the metallic heat pipe wall is increased significantly, thereby increasing the effective wall resistance. This, in turn, reduces the magnitude of the MHD pressure drop. The same principle can also be applied to flows of liquid metal coolants in a magnetic field.

R. W. Wong, A. K. Chargin, and B. G. Logan, *TMX-Axisymmetric Magnet Set Design Study,* Lawrence Livermore National Laboratory, Livermore, CA, UCRL-85988 (1981). Prepared for the 9th Symp. on Engineering Problems of Fusion Research, Chicago, IL, October 26–29, 1981.

Studies are currently being made to design an axisymmetric modification to the TMX-Upgrade experiment. The existing TMX-Upgrade quadrupole plug and transition magnet sets are replaced by the circular coils of an axisymmetric plug.

RM

U. S. Government Printing Office: 1982/2-587-002/4046

Technical Information Department · Lawrence Livermore National Laboratory
University of California · Livermore, California 94550

First Class Mail